Universitat Autònoma de Barcelona

SYNTHESIS AND PROPERTIES OF MULTIFUNCTIONAL SINGLE MOLECULE MAGNETS

MATHIEU GONIDEC

Doctoral Thesis

Programa de doctorat en Ciència de Materials

Supervised by David B. Amabilino and Jaume Veciana Miró

Departament de Química
Facultat de Ciències

2010

CHAPTER 6

A LIQUID CRYSTALLINE SINGLE-MOLECULE MAGNET

6-1 Introduction

The preparation of a chiral double decker complex that behaves as a SMM was one of the principal objectives of this thesis, because the stereogenic centers might induce a chiral arrangement upon the coordination sphere of the metal ion and therefore give rise to some interesting magneto-chiral effect.[1-3] On the other hand, the supramolecular organization beyond the molecule is also of interest,[4-8] since the different supramolecular assemblies of these compounds, facilitated by the incorporation of long alkyl chains,[9-16] can provide a rich variety of magnetic behavior.

For these reasons, we prepared the compound *(S,S,S,S,S,S,S,S,S,S,S,S,S,S,S,S)*-**27**, from now on referred to as **27**, a chiral derivative of the double-decker phthalocyanine terbium complex. The stereogenic centers were envisaged at every 4,5 positions of the phenyl rings so as to avoid the possibility to obtain mixtures of constitutional isomers, while at the same time maximizing the "chiral content". Thus, molecule **27** contains no less than 16 stereogenic centers of the same absolute configuration. The sixteen long

[1] C. Train, R. Gheorghe, V. Krstic, L.-M. Chamoreau, N. S. Ovanesyan, G. L. J. A. Rikken, M. Gruselle and M. Verdaguer, *Nat. Mater.* **2008**, *7*, 729-734.
[2] G. L. J. A. Rikken and E. Raupach, *Nature* **1997**, *390*, 493-494.
[3] G. L. J. A. Rikken and E. Raupach, *Nature* **2000**, *390*, 932-935.
[4] Y. Qiu, P. Chen and M. Liu, *Langmuir* **2008**, *24*, 7200-7207.
[5] P. P. Bose, M. G. B. Drew, A. K. Das and A. Banerjee, *Chem. Commun.* **2006**, 3196-3198.
[6] M. Linares, P. Iavicoli, K. Psychogyiopoulou, D. Beljonne, S. De Feyter, D. B. Amabilino and R. Lazzaroni, *Langmuir* **2008**, *24*, 9566-9574.
[7] P. Iavicoli, M. Linares, Á. Pérez del Pino, R. Lazzaroni and D. B. Amabilino, *Superlattices Microstruct.*, *44*, 556-562.
[8] P. Iavicoli, M. Simon-Sorbed and D. B. Amabilino, *New J. Chem.* **2009**, *33*, 358-365.
[9] S. Dong, H. Tian, D. Song, Z. Yang, D. Yan, Y. Geng and F. Wang, *Chem. Commun.* **2009**, 3086-3088.
[10] A. S. Klymchenko, J. Sleven, K. Binnemans and S. De Feyter, *Langmuir* **2006**, *22*, 723-728.
[11] F. Nekelson, H. Monobe and Y. Shimizu, *Mol. Cryst. Liq. Cryst.* **2007**, *479*, 205-211.
[12] F. Nekelson, H. Monobe, M. Shiro and Y. Shimizu, *J. Mater. Chem.* **2007**, *17*, 2607-2615.
[13] S. Sergeyev, E. Pouzet, O. Debever, J. Levin, J. Gierschner, J. Cornil, R. G. Aspe and Y. H. Geerts, *J. Mater. Chem.* **2007**, *17*, 1777-1784.
[14] Z. Belarbi, C. Sirlin, J. Simon and J. J. Andre, *J. Phys. Chem.* **1989**, *93*, 8105-8110.
[15] D. D. Diaz, T. Torres, R. Zentel, R. Davis and M. Brehmer, *Chem. Commun.* **2007**, 2369-2371.
[16] F. Nekelson, H. Monobe and Y. Shimizu, *Chem. Commun.* **2006**, 3874-3876.

alkyl chains of this molecule can favor the appearance of several mesophases as is has been previously observed for analogous situations. [17]

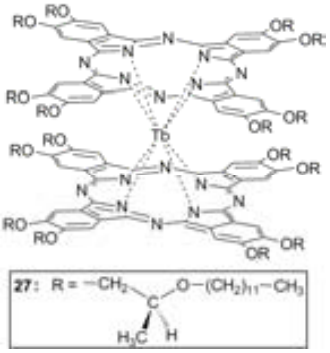

It turned out that the material may behave both as a chiral liquid crystal at room temperature, and as a single molecule magnet at low temperatures. Importantly, when the material is cooled at different rates the magnetic properties may vary because of different degrees and types of supramolecular order, bringing the opportunity to know about the influence of the intermolecular magnetic interactions on the SMM behavior of this compound.

In this chapter, we describe the preparation and characterization of the liquid crystalline terbium double-decker phthalocyanine complex **27** and how its mesomorphic properties can be used as a tool to adjust reversibly at will its magnetic properties. The Tb ion is used here as a direct and very sensitive probe of the structural changes occurring at low temperature where magnetic relaxation is dominated by direct – phonon induced – tunneling transitions.

6-2 Synthesis and characterization of the studied compound

The chiral bromoalkyl derivative *(S)*-**34**, a precursor of **27**, was synthesized in five steps from methyl lactate following a known route (see Scheme 6-1). [18] *(S)*-(-)-Methyl lactate was reacted with n-dodecyl iodide in the presence of silver (I) oxide without any other solvent, and the carboxylic acid *(S)*-**30** was obtained after hydrolisys of the impure ester with lithium hydroxide in methanol, to facilitate its purification. The pure acid was then converted back to the methyl ester *(S)*-**31** by refluxing it in methanol in presence of a catalytic amount of sulfuric acid. The chiral alcohol *(S)*-**32** was obtained by reduction

[17] K. Binnemans and C. Gorller-Walrand, *Chem. Rev.* **2002**, *102*, 2303-2346.
[18] E. Gomar-Nadal, C. Rovira and D. B. Amabilino, *Tetrahedron* **2006**, *62*, 3370-3379.

of *(S)*-**31** with lithium aluminum hydride in refluxing ether and the corresponding tosylate *(S)*-**33** was prepared by reacting *(S)*-**32** with tosyl chloride in the presence of triethylamine and a catalytic amount of dimethyl aminopyridine (DMAP). Finally, the chiral bromoalkyl ether *(S)*-**34** was prepared by reacting tosylate *(S)*-**33** with a large excess of lithium bromide in refluxing acetone.

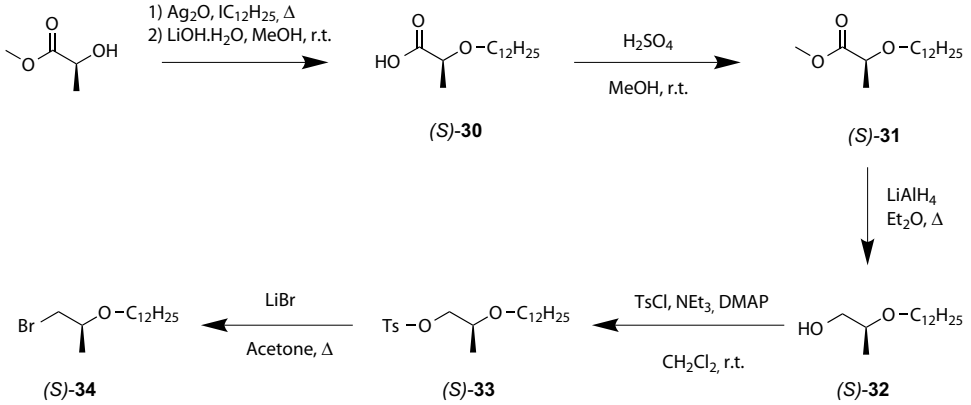

Scheme 6-1. Synthesis of the chiral bromoalkyl *(S)*-**34**.

The corresponding di-alkoxy phthalonitrile *(S,S)*-**9** was prepared from *(S)*-**34** in two steps using the procedures described in Chapter 2 (see Scheme 6-2). More precisely, dibromocatechol, prepared by bromination of the commercial pyrocatechol as described elsewhere, [19] was reacted with the bromoalkyl derivative in the presence of potassium carbonate in DMF [20] and the phthalonitrile was prepared in good yield by cyanation of the obtained dialkoxy dibromo aryl derivative *(S,S)*-**4** by reaction with zinc cyanide and tetrakis triphenyl phosphine palladium(0).

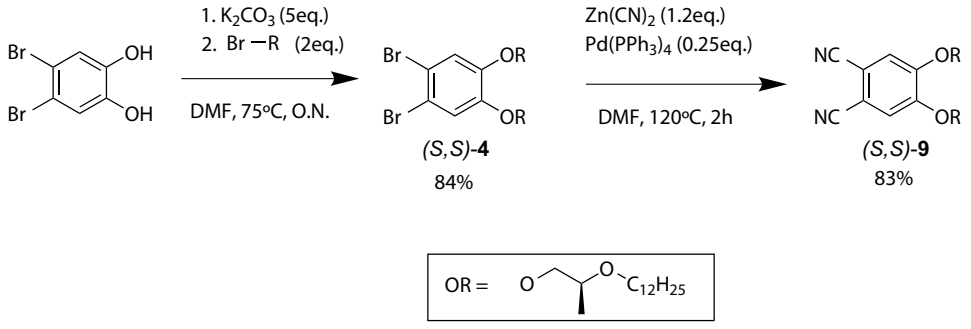

Scheme 6-2. Synthesis of the chiral phthalonitrile *(S,S)*-**9**.

[19] M. Kohn, *J. Am. Chem. Soc.* **1951**, *73*, 480.

[20] C. Piechocki, J. Simon, J.-J. Andre, D. Guillon, P. Petit, A. Skoulios and P. Weber, *Chem. Phys. Lett.* **1985**, *122*, 124-128.

Compound *(S,S)*-**9** was purified by silicagel chromatography and characterized by NMR spectroscopy, IR spectroscopy and polarimetry to determine its optical rotation.

The chiral metal-free phthalocyanine *(S,S,S,S,S,S,S,S)*-**22**, from now on **22**, bearing eight identical stereocenters, was prepared by cyclotetramerization of *(S,S)*-**9** in n-hexanol in the presence of DBU and KOAc.

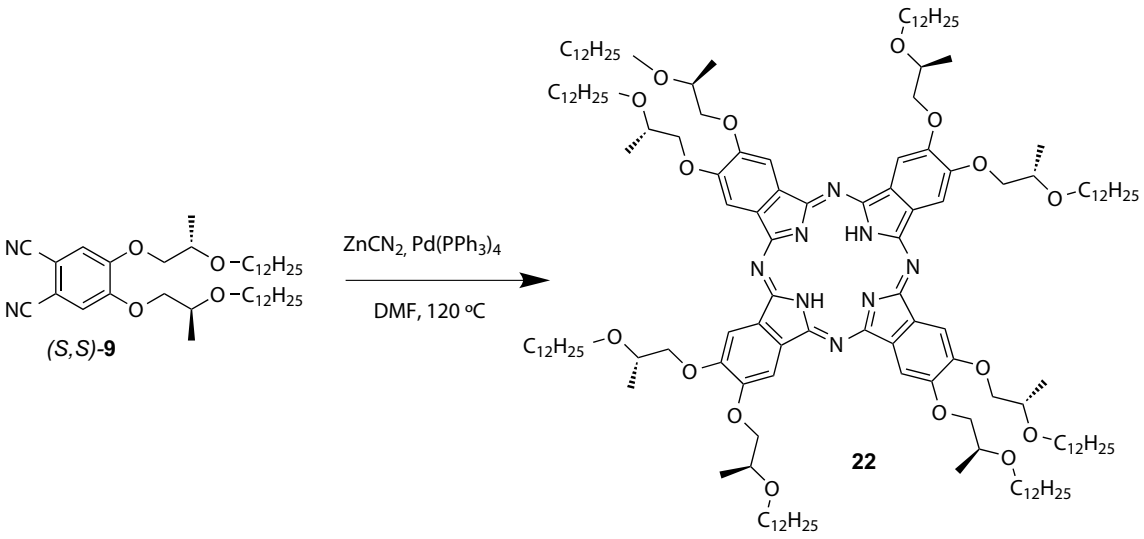

Scheme 6-3. Synthesis of the chiral phthalocyanine **22**.

The corresponding terbium double-decker complex **27** was prepared by reacting **22** with anhydrous terbium chloride and N,N-bis-trimethylsilylamide, with minor changes from a published method for other terbium double-decker phthalocyanine complexes. [21]

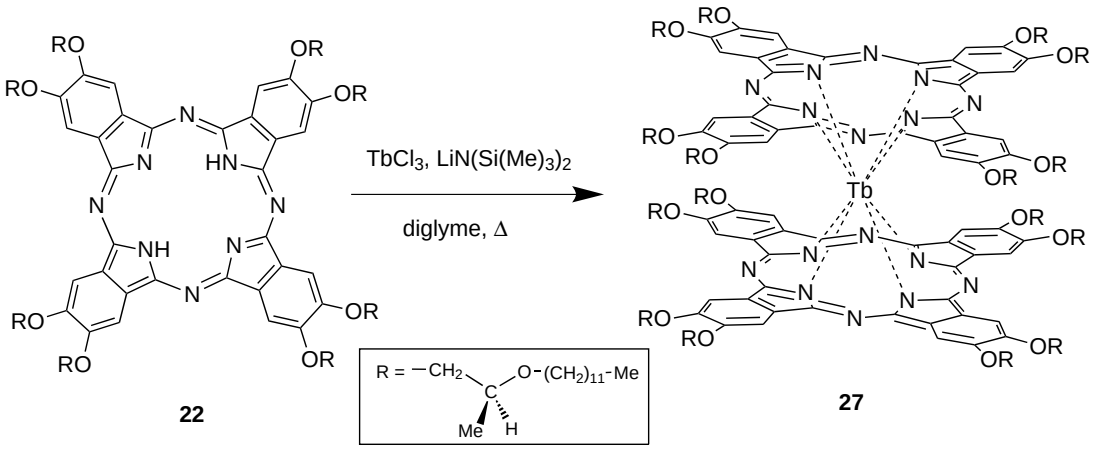

Scheme 6-4. Synthesis of the chiral complex **27**.

[21] T. Gross, F. Chevalier and J. S. Lindsey, *Inorg. Chem.* **2001**, *40*, 4762-4774.

The new compounds **22** and **27** were thoroughly purified by repeated silicagel column chromatography and gel permeation chromatography, and were characterized by LDI-TOF mass spectrometry, IR, UV-Vis absorption spectroscopy, and circular dichroism spectroscopy.

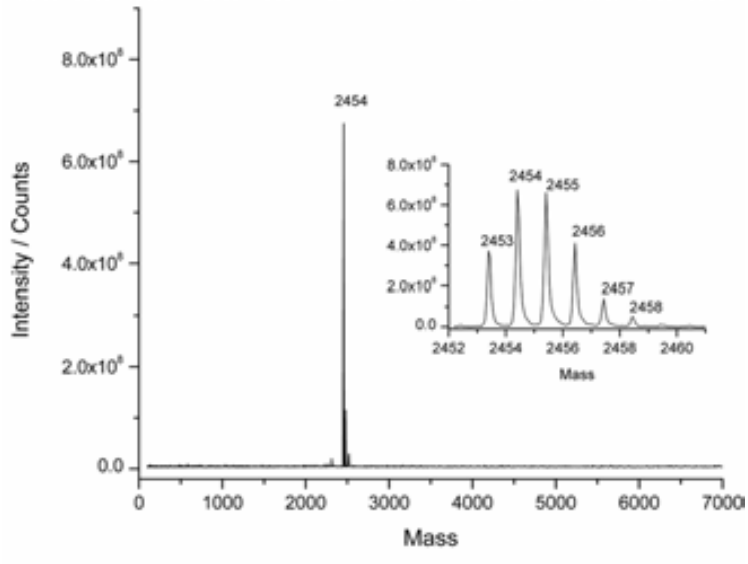

Figure 6-1. LDI-TOF mass spectrum of the free base phthalocyanine **22** with positive polarization. Inset, an enlargement of the molecular ion peak region, showing the isotopic distribution.

The laser desorption ionization mass spectrum of compound **22** showed a very clean spectrum with a molecular ion peak at $[M]^+$ = 2454 (see Figure 6-1) confirming the proposed molecular structure.

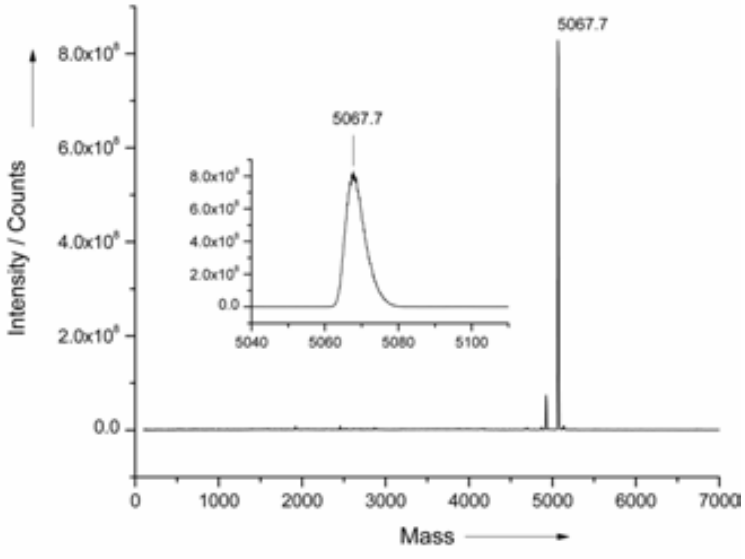

Figure 6-2. LDI-TOF mass spectrum of complex **27** with positive polarization. Inset, enlargement of the molecular ion region.

In addition, the isotopic distribution of the molecular ion peak could be resolved and corresponds to the expected one. The mass spectrum of the complex **27** on the other hand, shows a molecular ion peak at $[M]^+$ = 5068, in agreement with the proposed molecular structure, but its isotopic distribution could not be resolved (see Figure 6-2).

The absorption spectra of **22** and **27** show the characteristic bands of free base phthalocyanines and neutral double-decker complexes, respectively. [22-24]

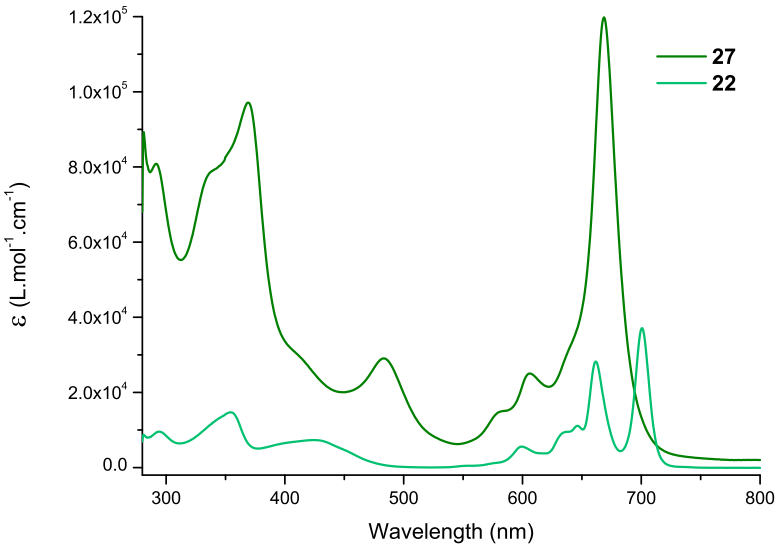

Figure 6-3. UV-Vis spectra of a solution of the terbium double-decker complex **27** in toluene (dark green) and of a solution of the metal free phthalocyanine **22** in toluene (light green).

Namely, the free base phthalocyanine **22** (see Figure 6-3) exhibits a split Q-band with peaks at 700 and 661 nm, a vibronic band at 599 nm, and a Soret band at 354 nm, while the double-decker complex **27** (see Figure 6-3) shows an intense Q-band absorption at 668 nm, vibronic bands at 605 and 581 nm, a fingerprint π radical band at 483 nm and a split Soret band at 337 and 369 nm.

The optical activity of the compounds was proved by circular dichroism (CD) spectroscopy.[i] Compound **27** shows Cotton effects at 668, 610, 455, and 368 nm, indicating that the chromophore groups of this molecule is immersed in a chiral environment. In contrast, the CD spectrum of the free base phthalocyanine **22** is dramatically less intense (see Figure 6-4).

---

[22] A. De Cian, M. Moussavi, J. Fischer and R. Weiss, *Inorg. Chem.* **1985**, *24*, 3162-3167.
[23] J. Jiang and D. K. P. Ng, *Acc. Chem. Res.* **2009**, *42*, 79-88.
[24] N. Ishikawa, *J. Porphyrins Phthalocyanines* **2001**, *5*, 87-101.
[i] *The optical rotation of those complexes cannot be measured by polarimetry because of their very high molar absorptivities at the normal wavelength of the sodium D line.*

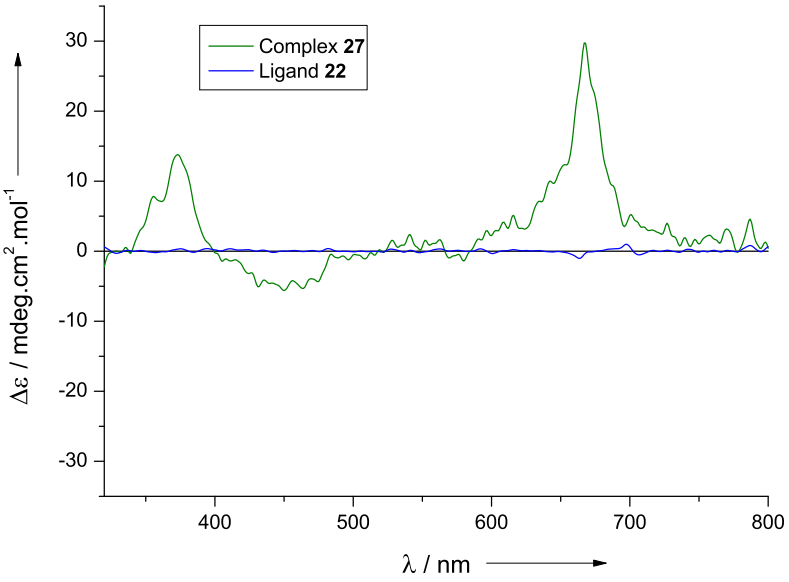

Figure 6-4. Circular dichroism spectra of compounds **27** and **22** in toluene

The lack of significant optical activity in compound **22**, in the region of 300-800 nm can be explained by the fact that despite the fact that this molecule contains no less than 8 stereogenic centers, they are positioned far enough away from the π-conjugated core not to influence significantly the geometry of the chromophore and do not therefore provide a strong chiral environment affecting the electronic absorptions. On the other hand, the double-decker complex **27** not only doubles the amount of stereogenic centers but the vicinity of the two phthalocyanine rings probably also forces the sterically hindered molecule to adopt a chiral conformation which is reflected in a stronger transfer of chirality from the peripheral chiral centers to the phthalocyanine chromophore. Even so, the intensity of the Cotton effects is relatively small, given the number of stereogenic centers, and may arise from a small number of contributing conformations.

6-3 Study of the mesomorphic behaviors of compounds 22 and 27

Variable temperature polarizing optical microscopy (POM) shows that compound **27** is mesomorphic with a clearing point at 304 K and an optical texture at room temperature suggesting a columnar (Col) mesophase (Figure 6-5) which is consistent with previously described mesomorphic double-decker phthalocyanine complexes. [11, 12, 14, 16, 17, 25-27]

[11] F. Nekelson, H. Monobe and Y. Shimizu, *Mol. Cryst. Liq. Cryst.* **2007**, *479*, 205-211.

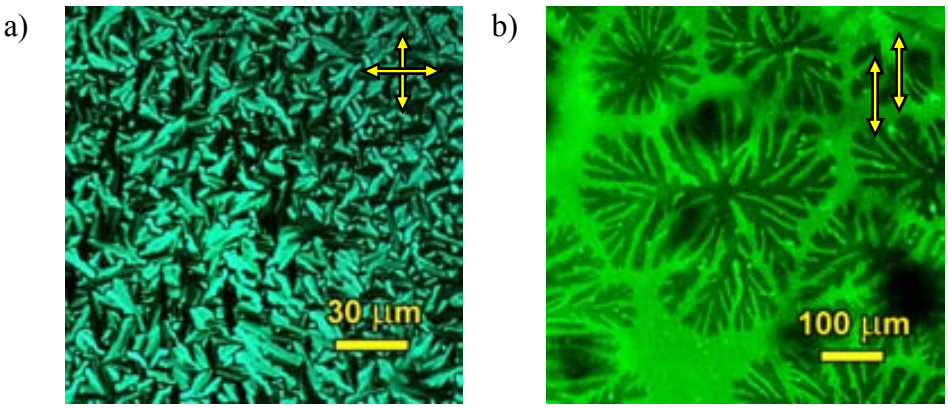

Figure 6-5. POM images of the mesophase of **27** at 298 K, showing: a) the optical texture with crossed polarizing filters, and b) the fan texture of the homeotropic alignment, as seen with parallel polarizing filters.

The observed optical texture corresponds to a dynamic phase. Indeed, if one monitors the same area over a prolonged period of time, the dark and light domains flip over time and tend to unite into ever bigger domains.

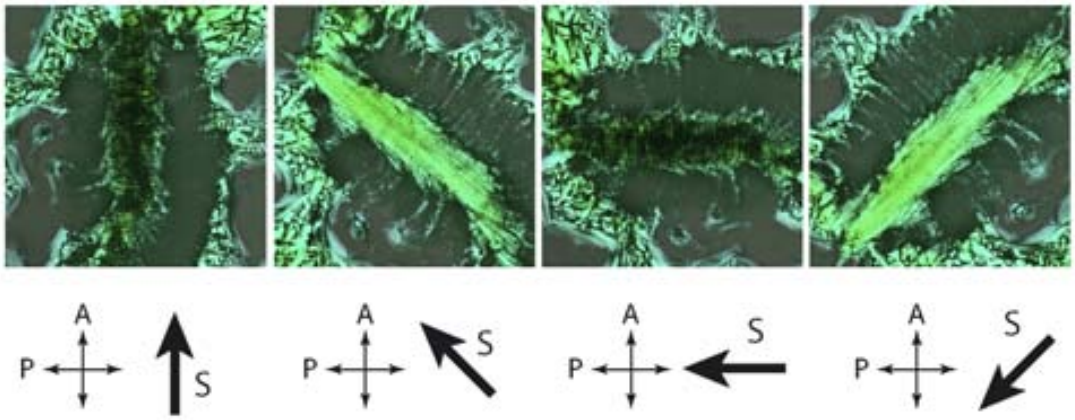

Figure 6-6. POM images of **27** at 298 K, showing the optical texture depending on the relative angle between the analyzer (A) and the shear direction (S). The image size is 200×200 µm.

[12] F. Nekelson, H. Monobe, M. Shiro and Y. Shimizu, *J. Mater. Chem.* **2007**, *17*, 2607-2615.
[16] F. Nekelson, H. Monobe and Y. Shimizu, *Chem. Commun.* **2006**, 3874-3876.
[17] K. Binnemans and C. Gorller-Walrand, *Chem. Rev.* **2002**, *102*, 2303-2346.
[25] K. Ban, K. Nishizawa, K. Ohta, A. M. van de Craats, J. M. Warman, I. Yamamoto and H. Shirai, *J. Mater. Chem.* **2001**, *11*, 321-331.
[26] K. Binnemans, J. Sleven, S. De Feyter, F. C. De Schryver, B. Donnio and D. Guillon, *Chem. Mater.* **2003**, *15*, 3930-3938.
[27] A. G. Gurek, T. Basova, D. Luneau, C. Lebrun, E. Koltsov, A. K. Hassan and V. Ahsen, *Inorg. Chem.* **2006**, *45*, 1667-1676.
[14] Z. Belarbi, C. Sirlin, J. Simon and J. J. Andre, *J. Phys. Chem.* **1989**, *93*, 8105-8110.

Also, the material can be aligned by shearing of the liquid crystalline phase. After shearing, the whole affected area of the mesophase is predominantly oriented along the sheering direction as can be seen in Figure 6-6.

Upon cooling from the isotropic (I) liquid phase, some hexagonal dendritic growth could be observed in the optical texture of **27** under uncrossed polarizing filters at 298 K. The observation of this fan-like texture suggests a homeotropic alignment on glass of a columnar hexagonal (Col_h) mesophase.[11, 12, 16, 25]

Differential Scanning Calorimetry (DSC) of complex **27** (Figure 6-7) shows only one endothermic peak at 261 K corresponding to the crystal to hexagonal columnar (Cr → Col_h) transition with ΔH = 86.1 kJ.mol^{-1} and ΔS = 340.7 J.K^{-1}.mol^{-1}. However, this complex does not show any peak near 304 K corresponding to the clearing point observed by POM, presumably because of the small enthalpy difference between the two phases.

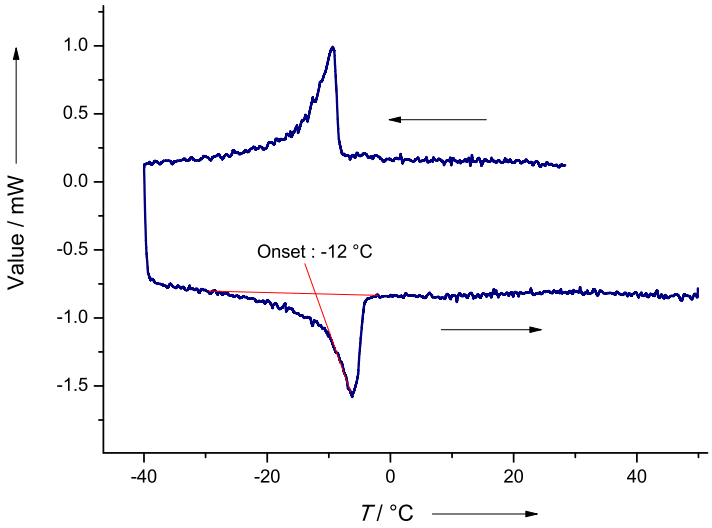

Figure 6-7. DSC trace of the terbium double-decker complex **27** with cooling and heating rates of 1 ºC.min^{-1}

Small angle x-ray scattering (SAXS) diffraction technique was used to confirm the nature of the observed mesophase. For complex **27**, only three reflections (see Figure 6-8) could be observed at 298 K in the small angle region of 0-8 º, with d spacing ratios of $1:\sqrt{3}:2$, allowing an unambiguous identification of a hexagonal lattice.

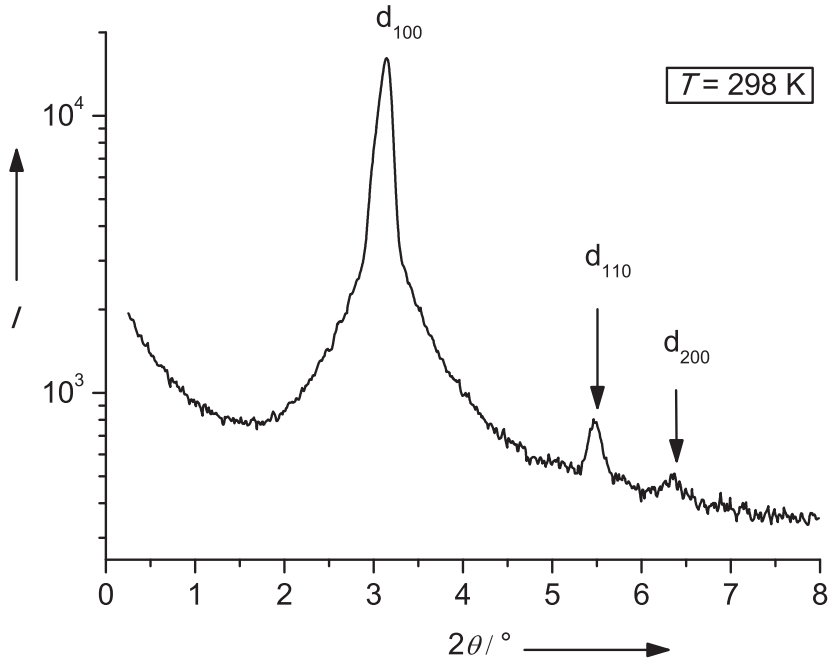

Figure 6-8. SAXS diffraction patterns of the hexagonal columnar mesophase of complex **27** at 298 K.

The observed reflections of complex **27**, obeying $(h^2 + hk + k^2)^{1/2}$, were labeled (100), (110), (200) and are given in Table 6-1. This observation confirms the hexagonal columnar mesophase, which is qualitatively consistent with previously reported mesomorphic double-decker compounds of cerium,[11, 12, 16] and various lanthanides.[17, 25, 26]

Table 6-1. Observed reflexions and calculated reflexions based on a hexagonal lattice obeying $(h^2 + hk + k^2)^{1/2}$. The calculated d values are calculated as $d = d_{100} / (h^2 + hk + k^2)^{1/2}$, where d_{100} is the main observed diffraction peak.

Compounds	Phase	Observed d / nm	Calculated d / nm	Label
22	Col_h	2.85	-	100
		1.64	1.65	110
		1.41	1.42	200
27	Col_h	2.78	-	100
		1.61	1.60	110
		1.38	1.39	200

The phase behavior of the free base phthalocyanine **22** is found to be qualitatively similar to the behavior of **27,** with the only difference of a considerable shift in the phase transition temperatures.

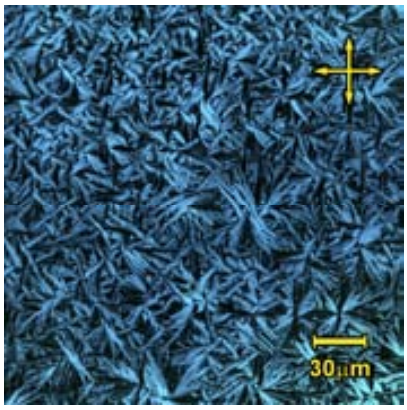

Figure 6-9. POM images of the mesophase of **22**, showing the optical texture at 298 K with crossed polarizing filters.

Thus, complex **22** also presents a hexagonal columnar mesophase as evidenced by POM (see Figure 6-9) and SAXS (Figure 6-10). Nevertheless, the clearing point is much lower in the complex **27** than in **22** (304 K compared with 415 K), as occurs in analogous systems.[14, 17, 25, 26] This could be due to a strong energy difference in the cofacial aggregation of free phthalocyanines and double-decker complexes.

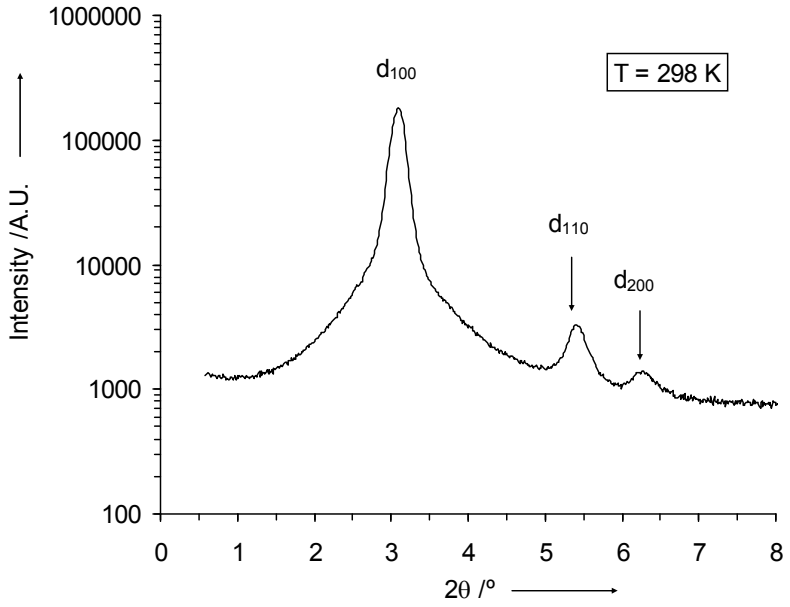

Figure 6-10. SAXS diffraction patterns of the hexagonal columnar mesophase of **22** at 298 K.

The metal center pulling most of the electron density of the rings in the interplanar space, making the outer face of the ligands less prone to aggregation than in the free base phthalocyanines.

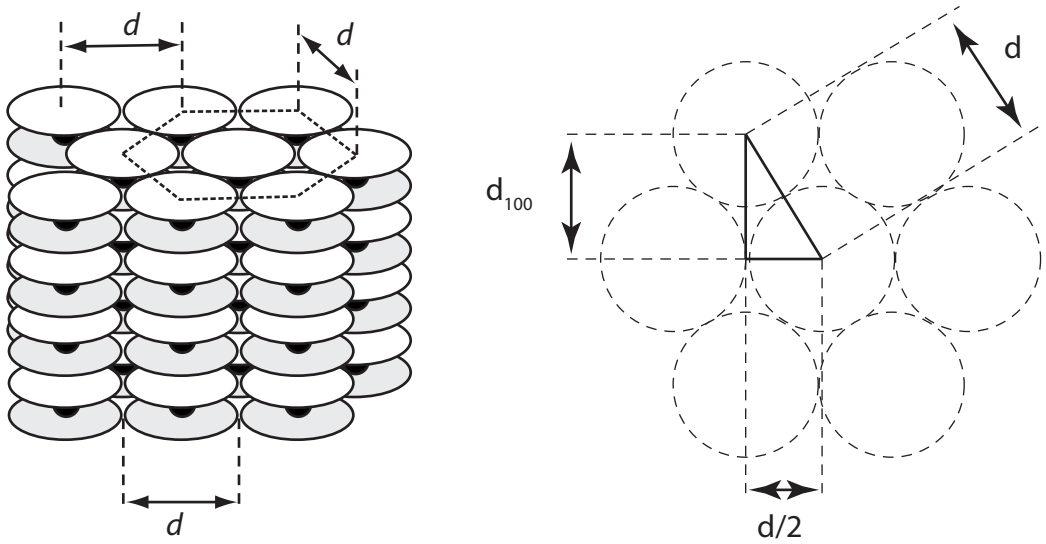

Figure 6-11. Representation of the arrangement of the double-decker phthalocyanine complexes in the hexagonal columnar mesophase. The inter-columnar repeat distance *d* is shown together with the inter-planar distance d_{100}.

The intercolumnar repeating distance (see Figure 6-11), was calculated for both compounds as $d = d_{100} \times 2 / \sqrt{3}$, where d_{100} is the main diffraction peak of the SAXS spectra, and was found to be identical, taking into account the experimental error, with a mean value of d = 3.2 nm.

6-4 Processing of the liquid crystalline complex 27 and preparation of samples with different supramolecular structures

The magnetic properties of single-molecule magnets can be very sensitive to the structural changes in the solid state because the relative arrangements of the molecules dictate the dipolar interactions among other issues. Indeed, differences of magnetic behavior have been seen in SMMs derived from dodecamanganese complexes and attributed to Jahn-Teller isomerism in the coordination sphere of the manganese. [28]

[28] S. M. J. Aubin, Z. Sun, H. J. Eppley, E. M. Rumberger, I. A. Guzei, K. Folting, P. K. Gantzel, A. L. Rheingold, G. Christou and D. N. Hendrickson, *Inorg. Chem.* **2001**, *40*, 2127-2146.

[29] N. Ishikawa, M. Sugita and W. Wernsdorfer, *Angew. Chem. Int. Ed.* **2005**, *44*, 2931-2935.

It has also been shown that the degree of dipolar interactions as well as changes in the matrix arrangements around the molecular core of double-decker lanthanide complexes can influence the magnetic behavior of these compounds.[29, 30] For this reason, the mesomorphism of **27** was extremely appealing since it can be seen as a tool to change the superstructure and probe the robustness of its magnetic properties in a variety of discrete structural situations. Since the SMM behavior and magnetic ordering occur at low temperatures, one can kinetically trap the sample in a given structural state, and measure and characterize its magnetic properties at low temperature. Namely, via suitable rates of cooling, one can prepare, from the same specimen, a glassy, structurally disordered sample $\mathbf{27_{Dis}}$, an intermediate partially ordered frozen mesophase sample $\mathbf{27_{PO}}$, or reach an ordered crystalline state $\mathbf{27_{Cr}}$. An illustration of the expected structures in the domains of the solid state of the different samples is given in Figure 6-12.

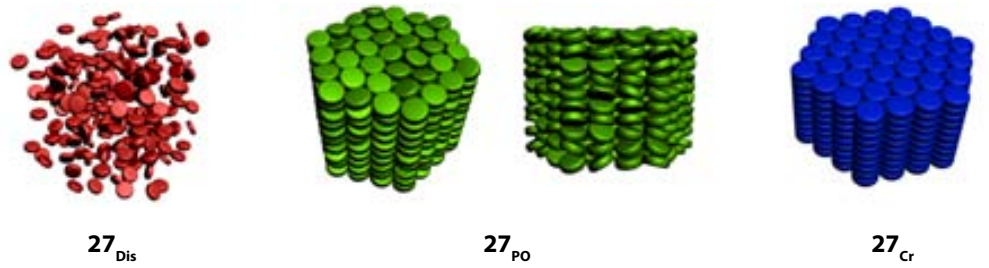

Figure 6-12. Idealized structures in the domains of the frozen solid states corresponding to sample $\mathbf{27_{Dis}}$, $\mathbf{27_{PO}}$ and $\mathbf{27_{Cr}}$. Each disk represents one double-decker molecule.

It is worth mentioning that all three samples should be on average isotropic, that is, even though the individual domains or microcrystals are expected to be anisotropic in the case of $\mathbf{27_{PO}}$ and $\mathbf{27_{Cr}}$, these domains or microcrystals should be randomly distributed across the whole sample, giving a macroscopic appearance of an isotropic material. Interestingly, a fourth sample could also be made by applying an external magnetic field while cooling down. If this is done at a strong enough magnetic field, the magnetic torque exerted on the magnetic dipoles could provide an oriented sample $\mathbf{27_{CrField}}$ which would be locally identical to $\mathbf{27_{Cr}}$ but presenting a long-range alignment of the microcrystals along the field direction (see Figure 6-13). Such a sample would be truly anisotropic, resembling an oriented single-crystal, and its properties might differ from those of $\mathbf{27_{Cr}}$.

[30] F. Branzoli, P. Carretta, M. Filibian, G. Zoppellaro, M. J. Graf, J. R. Galan-Mascaros, O. Fuhr, S. Brink and M. Ruben, *J. Am. Chem. Soc.* **2009**, *131*, 4387-4396.

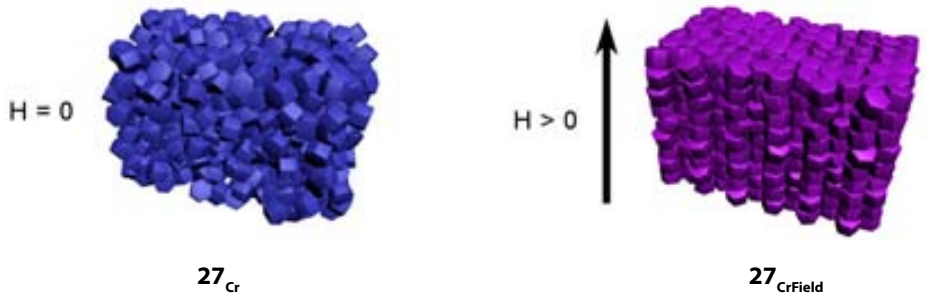

Figure 6-13. Comparison of the orientation of microcrystals of samples $\mathbf{27}_{\mathbf{Cr}}$ and $\mathbf{27}_{\mathbf{CrField}}$. Here, the hexagonal domains represent different microcrystals composed by many well-ordered double-decker molecules.

The glassy disordered sample $\mathbf{27}_{\mathbf{Dis}}$ was prepared by warming up the material ex-situ at 333 K for 2 minutes to reach the isotropic phase, and quenching the resulting phase at 150 K inside the susceptometer. The ordered sample $\mathbf{27}_{\mathbf{Cr}}$ was prepared entirely in-situ by warming up the same sample again and cooling it down slowly at a controlled rate. Sample $\mathbf{27}_{\mathbf{CrField}}$ was prepared exactly like sample $\mathbf{27}_{\mathbf{Cr}}$ with the exception that a constant magnetic field of 5 T, the maximum field that could be applied using the available equipment, was applied during the cooling procedure. Finally, after letting the isotropic phase sample equilibrate at room temperature (i.e. in the mesophase) for several weeks, it was quenched again to 150 K using the same protocol as that used for $\mathbf{27}_{\mathbf{Dis}}$, which afforded sample $\mathbf{27}_{\mathbf{PO}}$. The cooling rates of all the above mentioned processes are summarized in Scheme 6-5.

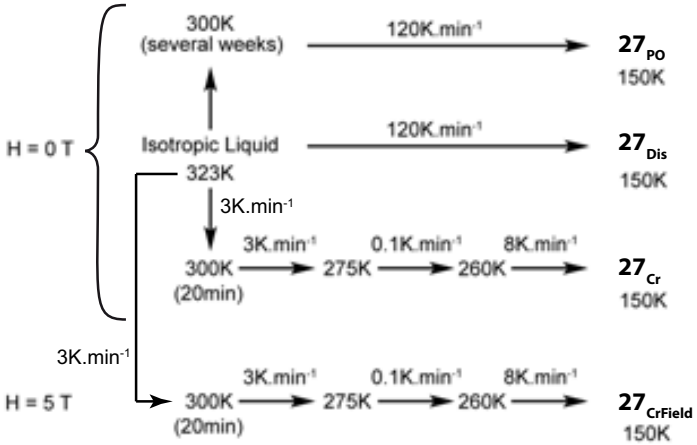

Scheme 6-5. Cooling procedures used to prepare samples $\mathbf{27}_{\mathbf{Dis}}$, $\mathbf{27}_{\mathbf{PO}}$, $\mathbf{27}_{\mathbf{Cr}}$ and $\mathbf{27}_{\mathbf{CrField}}$.

The distinct samples of complex **27** were studied by polarized optical microscopy so as to check the optical texture of the samples as a function of temperature treatment, confirming in this way the characteristics of the resulting superstructure. Thus, a sample of **27** was first quenched in conditions similar to those used to prepare sample $\mathbf{27}_{\mathbf{Dis}}$, and then it was warmed-up to room temperature and melted at 323 K. The resulting micrographs are shown in Figure 6-14.

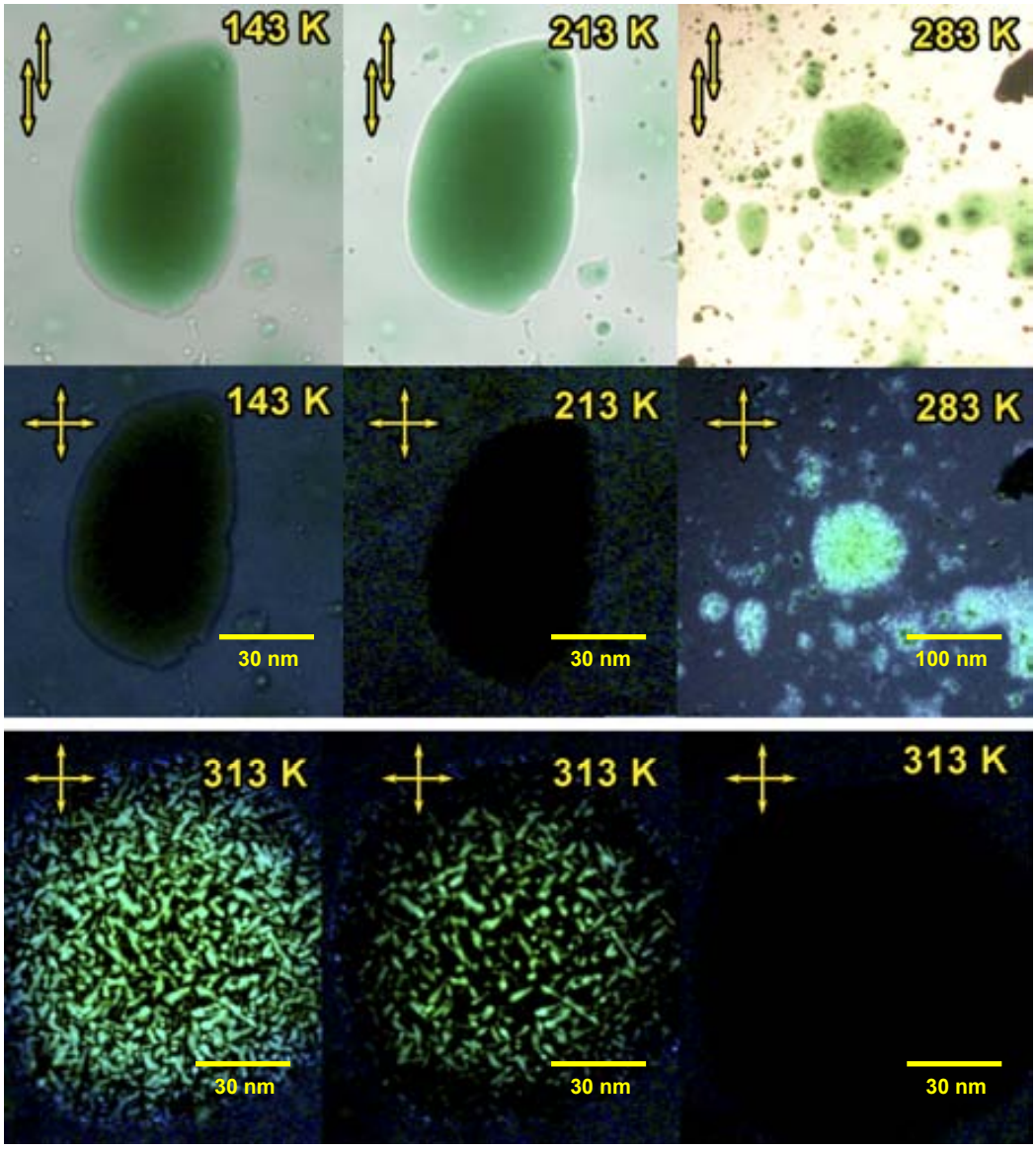

Figure 6-14. Changes in optical texture while heating a quenched sample of **27** from 143 K to 313 K at 30 K/min as seen with crossed polarizing filters (middle) and uncrossed polarizing filters (above). Evolution of the optical texture of **27** (enlargement of the bright circular motive seen at 283 K) over one minute when clearing at a constant temperature of 313 K (below) as seen with crossed polarizing filters.

The quenched sample looks effectively glassy at low temperatures between 143 K and 213 K. Upon further warming it started to flow at approximately 263 K and acquired an optical texture characteristic of the liquid-crystalline state quite rapidly. It started to melt to the isotropic liquid phase at 313 K and melted over a short period of time of approximately one minute (see Figure 6-14). This confirms that the quenched sample is really in a glassy state, i.e. $\mathbf{27}_{\mathbf{Dis}}$. In order to prepare a partially ordered structure of **27**, the isotropic liquid phase was then cooled down using the condition described in Scheme 6-5 for $\mathbf{27}_{\mathbf{PO}}$. The newly obtained frozen phase (see Figure 6-15) is optically very different from the starting glassy state of Figure 6-14. Namely, while the glass phase obtained upon quenching at 143 K is clearly isotropic when observed under crossed polarizing filters the sample obtained by cooling slowly from the isotropic melt is strongly birefringent at 271 K, indicating a partially ordered superstructure of a mesomorphic phase, i.e. $\mathbf{27}_{\mathbf{PO}}$.

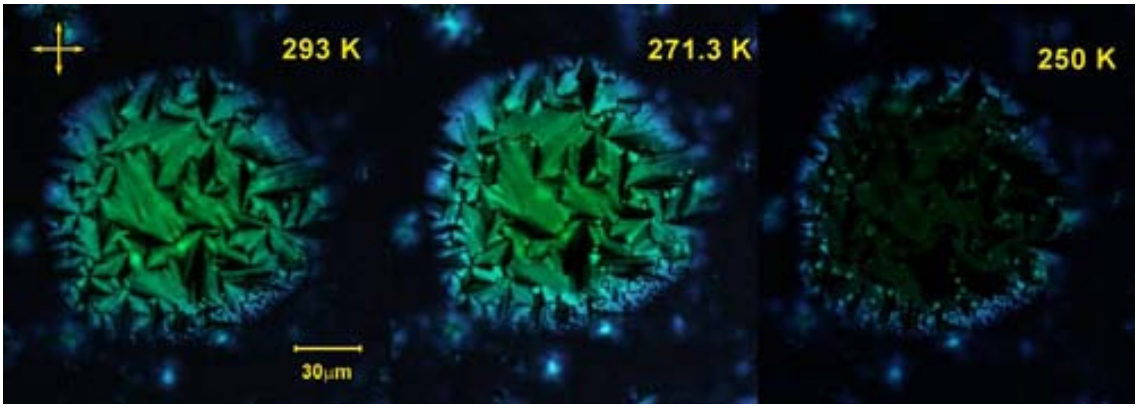

Figure 6-15. Changes in the optical texture while cooling down from 313 K using the cooling procedure described Scheme 6-5.

It is remarkable that upon further cooling the previous sample, it appears darker (see Figure 6-15). This transition, which was shown to be reproducible, is probably not a phase transition inherent of the bulk material but a surface related effect. A change in the orientation of the columnar mesophase might be responsible for the observed change in optical texture.

6-5 Study of the magnetic properties of materials deriving from 27 with different supramolecular structures.

Ac-magnetic susceptibility measurements of $\mathbf{27_{Dis}}$, $\mathbf{27_{PO}}$, $\mathbf{27_{Cr}}$ and $\mathbf{27_{CrField}}$, as a function of temperature and frequency of the oscillating magnetic field were done with a commercial superconducting quantum interference device (SQUID) magnetometer at the University of Zaragoza in collaboration with Dr. Fernando Luis.

It is important to stress here that the four samples of complex 27 used for this study were prepared using the very same sealed gelatin capsule, employed in the susceptometry experiments. Therefore, any change in composition − especially any loss of traces of solvent − is ruled out, the only difference from one sample to the other being the superstructure that is reached in the frozen solid state as a consequence of their different thermal treatments.

6-5-1 Temperature dependent ac magnetic susceptibility measurements

The temperature dependence of the in-phase (χ_M') and out-of-phase (χ_M'') susceptibilities measured at several frequencies in the range of 0.5 to 1500 Hz for samples $\mathbf{27_{Dis}}$, and $\mathbf{27_{Cr}}$ proved to be very similar to previously reported neutral double-decker complexes of terbium.[31] The χ_M'T product of the ordered and disordered samples (see Figure 6-16) converge above 54 K and for all the studied frequencies (0.5-1488 Hz) to approximately the same value of 9.4 ± 0.2 emu.mol^{-1}.

Similarly, the χ_M''(T) curves of $\mathbf{27_{Dis}}$ and $\mathbf{27_{Cr}}$ show qualitatively the same behavior under the above mentioned conditions (Figure 6-17). Having a closer look at the χ_M'T(T) data, one can however see the appearance of a second broad drop below 25 K in the χ_M'T(T) curves corresponding to the disordered sample $\mathbf{27_{Dis}}$, which becomes more evident below 15 Hz, that is not seen in the $\mathbf{27_{Cr}}$ sample. Small differences were also observed in the χ_M'' *vs.* T graphs for both samples. Thus, the peak in χ_M''(T) of $\mathbf{27_{Dis}}$ also appears to be shifted up by about 2-3 K with respect to that of $\mathbf{27_{Cr}}$ and the divergence at low temperature is notably higher for the disordered sample $\mathbf{27_{Dis}}$ than for the ordered one $\mathbf{27_{Cr}}$.

[31] N. Ishikawa, M. Sugita, N. Tanaka, T. Ishikawa, S.-y. Koshihara and Y. Kaizu, *Inorg. Chem.* **2004**, *43*, 5498-5500.

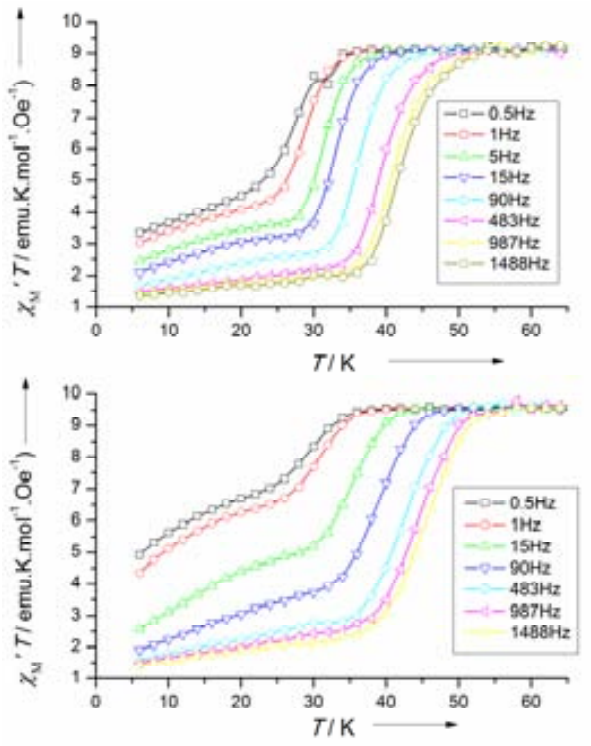

Figure 6-16. χ_M'T product of sample $\mathbf{27_{Cr}}$ (above) and $\mathbf{27_{Dis}}$ (below) versus temperature at various frequencies of the oscillating magnetic field.

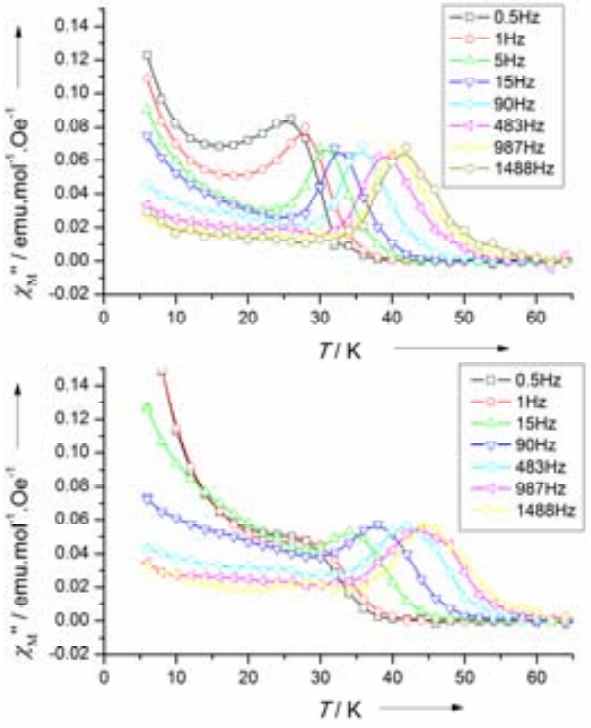

Figure 6-17. Imaginary part of the ac magnetic susceptibility χ_M'' of sample $\mathbf{27_{Cr}}$ (above) and $\mathbf{27_{Dis}}$ (below) versus temperature at various frequencies of the oscillating magnetic field.

The difference between samples 27Dis and 27Cr can also be illustrated by a 3D plot versus the log of the frequency and the temperature as the two horizontal axes (see Figure 6-18).

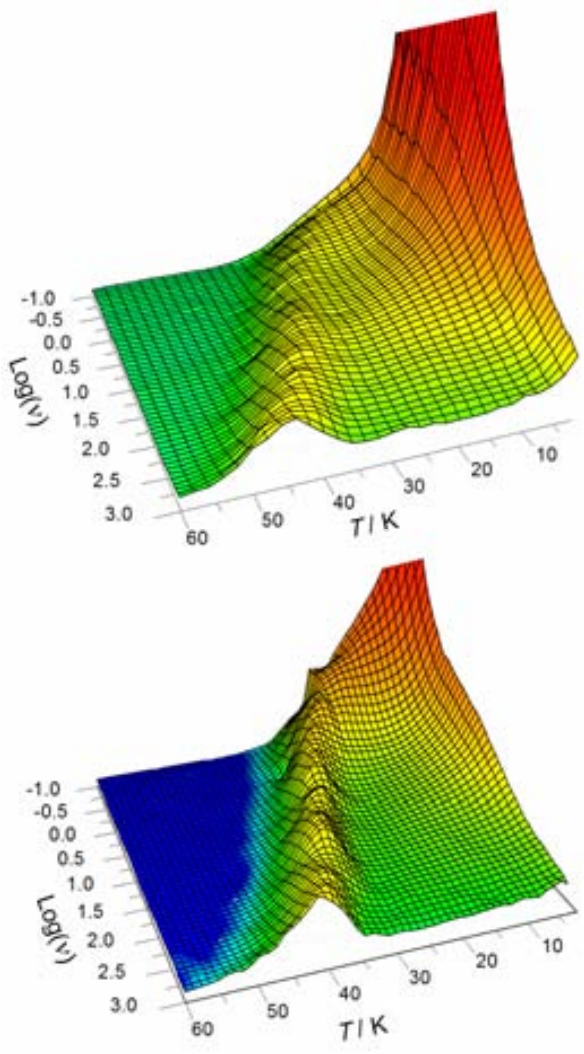

Figure 6-18. 3D graph of $\chi_M''(\log(\nu), T)$ for samples $\mathbf{27_{Dis}}$ (above) and $\mathbf{27_{Cr}}$ (below)

The magnetic measurements of sample $\mathbf{27_{CrField}}$ were found to be identical to those of sample $\mathbf{27_{Cr}}$ for all frequencies and at all temperatures as it is clearly shown in Figure 6-19. The identical magnetic behavior of both samples indicates that the external magnetic field does not produce any significant effect on the supramolecular organization of the sample $\mathbf{27_{CrField}}$. This result suggests that the magnitude of the total magnetic dipole moment of the molecules is too small for them to be aligned by the external magnetic field of 5 T used in the experiment.

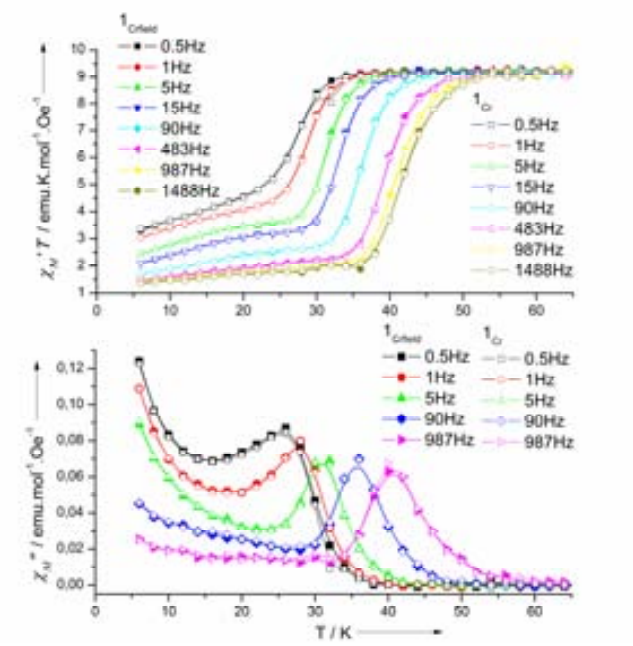

Figure 6-19. χ_M'T product (top) and χ_M'' (bottom) of sample **27$_{Cr}$** (empty symbols) and **27$_{CrField}$** (full symbols) versus temperature at various frequencies of the oscillating magnetic field.

The small magnitude of the magnetic dipole moment is somewhat surprising because it is in principle given by the sum of the diamagnetic and paramagnetic contributions and one would expect a large diamagnetic contribution with a high anisotropy for a largw aromatic molecule like **27**. Another consideration deserves the paramagnetic contribution of the Tb^{3+} ion to the total magnetic dipole moment of **27**. In fact, if the magnetic dipole moment of **27** comes entirely from the Tb(III) ion present in its structure, its expected magnitude must be very small and can be evaluated by the following formula:

$$m = g_J \sqrt{J(J+1)}\,\mu_B$$

where m is the magnetic moment and g_J is the Landé factor of the considered atom, being J its total angular momentum and μ_B is the Bohr magneton. In the case of a Tb^{3+} ion with $g_J = 3/2$ and $J = 6$ it gives $m = 9.72\ \mu_B$. Thus, the torque $\boldsymbol{\tau}$ exerted on a magnetic moment m by an external magnetic field **B** is given by:

$$\boldsymbol{\tau} = \boldsymbol{m} \times \boldsymbol{B}$$

The magnitude of the torque is therefore equal to mBsin(θ), where B is the applied magnetic field and θ is the value of the angle between the field and the magnetic moment. In our case, if there is only a paramagnetic contribution to the total magnetic moment, the maximum expected magnitude of the torque, at θ = 90º, for a 5 T field would therefore be of 4.51×10^{-22} J, which is equivalent to the thermal energy at 32.7 K. Therefore, at the crystallization temperature of the complex of 261 K, the thermal energy is huge in comparison with magnitude of the magnetic torque, preventing an effective alignment. It is therefore logical that this kind of paramagnetic contribution is not responsible for the alignment of the liquid crystal, under these conditions, and magnetic fields one order of magnitude larger would be required to achieve a molecular alignment at the crystallization temperature, that were not available in our laboratories. Thus, the diamagnetic contribution of **27** must be very small, being the cause of the lack of alignment.

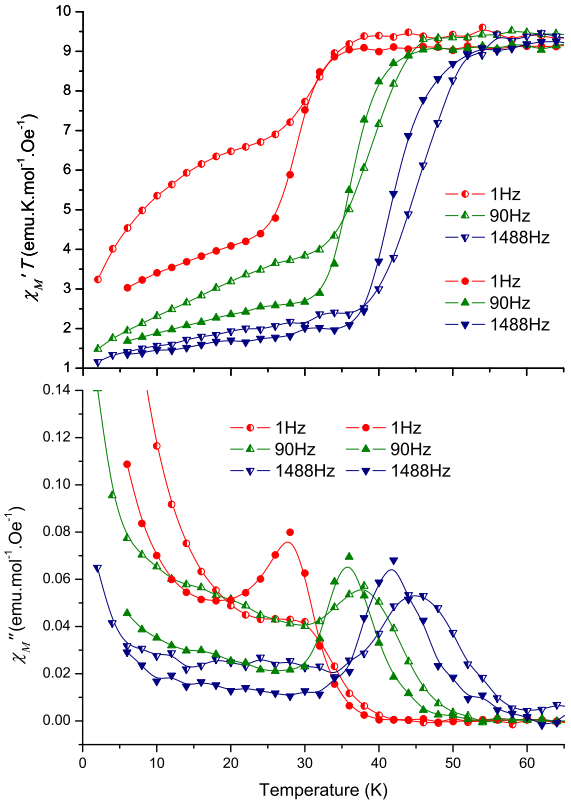

Figure 6-20. χ_M'T product (top) and χ_M'' (bottom) of sample $\mathbf{27_{PO}}$ (half-filled symbols) and $\mathbf{27_{Dis}}$(full symbols) versus temperature at various frequencies of the oscillating magnetic field.

The behavior of sample **27**$_{PO}$ was quite different from that of sample **27**$_{Dis}$, as shown in Figure 6-20, as it was initially expected, since the superstructure of **27**$_{PO}$ is also quite different from that of **27**$_{Dis}$.

6-5-2 Frequency dependent ac magnetic susceptibility measurements

The difference between the magnetization dynamics of samples **27**$_{Cr}$ and **27**$_{Dis}$ shows up more clearly in the frequency-dependent plots of the magnetic susceptibility (Figure 6-21) rather than in the already discussed temperature-dependent plots of the ac magnetic susceptibility (Figure 6-16 and Figure 6-17).

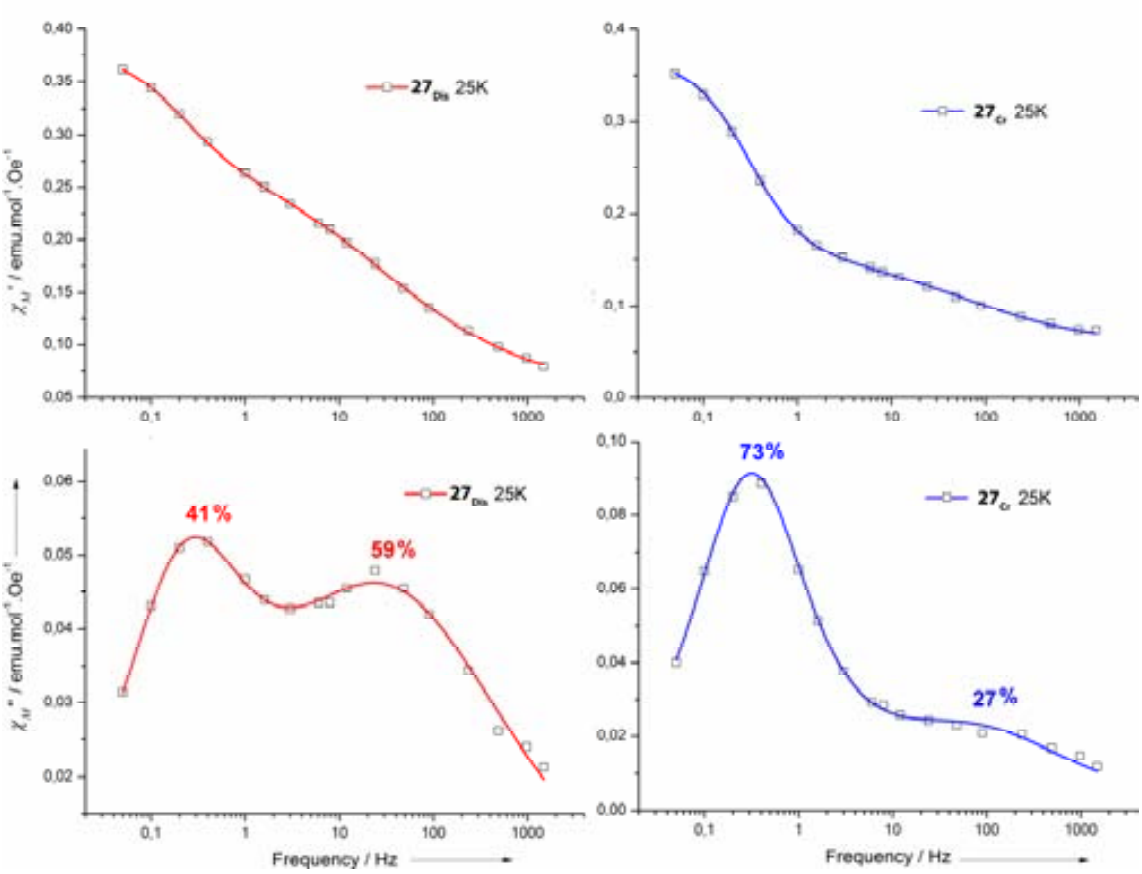

Figure 6-21. χ_M'(ν) (top) and χ_M''(ν) (bottom) graphs for samples **27**$_{Dis}$ (left) and **27**$_{Cr}$ (right). The solid lines are the best fits to the Cole-Cole model, and the percentage given on each peak correspond to the fraction of fast and slow relaxing species.

As a matter of example, while at 25 K the crystalline sample **27**$_{Cr}$ shows mainly one peak centered at 0.3 Hz in the χ_M'' vs. ν plot, the disordered sample **27**$_{Dis}$ clearly shows two peaks centered at 0.3 and 40 Hz. This striking difference evidences the coexistence

of two different magnetic relaxation processes, meaning that the sample behaves magnetically as a mixture of two different entities or species showing different relaxation rates. Since changes in the chemical composition can be ruled out, the nature of these slow and fast relaxing species must be associated with different molecular conformations or supramolecular arrangements. These structural changes can modify the anisotropy parameters and the intermolecular dipolar interactions, both of which may play a role in determining the magnetic relaxation rates. Deciding which of these two effects dominates requires a more detailed and quantitative analysis of the magnetic data, which we describe in what follows.

The χ_M'(ν) and χ_M''(ν) curves at 25 K of all four samples **27$_{Dis}$**, **27$_{Cr}$**, **27$_{PO}$** and **27$_{CrField}$** were fitted as the weighted sum of two Cole-Cole functions: [32]

$$\chi'(\omega) = f\left(\chi_{S1} + (\chi_{T1} - \chi_{S1})\frac{1 + (\omega\tau_1)^{1-\alpha_1}\sin(\pi\alpha_1/2)}{1 + 2(\omega\tau_1)^{1-\alpha_1}\sin(\pi\alpha_1/2) + (\omega\tau_1)^{2-2\alpha_1}}\right)$$

$$+ (1-f)\left(\chi_{S2} + (\chi_{T2} - \chi_{S2})\frac{1 + (\omega\tau_2)^{1-\alpha_2}\sin(\pi\alpha_2/2)}{1 + 2(\omega\tau_2)^{1-\alpha_2}\sin(\pi\alpha_2/2) + (\omega\tau_2)^{2-2\alpha_2}}\right)$$

$$\chi''(\omega) = f\,(\chi_{T1} - \chi_{S1})\frac{(\omega\tau_1)^{1-\alpha_1}\cos(\pi\alpha_1/2)}{1 + 2(\omega\tau_1)^{1-\alpha_1}\sin(\pi\alpha_1/2) + (\omega\tau_1)^{2-2\alpha_1}}$$

$$+ (1-f)(\chi_{T2} - \chi_{S2})\frac{(\omega\tau_2)^{1-\alpha_2}\cos(\pi\alpha_2/2)}{1 + 2(\omega\tau_2)^{1-\alpha_2}\sin(\pi\alpha_2/2) + (\omega\tau_2)^{2-2\alpha_2}}$$

where $\omega = 2\pi\cdot\nu$, ν is the frequency of the oscillating magnetic field, τ_1 and τ_2 are respectively the relaxation times of the fast and slow relaxing magnetic species, f is the fraction of the fast relaxing species, and α_1 and α_2 are parameters accounting for the width of ac susceptibility peaks of both species (the smaller α, the sharper the peaks). Finally, the parameters χ_T and χ_S are the isothermal and adiabatic limit susceptibilities. When $\omega\tau << 1$, $\chi = \chi_T$ and when $\omega\tau >> 1$, $\chi = \chi_S$. The fitting was made iteratively for χ_M'(ν) and χ_M''(ν) until reaching the best parameters fitting both χ_M'(ν) and χ_M''(ν).

In order to check the reproducibility of the obtained results on species showing different relaxations, we submitted the sample to the same thermal treatments after one

[32] K. S. Cole and R. H. Cole, *J. Chem. Phys.* **1941**, *9*, 341-351.

year. The new data proved to be nearly identical to the first set (see Figure 6-22), confirming a complete reproducibility.

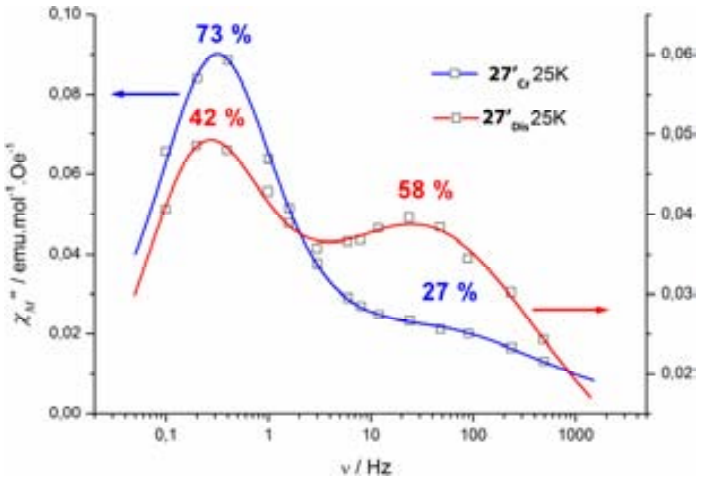

Figure 6-22. χ_M''(ν) for the sample **27$_{Dis}$** (squares) and **27$_{Cr}$** (circles) prepared again after one year. The solid lines are the best fits to the Cole-Cole model.

Similar fits were made for the χ_M'(ν) and χ_M''(ν) curves of samples **27$_{Dis}$** and **27$_{Cr}$** at seven different temperatures in the range of 5-30 K, obtaining analogous results, which reveals that the fraction of fast and slow relaxing species is independent of temperature in the range of study (see Figure 6-23) but is strongly dependent on the thermal history of the samples which control the supramolecular structure of the sample.

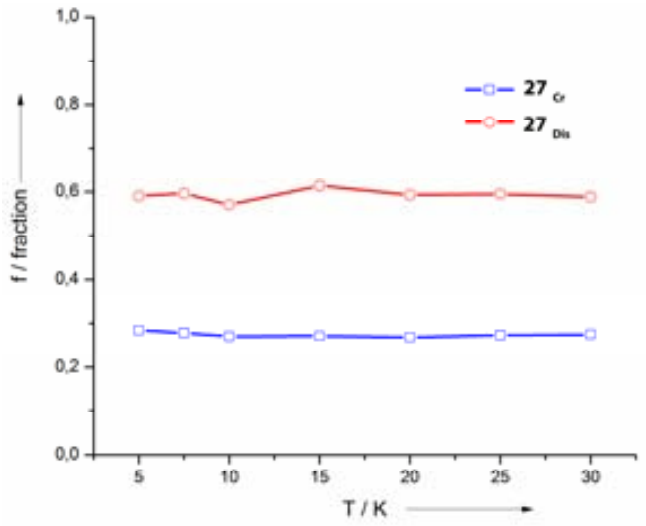

Figure 6-23. Fraction of the fast relaxing species, as a function of temperature for samples **27$_{Dis}$** (circles) and **27$_{Cr}$** (squares)

In fact, the fraction of the slow relaxing species at 25 K is almost doubled, changing from 41% to 73%, by switching from $\mathbf{27_{Dis}}$ to $\mathbf{27_{Cr}}$ (Figure 6-21), which indicates that this species is more abundant in the ordered state.

The same kind of analysis of the magnetic data was made for sample $\mathbf{27_{PO}}$, revealing that the ratio of fast relaxing species at 25 K in this partially ordered sample dropped increased even higher than in the disordered sample $\mathbf{27_{Dis}}$ to a value of 68% (see Figure 6-24). This result shed more light on the influence of the structural features, like different molecular conformations or supramolecular arrangements, on the relative abundance of the different relaxing species.

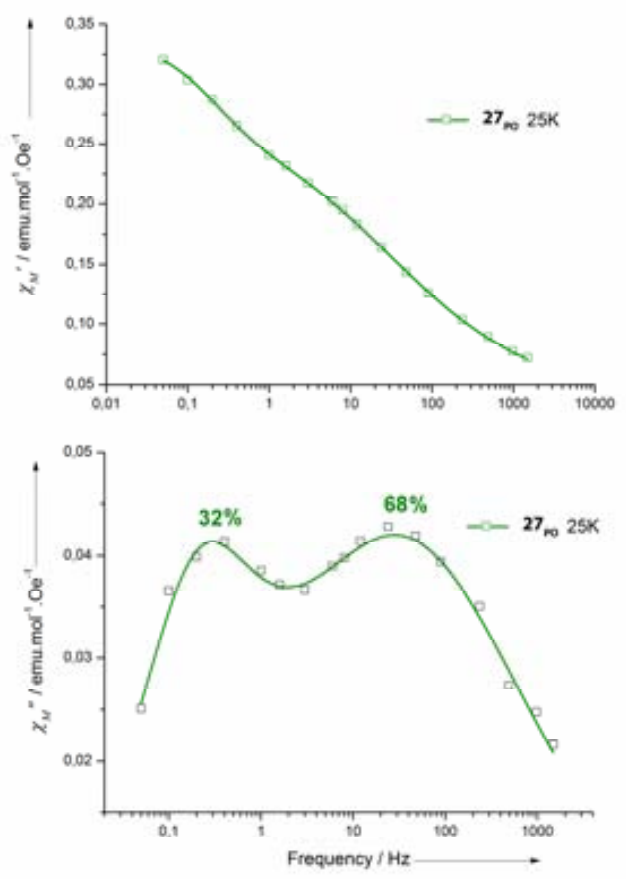

Figure 6-24. χ_M'(ν) (top) and χ_M''(ν) (bottom) for sample $\mathbf{27_{PO}}$. The solid lines are the best fits to the Cole-Cole model.

A deeper insight into the nature of the two species, and thus also on the origin of the differences in the relaxation rates, is provided by a detailed analysis of the temperature dependence of the relaxation times of the two species, τ_1 and τ_2, which are plotted in Figure 6-25, as a function of the reciprocal temperature. The relaxation times τ_1 and τ_2

of the two species are extracted from the fitting of the χ_M''(ν) plots while additional values of τ can be obtained from the maxima of the χ_M''(T) plots.

The analysis of the data for the two species found in both samples **27$_{Cr}$** and **27$_{Dis}$**, show that at high temperatures (T > 30 K) log(τ_2) is proportional to 1/T, which means that a thermally activated Orbach relaxation mechanism dominates. It is important to notice that, in this temperature range, the relaxation rates of the two species tend to merge.

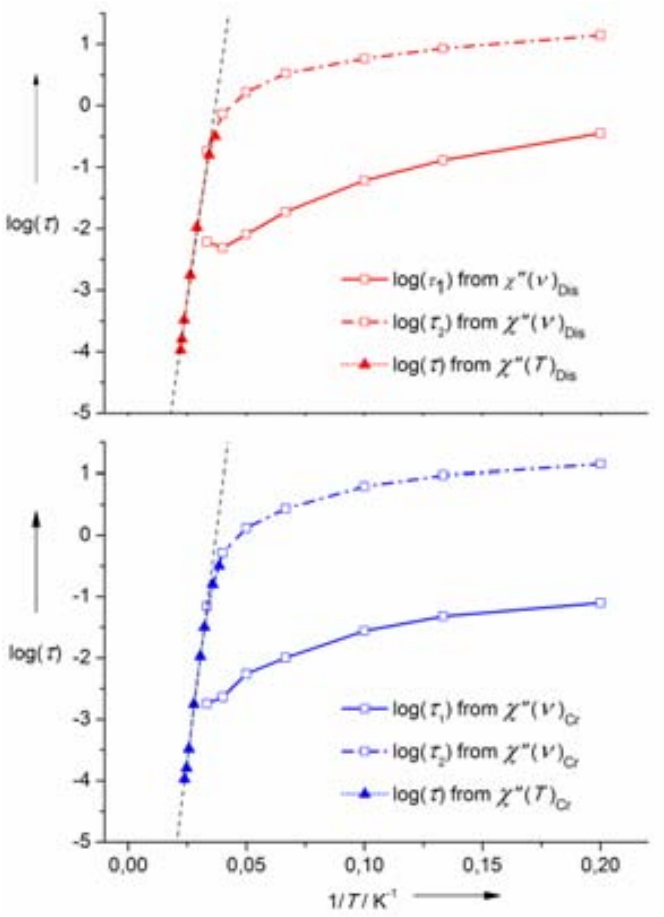

Figure 6-25. log(τ_1) and log(τ_2) (empty squares), obtained from χ_M''(ν), and of log(τ) (full triangles), obtained from χ''(T), as a function of 1/T, for samples **27$_{Dis}$** (top) and **27$_{Cr}$** (bottom). τ_1 and τ_2 are the relaxation times of the fast and slow relaxing species, respectively.

In fact, we only observe a single peak in the χ_M" vs. T characteristics, albeit broadened in the case of the amorphous sample (see Figure 6-17). The merging of the relaxation rates at higher temperatures suggests that the diagonal anisotropy terms, which largely determine the zero-field splitting and therefore also the activation energy of this process, are rather similar in the two species.

The Arrhenius analysis at high temperature gives an activation barrier Δ_{obs} = 4.80×10^2 cm^{-1} for sample **27$_{Cr}$** and Δ_{obs} = 4.22×10^2 cm^{-1} for sample **27$_{Dis}$**, which are in agreement with previously reported barrier heights for unsubstituted neutral terbium double-decker phthalocyanine complexes (see Table 6-2). [33]

Table 6-2. Comparison of barrier heights and pre-exponential factors obtained by the Arrhenius analysis of samples **27$_{Cr}$** and **27$_{Dis}$** together with literature data for standard $[Pc_2Tb]^0$

Samples	Δ_{obs} (cm^{-1})	τ_0^{-1} (s^{-1})
27$_{Cr}$	4.80×10^2	1.44×10^{11}
27$_{Dis}$	4.22×10^2	5.85×10^9
$[Pc_2Tb]^{0[33]}$	4.10×10^2	6.80×10^8

Below 30 K, the relaxation rates become weakly dependent on T, following more specifically a dependency like $\tau_2 \propto T^{-1}$ (see Figure 6-26).

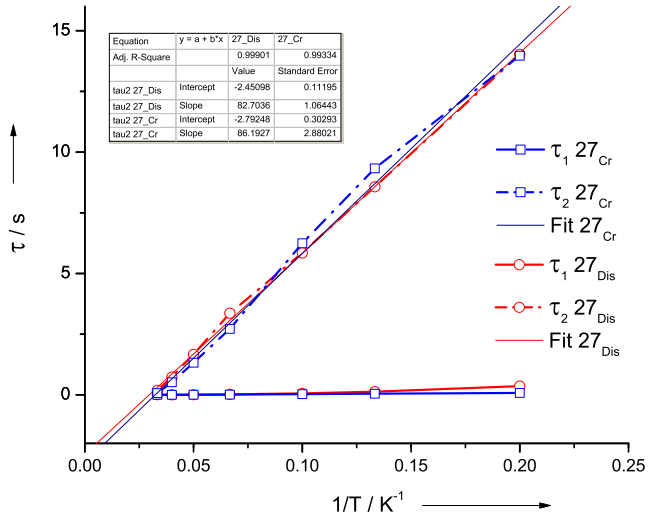

Figure 6-26. Linear plots of the fitted parameters τ_1 and τ_2 as a function of 1/T for samples **27$_{Dis}$** (circles) and **27$_{Cr}$** (squares) for 5 K < T < 30 K. In this range of temperature, τ_2 (dashed line) is clearly linear in 1/T which demonstrates the predominance of the direct phonon-induced tunneling process.

[33] N. Ishikawa, M. Sugita, T. Ishikawa, S.-y. Koshihara and Y. Kaizu, *J. Phys. Chem. B* **2004**, *108*, 11265-11271.

This behavior puts in evidence a crossover from the thermally activated Orbach mechanism, predominant at high temperature, to a direct or phonon-induced tunneling process taking over for T < 30 K. A crucial observation is that the relaxation times of the two species diverge dramatically in the low temperature (or tunneling) regime, where τ_1 becomes two orders of magnitude shorter than τ_2 (see Figure 6-25). It is important to notice that the tunneling rates measured for the slow relaxing species τ_2 for both samples **27**$_{Cr}$ and **27**$_{Dis}$ are the same, within experimental uncertainties.

Summarizing our observations, we can state that the anisotropy energy barriers of the two magnetic species are rather close to each other, but the probabilities of crossing these barriers by tunneling are very different. This strongly suggests that the nature of the fast relaxing species is associated with a lower molecular symmetry or, equivalently, a distorted molecule, and that the slow relaxing species must correspond to a well-defined molecular structure with the minimum allowed distortion from a pure axial symmetry. This hypothesis is supported by the sharp distribution, i.e. small α_2, of relaxation rates observed for the slow relaxing species, and the broader distribution, i.e. with larger α_1 values, observed for the faster ones in both samples (see Figure 6-27).

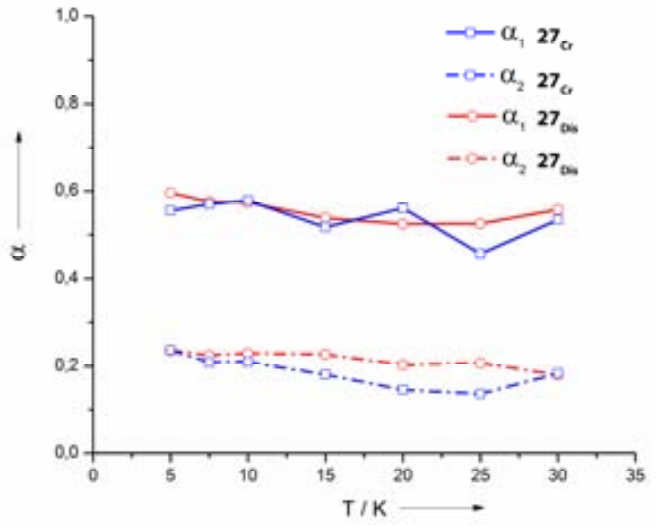

Figure 6-27. Fitted broadness parameters α_1 and α_2 of the fast and slow relaxing species, respectively, as a function of temperature for samples **27**$_{Dis}$ (circles) and **27**$_{Cr}$ (squares)

Another interesting result is found with the equilibrium susceptibilities of samples **27**$_{Dis}$ and **27**$_{Cr}$ measured above the blocking temperature at 90 Hz, which corresponds to the temperature of the peak in $\chi_M''(T)$ at the observed frequency. Plotting $1/\chi'_M$ vs. T

for both samples gave identical Curie constants of 0.104 ± 0.1 mol.emu^{-1}.K^{-1}, within experimental uncertainties, irrespective of the thermal history (see Figure 6-28). However, the Weiss temperature of the amorphous sample **27$_{Dis}$** was of 0.69 K, which is somewhat smaller than that of the crystalline sample **27$_{Cr}$** (θ = 2.1 K). This observation shows that the macroscopic average orientation of the anisotropy axes is not modified by the cooling procedure and that the average strength of intermolecular magnetic interactions depends on the thermal treatment. This is not completely unexpected, since dipolar interactions, with their long-range character, are sensitive to changes in parameters such as the intermolecular distances and the symmetry of the crystal structure.

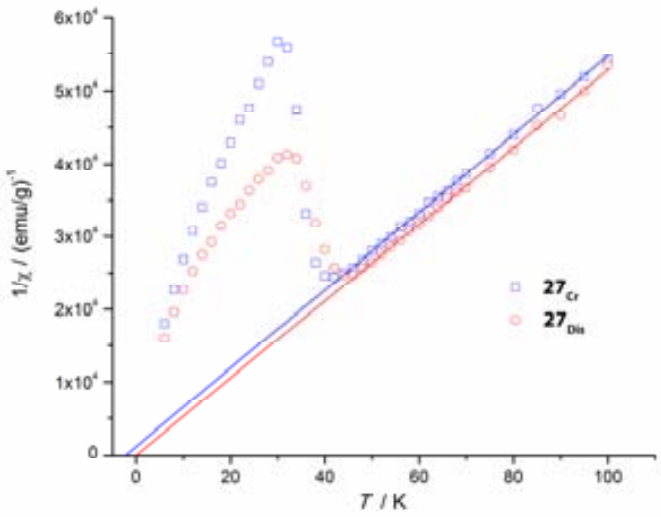

Figure 6-28. Comparison of the Curie-Weiss fits made for the equilibrium susceptibilities measured above the blocking temperatures at 90 Hz of samples **27$_{Cr}$** and **27$_{Dis}$**.

The weakening of magnetic dipolar interactions in the case of the amorphous sample **27$_{Dis}$** might, in principle, also lead to a faster tunneling, as it was experimentally observed, since this quantum phenomenon is suppressed by bias magnetic fields that detune spin-up and spin-down states. There is, however, a method to experimentally discriminate the relative effects of dipolar magnetic fields and molecular distortions. The effect of dipolar fields should be erased when the sample is submitted to external magnetic fields stronger than these typical dipolar fields that are typically of the order of a few 100 Oe. Ac magnetic susceptibility vs. H experiments, show that the dynamical magnetic responses of the two samples remain substantially different at any field (see Figure 6-29).

These experiments provide then solid arguments supporting the hypothesis that the two relaxation processes are mainly associated with different molecular distortions. More specifically, nearly undistorted molecules would be associated with the slow relaxing species, dominant in the crystalline material, while molecules distorted along the plane perpendicular to the magnetic easy axis constitute the fast relaxing species, which become dominant when the sample is quenched from the liquid state or the mesophase.

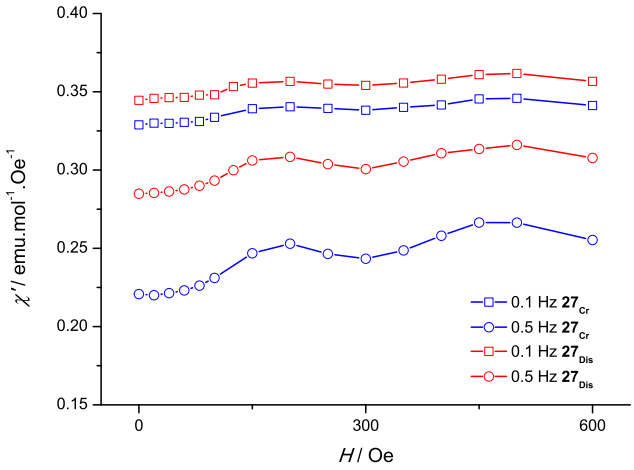

Figure 6-29. Real components of the ac magnetic susceptibility of samples $\mathbf{27_{Dis}}$ and $\mathbf{27_{Cr}}$, measured at 25 K, at 0.1 and 0.5 Hz as a function of DC magnetic field. The plot shows that, at any frequency and at all fields below 600 Oe, the molecular spins are farther from equilibrium in the $\mathbf{27_{Cr}}$ sample than they are in the $\mathbf{27_{Dis}}$ sample.

The big difference between τ_1 and τ_2 must then be associated with differences in the molecular conformation. Tunneling rates are determined by the intensity and symmetry of the off-diagonal anisotropy terms present in the spin Hamiltonian which, in its turn, reflect the local molecular symmetry and are, for this reason, extremely sensitive to even very weak distortions in the plane perpendicular to the easy magnetic axis. [34, 35]

[34] A. Cornia, L. Gregoli, C. Danieli, A. Caneschi, R. Sessoli, L. Sorace, A.-L. Barra and W. Wernsdorfer, *Inorg. Chim. Acta* **2008**, *361*, 3481-3488.

[35] M. Evangelisti, F. Luis, F. L. Mettes, N. Aliaga, G. Aromí, J. J. Alonso, G. Christou and L. J. de Jongh, *Phys. Rev. Lett.* **2004**, *93*, 117202.

While the coexistence of two different relaxation processes is a common feature in some SMMs,[28, 36] it is the first time that this phenomenon is observed in lanthanide double-decker complexes, and it is the only system, to date, in which the ratio between these responses has been shown to be reversibly modified via simple thermal treatments.

To conclude, we have shown the important influence that the structural environment of a single molecule magnet has on its dynamic magnetic behavior, taking advantage of the phase behavior of the complex. A reversible change of the magnetic properties was achieved by simple heating and cooling cycles.

Here, the absence of compositional change was demonstrated by the reversibility of the process, putting in evidence the structural origin of the modification of the magnetic behavior, because of variations in the arrangement of the molecules. This discovery was made possible by the synthesis of a room temperature liquid crystalline molecular material whose phase behavior depends critically on the chiral substituents.

Now that the in-depth dynamic magnetic behavior of complex **27** has been elucidated, it opens-up some perspective towards performing magneto-chiral experiments with the chiral complex **27**.

[36] E. Terazzi, C. Bourgogne, R. Welter, J.-L. Gallani, D. Guillon, G. Rogez and B. Donnio, *Angew. Chem. Int. Ed.* **2008**, *47*, 490-495.

Bibliography

[1] C. Train, R. Gheorghe, V. Krstic, L.-M. Chamoreau, N. S. Ovanesyan, G. L. J. A. Rikken, M. Gruselle, M. Verdaguer, *Nat. Mater.* **2008**, *7*, 729-734.

[2] G. L. J. A. Rikken, E. Raupach, *Nature* **1997**, *390*, 493-494.

[3] G. L. J. A. Rikken, E. Raupach, *Nature* **2000**, *390*, 932-935.

[4] Y. Qiu, P. Chen, M. Liu, *Langmuir* **2008**, *24*, 7200-7207.

[5] P. P. Bose, M. G. B. Drew, A. K. Das, A. Banerjee, *Chem. Commun.* **2006**, 3196-3198.

[6] M. Linares, P. Iavicoli, K. Psychogyiopoulou, D. Beljonne, S. De Feyter, D. B. Amabilino, R. Lazzaroni, *Langmuir* **2008**, *24*, 9566-9574.

[7] P. Iavicoli, M. Linares, Á. Pérez del Pino, R. Lazzaroni, D. B. Amabilino, *Superlattices Microstruct.*, *44*, 556-562.

[8] P. Iavicoli, M. Simon-Sorbed, D. B. Amabilino, *New J. Chem.* **2009**, *33*, 358-365.

[9] S. Dong, H. Tian, D. Song, Z. Yang, D. Yan, Y. Geng, F. Wang, *Chem. Commun.* **2009**, 3086-3088.

[10] A. S. Klymchenko, J. Sleven, K. Binnemans, S. De Feyter, *Langmuir* **2006**, *22*, 723-728.

[11] F. Nekelson, H. Monobe, Y. Shimizu, *Mol. Cryst. Liq. Cryst.* **2007**, *479*, 205-211.

[12] F. Nekelson, H. Monobe, M. Shiro, Y. Shimizu, *J. Mater. Chem.* **2007**, *17*, 2607-2615.

[13] S. Sergeyev, E. Pouzet, O. Debever, J. Levin, J. Gierschner, J. Cornil, R. G. Aspe, Y. H. Geerts, *J. Mater. Chem.* **2007**, *17*, 1777-1784.

[14] Z. Belarbi, C. Sirlin, J. Simon, J. J. Andre, *J. Phys. Chem.* **1989**, *93*, 8105-8110.

[15] D. D. Diaz, T. Torres, R. Zentel, R. Davis, M. Brehmer, *Chem. Commun.* **2007**, 2369-2371.

[16] F. Nekelson, H. Monobe, Y. Shimizu, *Chem. Commun.* **2006**, 3874-3876.

[17] K. Binnemans, C. Gorller-Walrand, *Chem. Rev.* **2002**, *102*, 2303-2346.

[18] E. Gomar-Nadal, C. Rovira, D. B. Amabilino, *Tetrahedron* **2006**, *62*, 3370-3379.

[19] M. Kohn, *J. Am. Chem. Soc.* **1951**, *73*, 480.

[20] C. Piechocki, J. Simon, J.-J. Andre, D. Guillon, P. Petit, A. Skoulios, P. Weber, *Chem. Phys. Lett.* **1985**, *122*, 124-128.

[21] T. Gross, F. Chevalier, J. S. Lindsey, *Inorg. Chem.* **2001**, *40*, 4762-4774.

[22] A. De Cian, M. Moussavi, J. Fischer, R. Weiss, *Inorg. Chem.* **1985**, *24*, 3162-3167.

[23] J. Jiang, D. K. P. Ng, *Acc. Chem. Res.* **2009**, *42*, 79-88.

[24] N. Ishikawa, *J. Porphyrins Phthalocyanines* **2001**, *5*, 87-101.

[25] K. Ban, K. Nishizawa, K. Ohta, A. M. van de Craats, J. M. Warman, I. Yamamoto, H. Shirai, *J. Mater. Chem.* **2001**, *11*, 321-331.

[26] K. Binnemans, J. Sleven, S. De Feyter, F. C. De Schryver, B. Donnio, D. Guillon, *Chem. Mater.* **2003**, *15*, 3930-3938.

[27] A. G. Gurek, T. Basova, D. Luneau, C. Lebrun, E. Koltsov, A. K. Hassan, V. Ahsen, *Inorg. Chem.* **2006**, *45*, 1667-1676.

[28] S. M. J. Aubin, Z. Sun, H. J. Eppley, E. M. Rumberger, I. A. Guzei, K. Folting, P. K. Gantzel, A. L. Rheingold, G. Christou, D. N. Hendrickson, *Inorg. Chem.* **2001**, *40*, 2127-2146.

[29] N. Ishikawa, M. Sugita, W. Wernsdorfer, *Angew. Chem. Int. Ed.* **2005**, *44*, 2931-2935.
[30] F. Branzoli, P. Carretta, M. Filibian, G. Zoppellaro, M. J. Graf, J. R. Galan-Mascaros, O. Fuhr, S. Brink, M. Ruben, *J. Am. Chem. Soc.* **2009**, *131*, 4387-4396.
[31] N. Ishikawa, M. Sugita, N. Tanaka, T. Ishikawa, S.-y. Koshihara, Y. Kaizu, *Inorg. Chem.* **2004**, *43*, 5498-5500.
[32] K. S. Cole, R. H. Cole, *J. Chem. Phys.* **1941**, *9*, 341-351.
[33] N. Ishikawa, M. Sugita, T. Ishikawa, S.-y. Koshihara, Y. Kaizu, *J. Phys. Chem. B* **2004**, *108*, 11265-11271.
[34] A. Cornia, L. Gregoli, C. Danieli, A. Caneschi, R. Sessoli, L. Sorace, A.-L. Barra, W. Wernsdorfer, *Inorg. Chim. Acta* **2008**, *361*, 3481-3488.
[35] M. Evangelisti, F. Luis, F. L. Mettes, N. Aliaga, G. Aromí, J. J. Alonso, G. Christou, L. J. de Jongh, *Phys. Rev. Lett.* **2004**, *93*, 117202.
[36] E. Terazzi, C. Bourgogne, R. Welter, J.-L. Gallani, D. Guillon, G. Rogez, B. Donnio, *Angew. Chem. Int. Ed.* **2008**, *47*, 490-495.

CHAPTER 7

EXPERIMENTAL

7-1 Techniques and instruments

Nuclear Magnetic Resonance spectroscopy (NMR)

NMR spectra were recorded at the Servei de Ressonància Magnètica Nuclear of the Universitat Autònoma de Barcelona on the following spectrometers: Bruker Avance 250 MHz, 360MHz and 400 MHz spectrometers as specified. The solvent residual peak was used to calibrate the spectra using literature reference δ ppm values. [1]

Ultraviolet-visible absorption spectroscopy (UV-Vis)

UV-Vis absorption spectra were collected on a Varian Cary 5000 spectrometer, at one data point every 0.66 nm and measured at a scanning rate of 1200 $nm.min^{-1}$.

UV-Vis Spectroelectrochemistry

The UV/vis spectroelectrochemical experiments were carried out with an optically transparent electrochemical (OTE) cell (modified quartz cuvette, optical pathlength: 0.5 mm). [2] A three-electrode configuration, consisting a Pt/Rh gauze working electrode, a Pt wire secondary electrode (in a fritted PTFE sleeve) and a saturated calomel electrode, chemically isolated from the test solution via bridge tube containing electrolyte solution and terminated in a porous frit, was used in the cell. The potential at the working electrode was controlled by a Sycopel Scientific Ltd. DD10M potentiostat. The UV/vis spectra were recorded on a Perkin Elmer Lambda 16 spectrophotometer at the University of Nottingham.

Circular Dichroism spectroscopy (CD)

CD data were recorded on a Jasco J275 spectropolarimeter at room temperature without using any thermostat. The solvent spectrum was substracted from the solution spectra, and the processing was done with the standard JASCO software.

---

[1] H. E. Gottlieb, V. Kotlyar and A. Nudelman, *J. Org. Chem.* **1997**, *62*, 7512-7515.

[2] S. A. Macgregor, E. McInnes, R. J. Sorbie and L. J. Yellowlees, Molecular Electrochemistry of Inorganic, Bioinorganic and Organometallic Compounds, Kluwer Academic Publishers, **1993**.

Infrared absorption spectroscopy (IR)

Infrared spectra were recorded on a Perkin Elmer Spectrum One Fourier Transform spectrometer, using NaCl plates for the characterization of oily compounds and attenuated total reflection (ATR) mode for solid and waxy compounds.

Small Angle X-ray Scattering spectroscopy (SAXS):

Small Angle X-ray Scattering data were recorded using a S3 MICRO instrument (Hecus X-ray Systems, Graz, Austria) with point beam focalization at the IIQAB (Barcelona) with Dr. Jordi Esquena.

Differential Scanning Calorimetry (DSC):

The phase transition temperatures enthalpies and entropies were measured by Differential Scanning Calorimetry on a Mettler-Toledo DSC-822e/400 calorimeter.

Cyclic Voltammetry (CV)

Cyclic voltammetric studies were carried out using an Autolab PGSTAT20 potentiostat. Standard cyclic voltammetry was carried out under an atmosphere of argon using a three-electrode arrangement in a single compartment cell. A glassy carbon working electrode, a Pt wire secondary electrode and a saturated calomel reference electrode, chemically isolated from the test solution via a bridge tube containing electrolyte solution and fitted with a porous Vycor frit, were used in the cell. Compensation for internal resistance was not applied.

Laser Desorption Ionization – Time of Flight Mass Spectrometry (LDI-TOF MS)

Mass spectra were recorded on a Bruker Ultraflex LDI-TOF spectrometer.

Polarizing Optical Microscopy

Polarized Optical Micrographs were recorded with an Olympus DP20 camera on an Olympus BX51 microscope. The temperature was controlled by a Linkam Scientific TMS94 control unit.

7-2 Reactants and chromatography

Reagents and starting materials were used as otbained from SDS, Fluka, Aldrich and Merck. Size exclusion chromatography were done using swollen biobeads media from Bio-Rad and silica gel column chromatography was done using Silica gel 60 (35-70 mesh) from SDS.

7-3 Synthesis and characterization

4,5-Dibromocatechol (1) [3]

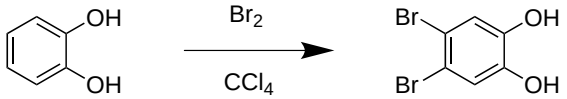

1

In a 500mL three neck round bottom flask under nitrogen, equipped with a reflux condenser, an addition funnel and a gas outlet connected to a bubbler filled with a 10% NaOH aqueous solution, was suspended catechol (136 mmol, 15.0 g, 1 eq.) in CCl_4 (150 mL). Bromine (272 mmol, 43.5 g, 2 eq.) diluted in CCl_4 (20mL) was added dropwise at 0 °C over 4.5 h. The excess of bromine was neutralized with aqueous $NaHSO_3$ (150 mL, 40% solution). The mixture was filtrated and the solids were dissolved in CCl_4, washed with water and dried in vacuum. The obtained 4,5-dibromocatechol **1** (30.2 g) was then recrystallized from $CHCl_3$ (220 mL) to afford a white crystalline solid (22.5 g, 62%).

M.W.: 267.9 $g.mol^{-1}$. **m.p.:** 126 ºC. **FT-IR:** 3600 (s), 3216 (s), 1605 (m), 1503 (s), 1419 (s), 1326 (s), 1270 (s), 1228 (s), 1209 (s), 1181 (s), 1101 (m), 911 (w), 871 (m), 846 (w), 806 (m), 679 (m), 646 (s), 635 (s), 605 (m), 526 (w) cm^{-1}. **^{1}H NMR** (250 MHz, *$CDCl_3$*): δ 7.14 (s, 2 H, Ar-**H**), 5.43 (s, 2 H, **-OH**) ppm. **^{13}C NMR** (63 MHz, $CDCl_3$) δ 143.63, 120.07, 115.02 ppm.

[3] M. Kohn, *J. Am. Chem. Soc.* **1951**, *73*, 480.

1,2-Dibromo-4,5-bispentadecyloxybenzene (2) [4]

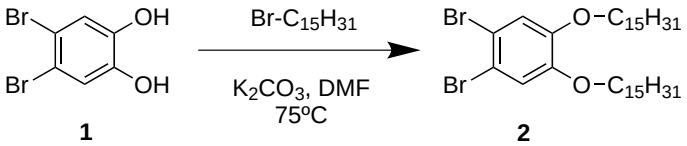

1 2

To a suspension of dry K_2CO_3 (93 mmol, 12.9 g, 5 eq.) in dry DMF distilled over CaH_2 (100 mL) was added 4,5-dibromocatechol **1** (18.7 mmol, 5.0 g, 1 eq.). The mixture was stirred at 40 ºC for 15 minutes before addition of 1-bromo-pentadecane (37.3 mmol, 10.9 g, 2 eq.). The reaction mixture was then stirred at 75 ºC overnight. Water (200 mL) was added to precipitate the reaction product. After filtration, the solids were dissolved in DCM, dried over $MgSO_4$ and the solvent evaporated. The residue was purified by column chromatography of silica gel using toluene as an eluent. 1,2-Dibromo-4,5-bispentadecyloxybenzene **2** was obtained as a white crystalline solid (11.0 g, 86%).

M.W.: 688.7 g.mol^{-1}. **FT-IR:** 2950 (m), 2917 (s), 2849 (s), 1585 (w), 1500 (s), 1481 (m), 1471 (s) 1398 (w), 1384 (w), 1354 (m), 1319 (w), 1250 (s), 1201 (s), 1151 (w), 1118 (w), 1059 (w), 1027 (w), 1010 (w), 978 (w), 946 (w), 896 (w), 859 (m), 853 (w), 812 (w), 784 (w), 758 (w), 718 (s), 668 (w), 649 (m), 628 (w) cm^{-1}. **^{1}H NMR** (250 MHz, $CDCl_3$): δ 7.06 (s, 2 H, Ar-**H**), 3.94 (t, *J* = 6.7 Hz, 4 H, -O-**CH_2**-), 1.80 (m, 4 H, -O-CH_2-**CH_2**-), 1.26 (m, 48 H, , -O-CH_2-CH_2-**$(CH_2)_{12}$**-), 0.88 (t, *J* = 6.8 Hz, 6 H, **$-CH_3$**) ppm. **^{13}C NMR** (63 MHz, $CDCl_3$) δ 149.21, 118.21, 114.82, 69.79, 32.09, 29.88, 29.53, 29.50, 29.21, 26.09, 22.86, 14.28.

1,2-Dibromo-4,5-bisdocosyloxybenzene (3) [4]

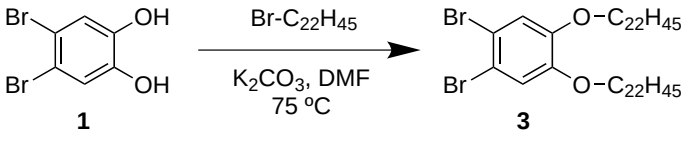

1 3

To a suspension of dry K_2CO_3 (41.0 mmol, 5.66 g, 2.2 eq.) in dry DMF distilled over CaH_2(200 mL) was added 4,5-dibromocatechol **1** (18.7 mmol, 5.00 g, 1 eq.). The mixture was stirred at 40 ºC for 15 minutes before addition of docosyl bromide (37.5

[4] K. Binnemans, J. Sleven, S. De Feyter, F. C. De Schryver, B. Donnio and D. Guillon, *Chem. Mater.* **2003**, *15*, 3930-3938.

mmol, 14.6 g, 2 eq.). The reaction mixture was then stirred at 75 ºC during 60 h. The cooled reaction mixture was filtered a 4 ºC and washed with cold DMF (150 mL). The solids were extracted from water with DCM (500 mL). The organic layer and undissolved solids were cooled at 4 ºC and filtered. The obtained 1,2-dibromo-4,5-bisdocosyloxybenzene **3** was washed with diethyl ether (200 mL) affording a beige solid (13.6 g, 82%).

M.W.: 885.1 g.mol^{-1}. **m.p.:** 82 ºC. **FT-IR:** 2956 (m), 2917 (s), 2849 (s), 1584 (w), 1497 (s), 1472 (s), 1448 (m), 1396 (w), 1353 (m), 1327 (w), 1251 (s), 1199 (s), 1119 (w), 1077 (w), 1062 (w), 1045 (w), 1027 (w), 988 (w), 966 (w), 920 (w), 889 (w), 877 (w), 858 (m), 834 (w), 816 (w), 797 (w), 717 (m), 650 (w), 638 (w) cm^{-1}. **^{1}H NMR** (250 MHz, *$CDCl_3$*): δ ppm 7.04 (s, 2 H, Ar-**H**), 3.62 (t, *J* = 7.2 Hz, 4 H, -O-**CH_2**-), 1.30 (quint, 4 H, -O-CH_2-**CH_2**-), 0.68 (s, 76 H, -O-CH_2-CH_2-**$(CH_2)_{19}$**-), 0.27 (t, *J* = 7.1 Hz, 6 H, -**CH_3**) ppm. **^{13}C NMR** (63 MHz, $CDCl_3$) δ 149.21, 118.21, 114.82, 69.79, 32.09, 29.88, 29.53, 29.50, 29.21, 26.09, 22.86, 14.28.

1,2-Dicyano-4,5-bispentadecyloxybenzene (7)

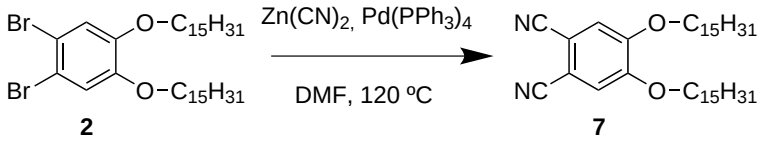

2 **7**

In a 50mL round bottom flask under argon were dissolved of 1,2-dibromo-4,5-bispentadecyloxybenzene **2** (8.71 mmol, 6.0 g, 1.0 eq.), zinc cyanide (10.5 mmol, 1.23 g, 1.2 eq.) and tetrakis-triphenylphosphinepalladium (0) (0.87 mmol, 1.01 g, 0.1 eq.) in DMF (16.5 ml). The mixture was stirred at 120 °C for 2 h after which ammonia (37%, 100 mL) was added, and the resulting precipitate was filtrated, washed with more ammonia (100 mL) and purified by column chromatography of silica gel using toluene as an eluent, affording 1,2-dicyano-4,5-bispentadecyloxybenzene **7** (3.29 g, 65%) as a white solid.

M.W.: 580.9 g.mol^{-1}. **m.p.:** 106 ºC. **FT-IR:** 3127 (w), 3063 (w), 2957 (m), 2919 (s), 2849 (s), 2229 (m), 1763 (w), 1621 (w), 1591 (s), 1568 (m), 1528 (s), 1467 (s), 1415 (w), 1404 (w), 1393 (m), 1365 (m), 1298 (s), 1230 (s), 1217 (m), 1197 (w), 1090 (s), 1058 (w), 1040 (w), 1009 (w), 996 (w), 975 (w), 943 (w), 908 (w), 888 (m), 853 (w), 721 (m), 637 (w), 536 (m) cm^{-1}. **^{1}H NMR** (250 MHz, $CDCl_3$) δ 7.10 (s, 2 H, Ar-**H**),

4.04 (t, *J* = 6.7 Hz, 4 H, -O-**CH$_2$**-), 1.80 (m, 4 H,-O-CH$_2$-**CH$_2$**-), 1.25 (m, 48H), 0.88 (t, *J* = 6.6 Hz, 6 H, -**CH$_3$**) ppm. **^{13}C NMR** (63 MHz, $CDCl_3$) δ 164.51, 136.87, 134.19, 118.42, 114.40, 67.67, 31.72, 28.69, 25.86, 22.86, 14.33.

1,2-Dibromo-4,5-bisdocosyloxybenzene (8)

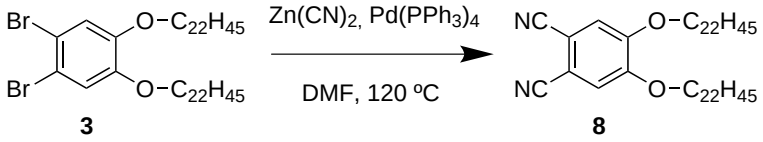

3 **8**

In a 5 mL round bottom flask under argon were dissolved 1,2-dibromo-4,5-bisdocosyloxybenzene **3** (0.64 mmol, 570 mg, 1.0 eq.), zinc cyanide (0.77 mmol, 91 mg, 1.2 eq.) and tetrakis-triphenylphosphinepalladium (0) (0.064 mmol, 74 mg, 0.1 eq.) in DMF (1.5 ml). The mixture was stirred at 120 °C for 2 h after which ammonia (37%, 5 mL) was added, and the resulting precipitate was filtrated, washed with more ammonia (20 mL) and water, and purified by column chromatography of silica gel using toluene as an eluent, affording 1,2-dicyano-4,5-bisdocosyyloxybenzene **8** (420 mg, 84%) as a white solid.

M.W.: 777.3 g.mol^{-1}. **m.p.:** 106 ºC. **FT-IR:** 2916 (s), 2849 (s), 2233 (m), 1591 (m), 1568 (m), 1526 (s), 1465 (s), 1393 (w), 1365 (s), 1297 (s), 1229 (s), 1216 (m), 1095 (m), 1029 (w), 984 (w), 962 (w), 937 (w), 893 (w), 720 (s) cm^{-1}. **^{1}H NMR** (250 MHz, $CDCl_3$): δ 7.10 (s, 2 H, Ar-**H**), 4.04 (t, *J*= 6.5 Hz, 4 H, -O-**CH$_2$**-), 1.85 (quint, *J* = 6.5 Hz, 4 H,-O-CH$_2$-**CH$_2$**-), 1.28 (m, 76 H, -O-CH$_2$-CH$_2$-(**CH$_2$)$_{19}$**-), 0 .88 (t, *J*=6.7 Hz, 6 H, -**CH$_3$**) ppm.

Octakis-pentadecyloxy-phthalocyanine (20) [7]

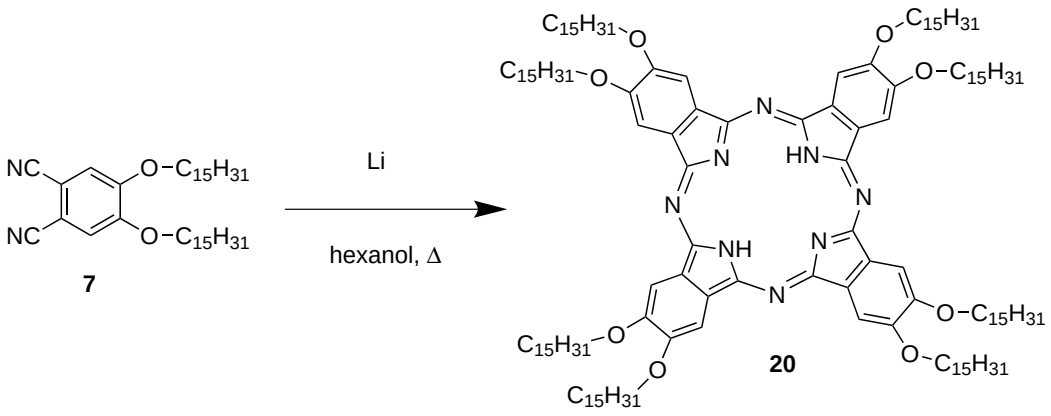

In a dry Schlenk was introduced 4,5-bis(pentadecyloxy)phthalonitrile **7** (0.172 mmol, 100 mg, 1 eq.). The Schlenk was evacuated and filled with argon three times. A freshly prepared 2 M solution of lithium in hexanol (0.408 mmol, 210 µL, 2.3 eq.) was added, and the mixture was heated at reflux temperature for 30 minutes. After that time glacial acetic acid (1mL) was added to neutralize the mixture and precipitate the free base phthalocyanine. The solids were filtered out and washed with more acetic acid (50 mL) and acetonitrile (20 mL). The title compound was obtained as a dark green solid (64 mg, 64%).

M.W.: 2325.7 g.mol^{-1}. **m.p.:** 189 ºC. **MS m/z:** 2323.0 (M^+). **FT-IR:** 2917 (s), 2850 (s), 1600 (m), 1493 (s), 1465 (s), 1376 (m), 1349 (m), 1278 (s), 1205 (m), 1045 (m), 852 (m), 720 (s) cm^{-1}. **^{1}H NMR** ($CDCl_3$): δ 8.58 (s, 8 H, Ar-**H**), 4.56 (m, 16 H, -O-**CH_2**-), 2.16 (m, 16 H, -O-CH_2-**CH_2**-), 1.74 (m, 16 H, -O-$(CH_2)_2$-**CH_2**-), 1.27 (m, 176 H, -O-$(CH_2)_3$-**$(CH_2)_{11}$**-), 0.88 (t, *J* = 6.7 Hz, 24 H, -**CH_3**) ppm. **UV-Vis** (log(ε)): 294 (4.63), 353 (4.70), 424 (4.41), 601 (4.24), 647 (4.51), 662 (4.82), 701 (4.91) nm. **Elemental Analysis (%):** Calculated C, 78.50; H, 11.18; N, 4.82. Found C, 77.00; H, 11.16; N, 4.31.

[7] R. P. Linstead and M. Whalley, *J. Chem. Soc.* **1952**, 4839-4846.

Octakis-docosyloxy-phthalocyanine (21) [7]

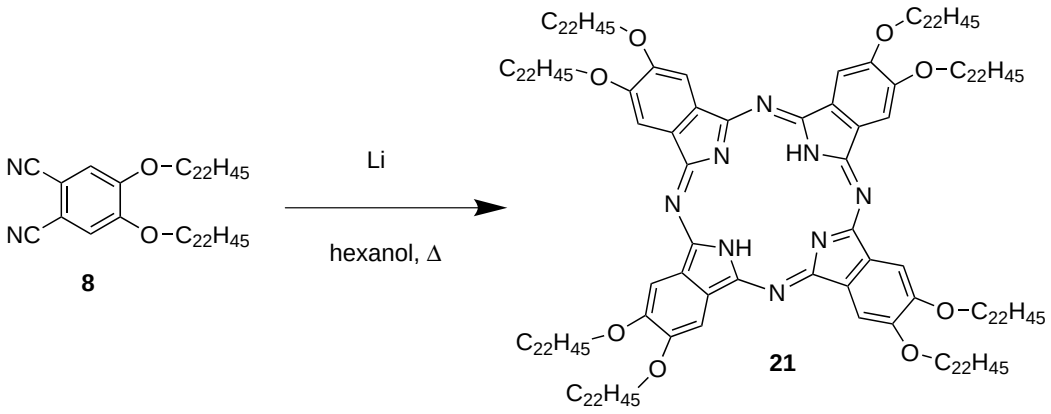

A fresh solution of lithium hexanolate was prepared by adding lithium (67 mg, 9.65 mmol, 15 eq.) to n-hexanol (4 mL) and warming up at 100 ºC for 2 h. 4,5-Bis(docosyloxy)phthalonitrile **8** (0.64 mmol, 500 mg, 1 eq.) was then introduced and the mixture was refluxed for 12 h. After that time glacial acetic acid was added (50 mL) to neutralize the mixture and precipitate the free base phthalocyanine. The solids were filtered out and washed with more acetic acid (50 mL) and acetonitrile (20 mL). The dark green residues were then crystallized three times from warm toluene and washed with DCM. The title compound was obtained as a dark green solid (273 mg, 54%).

M.W.: 3111.2 g.mol^{-1}. **MS m/z:** 3111.1 (M^+). **m.p.:** 195 ºC. **FT-IR:** 3299 (w), 2917 (s), 2850 (s), 1604 (m), 1491 (m), 1466 (s), 1420 (w), 1384 (m), 1330 (w), 1277 (s), 1201 (s), 1099 (m), 1046 (m), 1027 (m), 938 (w), 912 (w), 862 (w), 793 (w), 741 (m), 719 (s) cm^{-1}. **UV-Vis** (log(ε)): 701(4.92), 662(4.82), 646(4.48), 633(4.37), 600(4.13), 420(4.30), 354(4.65) nm.

Bis-(octakis-pentadecyloxy-phthalocyaninato) terbium(III) (25)

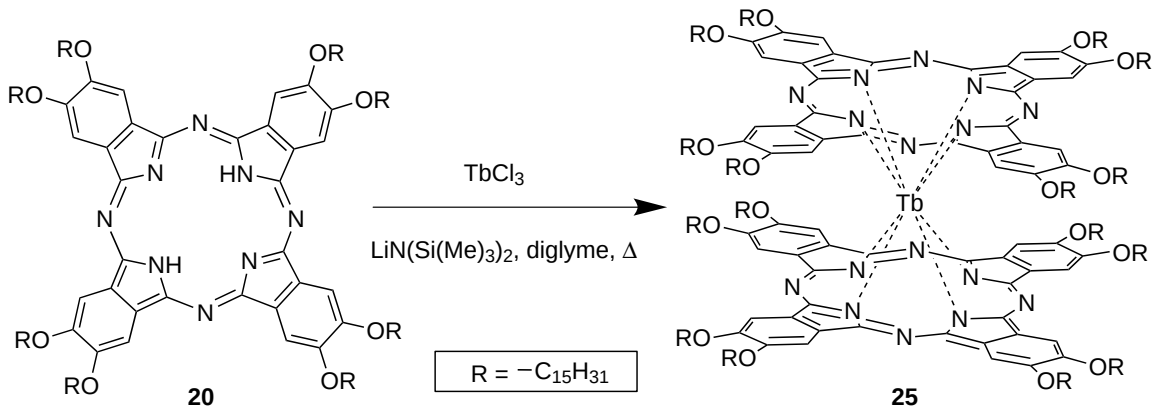

In a dry Schlenk tube under argon were introduced octakis-pentadecyloxy-phthalocyanine **20** (21 μmol, 50 mg, 2.0 eq.) and anhydrous terbium (III) chloride (12 μmol, 3.14 mg, 1.1 eq.). The solids were degassed for 10 minutes under vacuum, after which the mixture was cooled to 0 ºC with an ice bath. diglyme (2 mL) and N,N-bis(trimethylsilyl)lithium amide 1 M solution in THF (24 μmol, 23.6 μL, 2.2 eq.) were added with a syringe. The reaction was then stirred at 0 ºC for 1 h and refluxed for 2 h. After cooling down, methanol was added, and the dark green waxy residue was decanted and washed several times with warm methanol, it was then dissolved in hexane and the insoluble impurities were filtered out. After evaporation of the solvent, the residue was purified by repeated size exclusion chromatography (BioBeads SX1) using toluene as an eluent, affording a waxy dark green solid (38 mg, 74%).

M.W.: 4806.3 g.mol^{-1}. **m.p.:** 181 ºC. **MS m/z:** 4804 (M^+). **FT-IR:** 2916 (s), 2850 (s), 1601 (m), 1496 (m), 1453 (s), 1376 (s), 1318 (m), 1272 (s), 1195 (m), 1097 (w), 1078 (w), 1044 (m), 909 (w), 859 (m), 831 (w), 753 (m), 720 (m) cm^{-1}. **UV-Vis** (log(ε)): 292 (5.02), 335 (5.03), 369 (5.11), 471 (4.60), 576 (4.30), 601 (4.48), 662 (5.13) nm.

Bis-(octakis-docosyloxy-phthalocyaninato) terbium(III) (26)

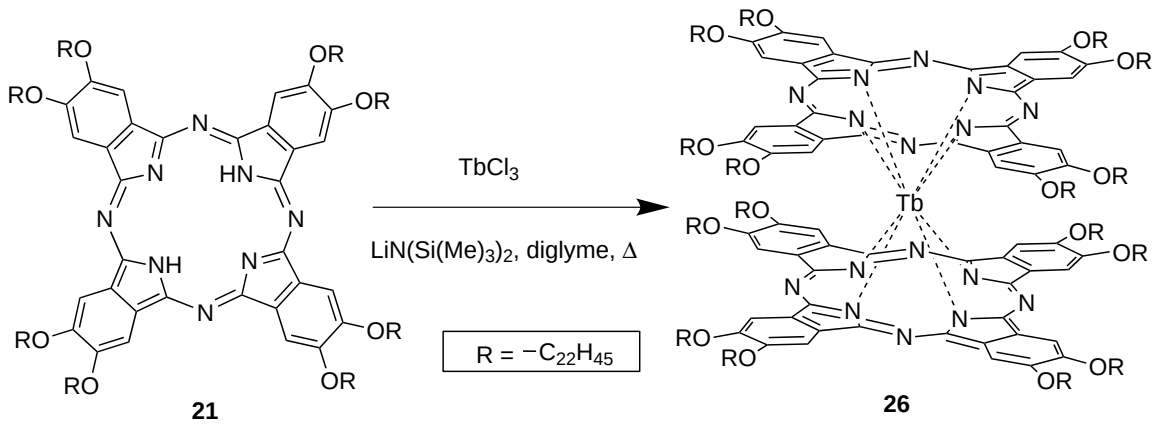

21 26

In a dry Schlenk tube under argon were introduced octakis-docosyloxy-phthalocyanine (32 μmol, 100 mg, 2.0 eq.) and anhydrous terbium (III) chloride (19 μmol, 5.12 mg, 1.2 eq.). The vessel was degassed for 10 minutes under vacuum, after which the mixture was cooled to 0 ºC with an ice bath. Diglyme (3.2 mL) and N,N-bis(trimethylsilyl)lithium amide 1 M solution in THF (39 μmol, 39 μL, 2.4 eq.) were added with a syringe. The reaction was then stirred at 0 ºC for 1 h and refluxed for 2 h. After cooling down, methanol was added, and the dark green waxy residue was decanted and washed several times with warm methanol, it was then dissolved in warm toluene and the insoluble impurities were filtered out. After evaporation of the solvent, the residue was purified by repeated size exclusion chromatography (BioBeads SX1) using toluene as an eluent, affording a waxy dark green solid (83 mg, 81%).

M.W.: 6377.3 g.mol^{-1}. **m.p.:** 124 ºC. **MS m/z:** 6371 (M^+). **FT-IR:** 2916 (s), 2850 (s), 1604 (w), 1496 (m), 1464 (s), 1378 (m), 1320 (w), 1275 (s), 1199 (m), 1079 (m), 1045 (m), 861 (w), 750 (m), 719 (s) cm^{-1}. **UV-Vis** (log(ε)): 663(5.05), 634(4.65), 601(4.58), 574(4.46), 474(4.63), 364(5.01), 336(5.09) nm. **Elemental Analysis (%):** Calculated C, 78.35; H, 11.63; N, 3.51. Found C, 78.39; H, 11.53; N, 3.39.

***(S)*-Methyl-2-dodecyloxypropanoate (31)** [5]

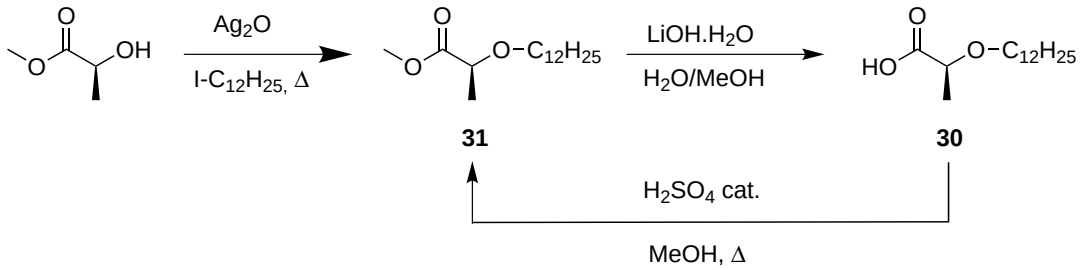

To a solution of *(-)*-methyl-L-lactate (9.1 g, 87 mmol, 1 eq.) and 1-iododododecane (60 g, 203 mmol, 2.3 eq.) was added silver (I) oxide (20 g, 87 mmol, 1 eq.). The mixture was sonicated for 10 min before refluxing for 24h in the dark. The resulting suspension was filtered through celite, washed with diethyl ether (3×200mL) and the solvent was removed under vacuum. To the remaining unpurified oil was added MeOH (300 mL), H_2O (120 mL) and LiOH.H_2O (11.7 g, 280 mmol, 3.2 eq.) and the mixture was stirred overnight at room temperature. After removal of the solvent in vacuum, aqueous NaOH (300 mL, 3.5%) was added and the mixture was extracted with diethyl ether (3×250 mL). The aqueous layer containing the chiral acid salt was then acidified with aqueous HCl and extracted with DCM (4×250mL). The organic layer was then dried over $MgSO_4$ and the solvent evaporated, to afford a yellow crude oil. The crude oil was purified by flash chromatography (hexane/AcOEt – 9/1) to afford the carboxylic acid **30** as a colorless oil (12 g, 53%).

M.W.: 258.4 g.mol^{-1}. **^{1}H NMR** ($CDCl_3$): δ 3.99 (q, *J* = 6.7 Hz, 1 H, HOOC-C(**H**)(CH_3)-), 3.52 (m, 2 H, -O-**CH_2**-), 1.61 (m, 2 H, -O-CH_2-**CH_2**-), 1.45 (d, *J* = 6.7 Hz, 3 H, HOOC-C(H)(**CH_3**)-), 1.26 (m, 18 H, -O-CH_2-CH_2-(**CH_2**)$_9$-), 0.88 (t, *J* = 6.6 Hz, 3 H, -**CH_3**) ppm.

A solution of *(S)*-2-Dodecyloxypropanoic acid **30** (12 g, 46 mmol, 1 eq.) and a catalytic amount sulphuric acid (ten drops) in MeOH (500 ml) was refluxed for 12 h. After this time, the mixture was cooled to room temperature and aqueous $NaHCO_3$ (100 mL, saturated solution) was added. The MeOH was evaporated and the aqueous phase was extracted with DCM (3×200 ml). The organic phase was washed with water (3×250 ml) and dried over $MgSO_4$, and the solvent evaporated. The remaining oil was purified

[5] E. Gomar-Nadal, C. Rovira and D. B. Amabilino, *Tetrahedron* **2006**, *62*, 3370-3379.

by flash chromatography using hexane–EtOAc [19/1] mixture as an eluent to obtain 10.2 g (81%) of a slightly yellow transparent oil characterized as **31.**

Overall Yield: 43%. **M.W.:** 272.4 g.mol^{-1}. $[\alpha]_{546}^{25}$ = –43.25 deg.cm^2.g^{-1}. **FT-IR:** 2923 (s), 2854 (s), 1757 (s), 1740 (s), 1457 (m), 1371 (w), 1272 (m), 1201 (m), 1146 (s), 1128 (s), 1075 (m), 982 (w), 843 (w), 754 (w), 722 (w), 667 (w) cm^{-1}. **^{1}H NMR** ($CDCl_3$): δ 3.96 (q, *J* = 6.7 Hz, 1 H, CH_3-OOC-C(**H**)(CH_3)-), 3.75 (s, 3 H, **CH_3**-OOC-C(H)(CH_3)-), 3.44 (m, 2 H, -O-**CH_2**-), 1.59 (m, 2 H, -O-CH_2-**CH_2**-), 1.40 (d, *J* = 6.7 Hz, 3 H, HOOC-C(H)(**CH_3**)-), 1.25 (m, 18 H, -O-CH_2-CH_2-(**CH_2**)$_9$-), 0.88 (t, *J* = 6.7 Hz, 3 H, -**CH_3**) ppm. **^{13}C NMR** (63 MHz, $CDCl_3$) δ 149.21, 118.21, 114.82, 69.79, 32.09, 29.88, 29.53, 29.50, 29.21, 26.09, 22.86, 14.28 ppm..

***(S)*-2-Dodecyloxypropan-1-ol (32)** [5]

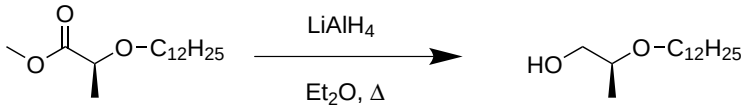

31 **32**

To a suspension of $LiAlH_4$ (1.67 g, 44 mmol) in dry diethyl ether (250 ml) was added drop-wise a solution of *(S)*-methyl-2-dodecyloxypropanoate **31** (10 g, 36.7 mmol) in dry diethyl ether (150 ml) over 15 min. The mixture was refluxed for 1 h. After this, the solution was cooled to 0ºC with an ice bath, and water was added dropwise to eliminate the remaining $LiAlH_4$. The reaction product was filtered from the white sludge. The sludge in the filter funnel was dissolved in sulphuric acid (aqueous, 20%) and the resulting solution was extracted with diethyl ether. The combined organic phases were dried over $MgSO_4$ and the solvent evaporated. The obtained oil was purified by flash chromatography using hexane-EtOAc [3/1] mixture as an eluent to obtain 7.03 g (78%) of a slightly yellow transparent oil characterized as **32**.

M.W.: 244.4 g.mol^{-1}. **^{1}H NMR** ($CDCl_3$): δ 3.65 (m, 5 H, HO-**CH_2**-C(**H**)(CH_3)-O-**CH_2**-), 1.57 (m, 2 H, -O-**CH_2**-CH_2-), 1.26 (m, 18 H, -O-CH_2-CH_2-(**CH_2**)$_9$-), 1.10 (d, *J* = 6.7 Hz, 3 H, HO-CH_2-C(H)(**CH_3**)-O-), 0.88 (t, *J* = 6.6 Hz, 3 H, - CH_2-**CH_3**) ppm.

***(S)*-2-Dodecyloxypropyl toluene-4-sulphonate (33)** [5]

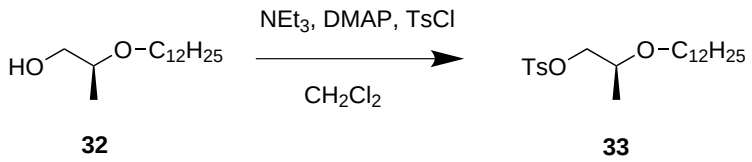

32 **33**

(S)-2-Dodecyloxypropan-1-ol **32** (29 mmol, 7.0 g, 1.0 eq.) was dissolved in DCM (500 ml) and cooled in an ice bath at 0ºC. Triethylamine (3.2 g, 31 mmol, 1.1 eq.) and dimethylaminopyridine (0.18 mg, 1.4 mmol, 0.5 eq.) were then added, followed by the addition of toluene-p-sulphonyl chloride (6.0 g, 31 mmol, 1.1 eq.) in small portions with constant stirring. The resulting solution was stirred overnight. Ice (250 g) and HCl (aqueous 10%, 400 ml) are added and the mixture was stirred until the ice was melted. The organic layer was washed with water (3×500 ml), dried over $MgSO_4$ and the solvent was evaporated. The remaining oil was purified by flash chromatography using hexane-DCM 1:2 mixture as an eluent to obtain 10.1 g (88%) of a slightly yellow transparent oil characterized as **33**.

M.W.: 398.6 g.mol^{-1}. **FT-IR:** 2925 (s), 2854 (s), 1919 (w), 1599 (m), 1496 (w), 1459 (m), 1365 (s), 1307 (w), 1292 (w), 1267 (w), 1210 (w), 1190 (s), 1178 (s), 1098 (s), 1020 (w), 988 (s), 830 (m), 814 (s), 792 (m), 738 (w), 706 (w), 667 (s), 625 (w), 576 (m), 555 (s) cm^{-1}. **^{1}H NMR** (250 MHz, $CDCl_3$): δ 7.80 (d, *J* = 8.2 Hz, 2 H, Ar-**H**), 7.34 (d, *J* = 8.0 Hz, 2 H, Ar-**H**), 4.10 (q, *J* = 7.2 Hz, 1 H, Ar-CH_2-C(**H**)(CH_3)-O-), 3.70-3.24 (m, 4 H, Ar-**CH_2**-C(H)(CH_3)-O-**CH_2**-), 2.45 (s, 3 H, **CH_3**-Ar-), 1.54 (m, 2 H, -O-CH_2-**CH_2**-), 1.25 (m, 18 H, -O-CH_2-CH_2-(**CH_2**)$_9$-), 1.10 (d, *J* = 6.0 Hz, 3 H, Ar-CH_2-C(H)(**CH_3**)-O-), 0.88 (t, *J* = 6.6 Hz, 3 H, -CH_2-**CH_3**) ppm.

***(S)*-1-Bromo-2-dodecyloxypropane (33)** [5]

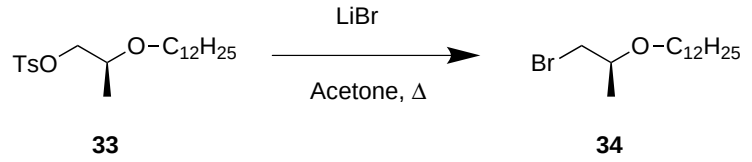

33 **34**

(S)-2-Dodecyloxypropyl toluene-4-sulphonate **33** (20.3 mmol, 8.1 g, 1.0 eq.) was dissolved in acetone (400 mL) and lithium bromide (0.53 mol, 45.9 g, 26 eq.) was added portionwise. The mixture was then refluxed overnight. The acetone was removed

and diethyl ether was added. The mixtured was filtered and the solids were washed with abundant ethyl ether. The solvent was removed in vacuum and the obtained pale yellow oil was purified by column chromatography of silica gel using hexane-DCM as an eluent, affording *(S)*-1-bromo-2-dodecyloxypropane **34** (5.7 g, 91%) as a pale yellow oil.

M.W.: 307.3 g.mol^{-1}. **FT-IR:** 2923 (s), 2853 (s), 1465 (s), 1458 (s), 1431 (m), 1376 (s), 13411326 (m), 1229 (m), 1195 (m), 1141 (m), 1096 (s), 918 (w), 872 (w), 824 (w), 722 (m), 668 (s) cm^{-1}. $[\alpha]_{546}^{25}$ = 3.92 deg.cm^2.g^{-1}. **^{1}H NMR** (250 MHz, $CDCl_3$): δ 3.64 (m, 1 H, -C**H**(CH_3)) 3.50 (t, *J* = 6.5 Hz, 2 H, -O-**CH_2**-), 3.41 (m, 1 H, Br-**CH_2**-), 3.39 (m, 1 H, Br-**CH_2**-), 1.74-1.18 (m, 23 H, -CH(**CH_3**)-O-CH_2-(**CH_2**)$_{10}$-), 0.88 (t, *J* = 6.7 Hz, 3 H, -O-(CH_2)$_{10}$-CH_3) ppm.

1,2-Dibromo-4,5-bis(*(S)*-2-(dodecyloxy)propoxy)benzene (4)

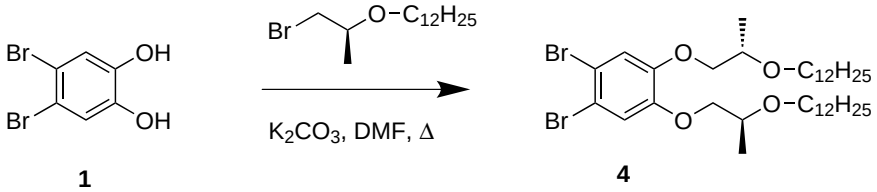

To a suspension of dry K_2CO_3 (22.3 mmol, 3.08 g, 5 eq.) in dry DMF distilled over CaH_2 (44 mL) was added 4,5-dibromocatechol **1** (4.46 mmol, 1.19 g, 1 eq.). The mixture was stirred at 40 ºC for 15 minutes before addition of *(S)*-1-bromo-2-dodecyloxypropane **34** (8.92 mmol, 2.74 g, 2 eq.). The reaction mixture was then stirred at 75 ºC overnight. Water (100 mL) was added to precipitate the reaction product. After filtration, the solids were dissolved in DCM, dried over MgSO4 and the solvent evaporated. The residue was purified by column chromatography of silica gel using toluene as an eluent. 1,2-dibromo-4,5-bis(*(S)*-2-(dodecyloxy)propoxy)benzene **4** was obtained as a pale yellow oil (2.7 g, 84%).

M.W.: 720.7 g.mol^{-1}. **FT-IR:** 2922 (s), 2853 (s), 1584 (w), 1496 (s), 1467 (s), 1454 (s), 1375 (m), 1354 (m), 1295 (w), 1249 (s), 1203 (s), 1107 (s), 1031 (s), 993 (m), 903 (m), 846 (m), 722 (m), 695 (w) cm^{-1}. **^{1}H NMR** 360 MHz, ($CDCl_3$): δ 7.09 (Ar-**H**, s, 2H), 3.95 (Ar-O-**CH_2**, m, 2H), 3.83 (Ar-O-**CH_2** and C**H**-CH_3, m, 4H), 3.54 (O-**CH_2**-CH_2, t, J = 6.7 Hz, 4H), 1.55 (O-CH_2-**CH_2**, m, 4H), 1.39-1.13 (CH-**CH_3** and O-CH_2-

CH_2-(**CH_2**)$_9$-CH_3, m, 42H), 0.88 (CH_2-**CH_3**, t, J = 6.6 Hz, 6H) ppm. $[\alpha]_{546}^{25}$ = 0.68 deg.cm^2.g^{-1}.

4,5-Bis(*(S)*-2-(dodecyloxy)propoxy)phthalonitrile (9)

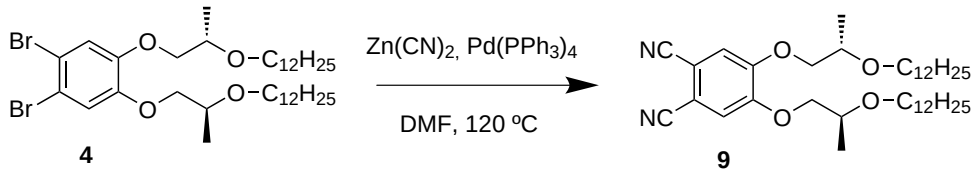

4 **9**

In a dry round-bottom flask under argon were suspended 1,2-Dibromo-4,5-bis(*(S)*-2-dodecyloxypropoxy)benzene **4** (3.75 mmol, 2.70 g, 1 eq.), tetrakis(triphenylphosphine) palladium (0) (1.04 mmol, 1.20 g, 0.28 eq.) and zinc (II) cyanide (4.50 mmol, 0.528 g, 1.2 eq.) in DMF (7.5 mL). The mixture was then heated at 120 ºC for 2 h after which ammonia (37%, 50 mL) was added, and the resulting precipitate was filtrated, washed with more ammonia (100 mL) and purified by column chromatography of silica gel using toluene as an eluent affording 4,5-bis(*(S)*-2-dodecyloxypropoxy)phthalonitrile **9** (1.9 g, 83%) as a white solid.

M.W.: 612.9 g.mol^{-1}. **m.p.:** 79 ºC. **FT-IR:** 3059 (w), 2919 (s), 2851 (s), 2230 (m), 1589 (m), 1566 (w), 1526 (s), 1468 (m), 1443 (w), 1411 (w), 1369 (m), 1351 (m), 1293 (s), 1231 (s), 1218 (w), 1164 (w), 1125 (m), 1085 (s), 1019 (m), 975 (m), 931 (w), 889 (m), 872 (w), 721 (m), 679 (w) cm^{-1}. **^{1}H NMR** 360 MHz, ($CDCl_3$): δ 7.18 (s, 2 H, Ar-**H**), 4.04 (m, 2 H, Ar-O-**CH_2**), 3.95 (m, 2 H, Ar-O-**CH_2**), 3.95 (m, 2 H, -***C*H**-CH_3), 3.54 (m, 4 H, O-**CH_2**-CH_2-), 1.55 (m, 4 H, O-CH_2-**CH_2**-), 1.39-1.14 (m, 42 H, CH-**CH_3** and O-CH_2-CH_2-**(CH_2)** $_9$-CH_3), 0.88 (t, *J* = 6.6 Hz, 6 H, CH_2-**CH_3**) ppm. **^{13}C NMR** (63 MHz, $CDCl_3$): δ 152.7, 116.9, 116.1, 109.0, 73.9, 73.7, 70.3, 32.3, 30.5, 30.0, 29.9, 29.7, 26.5, 23.0, 17.4, 14.5 ppm. $[\alpha]_{546}^{25}$ = 8.94 deg.cm^2.g^{-1}.

Octakis-(*(S)*-2-(dodecyloxy)propoxy)-phthalocyanine (22)

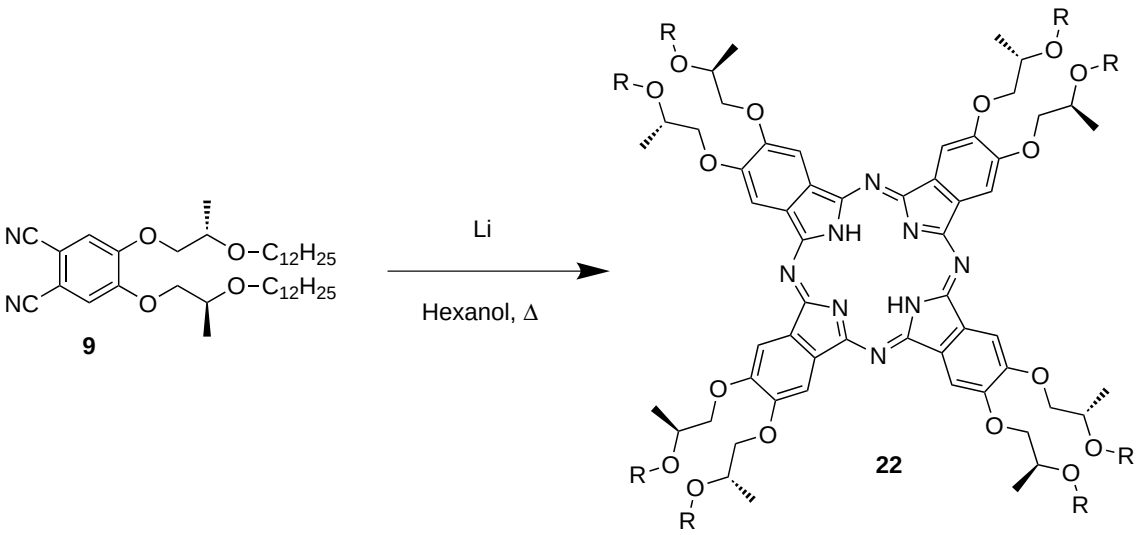

In a round bottom flask under nitrogen was added lithium (24.5 mmol, 170 mg, 60 eq.) in n-hexanol (10 mL). The mixture was heated at 100 ºC and stirred until complete disappearance of the lithium. 4,5-Bis(*(S)*-2-(dodecyloxy)propoxy)phthalonitrile **9** (1.63 mmol, 1.00 g, 4 eq.) was added and the mixture was stirred at 150 ºC overnight. Methanol was added, and the dark green waxy residue was decanted and washed several times with warm methanol, dissolved in hexane and the insoluble impurities were filtered out. The final residue was purified by repeated size exclusion chromatography (BioBeads SX1) using toluene as an eluent, affording a waxy dark green material (197 mg, 20%) characterized as **22**.

M.W.: 2453.7 g.mol^{-1}. **MS *m*/*z*:** 2454 (M^+). **FT-IR:** 2922 (s), 2853 (s), 1604 (m), 1447 (s), 1376 (m), 1331 (m), 1277 (s), 1203 (m), 1100 (s), 1022 (s), 874 (m), 803 (w), 744 (m), 720 (m) cm^{-1}. **^{1}H NMR** 360 MHz, ($CDCl_3$): δ 8.08 (N-*H*, s, 1H), 4.67 (N-*H*, s, 1H), 4.08 (Ar-O-*CH_2*, m, 8H), 3.96 (Ar-O-*CH_2*, m, 8H), 3.85 (*CH*-CH_3, m, 8H), 3.57 (O-*CH_2*-CH_2, m, 16H), 1.56 (O-CH_2-*CH_2*, m, 16H), 1.43-1.14 (CH-*CH_3* and O-CH_2-CH_2-*$(CH_2)_9$*-CH_3, m, 168H), 0.87 (CH_2-*CH_3*, m, 24H) ppm. **UV-Vis** (log(ε)): 700(4.57), 661(4.45), 646(4.05), 636(3.98), 599(3.74), 424(3.86), 354(4.17) nm. **CD** (Δε): 700(exciton 1.0), 661 (-1.0). **Col_h**142 **I**. **Elemental Analysis (%):** Calculated C, 74.40; H, 10.60; N, 4.57. Found C, 74.38; H, 10.69; N, 4.47.

Bis-(octakis-(*(S)*-2-(dodecyloxy)propoxy)-phthalocyaninato)terbium(III) (27)

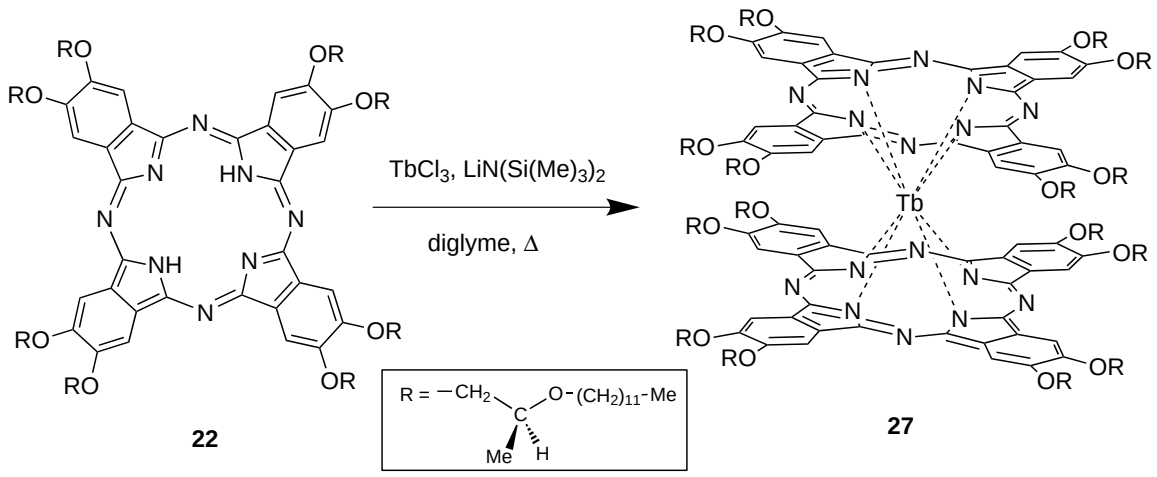

In a dry Schlenk tube under argon were introduced octakis-(*(S)*-2-(dodecyloxy)propoxy)-phthalocyanine **22** (31 µmol, 75 mg, 2.0 eq.) and anhydrous terbium chloride (7.6 µmol, 2.0 mg, 0.5 eq.). The vessel was degassed for 10 minutes under vacuum, after which the mixture was cooled to 0 ºC with an ice bath. Diglyme (3 mL) and N,N-bis(trimethylsilyl)lithium amide 1 M solution in THF (67 µmol, 67 µL, 4.4 eq.) were added with a syringe. The reaction was then stirred at 0 ºC for 1 h and refluxed for 2 h. After cooling down, methanol was added, and the dark green waxy residue was decanted and washed several times with warm methanol, dissolved in hexane and the insoluble impurities were filtered out. After evaporation of the solvent, the residue was purified by repeated size exclusion chromatography (BioBeads SX1) using toluene as an eluent, affording **27** as a waxy dark green material (52 mg, 67%) subsequently characterized as a room temperature liquid crystal.

M.W.: 5062.3 g.mol^{-1}. **MS *m/z*:** 5068 (M-), **FT-IR:** 2922 (s), 2853 (s), 1727 (w), 1600 (m), 1495 (m), 1450 (s), 1378 (s), 1319 (m), 1277 (s), 1201 (m), 1099 (s), 1050 (m), 877 (m), 823 (w), 754 (m), 721 (w) cm^{-1}. **UV-Vis** (log(ε)): 668(5.08), 605(4.40), 581(4.18), 483(4.47), 369(4.99), 337(4.90) nm. **C** -12 **Col$_h$** 31 **I**.

5,6-Dibromo-2,2-dimethyl-1,3-benzodioxole (5)

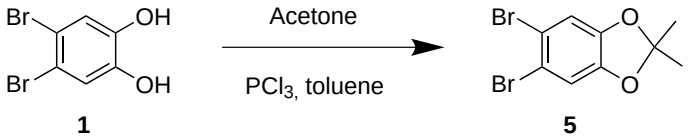

1 **5**

To a suspension of 4,5-dibromocatechol **1** (5 g, 18.66 mmol, 1.0 eq.) and acetone (1.64 ml, 22.4 mmol, 1.2 eq.), in dry toluene (30 ml) was added phosphorus trichloride (0.653 ml, 7.47 mmol, 0.4 eq.) dropwise at 20 ºC over 30 minutes. The reaction was stirred over night at room temperature. Potassium carbonate (25 g) was added and the solids were filtered and washed with toluene (50 mL). The organic layer was then washed with 10% NaOH (4×50 mL) dried on MgSO4 and the volatiles were evaporated on a rotatory evaporator affording 5,6-dibromo-2,2-dimethyl-1,3-benzodioxole **5** (2.4 g, 42%).

M.W.: 308.0 g.mol^{-1}. **m.p.:** 95 ºC. **FT-IR:** 3110 (w), 3058 (w), 2991 (w), 2929 (w), 1697 (w), 1649 (w), 1600 (w), 1488 (s), 1459 (m), 1379 (s), 1362 (m), 1259 (m), 1239 (s), 1206 (m), 1078 (m), 980 (m), 914 (m), 855 (s), 827 (w), 782 (m), 693 (w), 659 (w), 595 (w), 516 (m) cm^{-1}. **^{1}H NMR** (250 MHz, $(CD_3)_2CO$): δ 7.12 (s, 2 H, Ar-**H**), 1.69 (s, 6 H, -C(**CH_3**)$_2$) ppm.

4,5-Isopropylidenedioxyphthalonitrile (6)

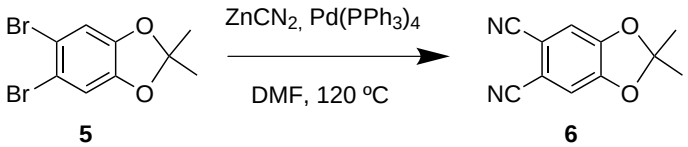

5 **6**

In a dry round-bottom flask under argon were suspended 5,6-dibromo-2,2-dimethyl-1,3-benzodioxole **5** (10 mmol, 3.08 g, 1.0 eq.), tetrakis(triphenylphosphine) palladium(0) (1.0 mmol, 1.15 g, 0.1 eq.) and zinc (II) cyanide (12.0 mmol, 1.41 g, 1.2 eq.) in DMF (20 mL). The mixture was then heated at 120 ºC for 2 h after which ammonia (37%, 100 mL) was added, and the resulting precipitate was filtered, washed with more ammonia (100 mL) and purified by column chromatography of silica gel using toluene as an eluent, affording 4,5-isopropylidenedioxyphthalonitrile **6** (1.7 g, 85%) as a white solid.

M.W.: 200.2 g.mol^{-1}. **m.p.:** 198 ºC.**FT-IR:** 3123 (w), 3067 (w), 2995 (w), 2943 (w), 2229 (s), 1741 (w), 1651 (w), 1598 (m), 1546 (w), 1501 (s), 1452 (m), 1402 (w), 1381 (s), 1282 (s), 1264 (m), 1255 (m), 1210 (s), 1165 (m), 1119 (m), 982 (s), 879 (s), 873 (s), 826 (s), 775 (m), 731 (w), 654 (m), 534 (s), 513 (w) cm^{-1}. **^{1}H NMR** (250 MHz, $CDCl_3$): δ 7.05 (s, 2H, Ar-**H**), 1.75 (s, 6H, -C(**CH_3**)$_2$) ppm.

Bis-(tetrakis-isopropylidenedioxy-phthalocyaninato) terbium(III) (28)

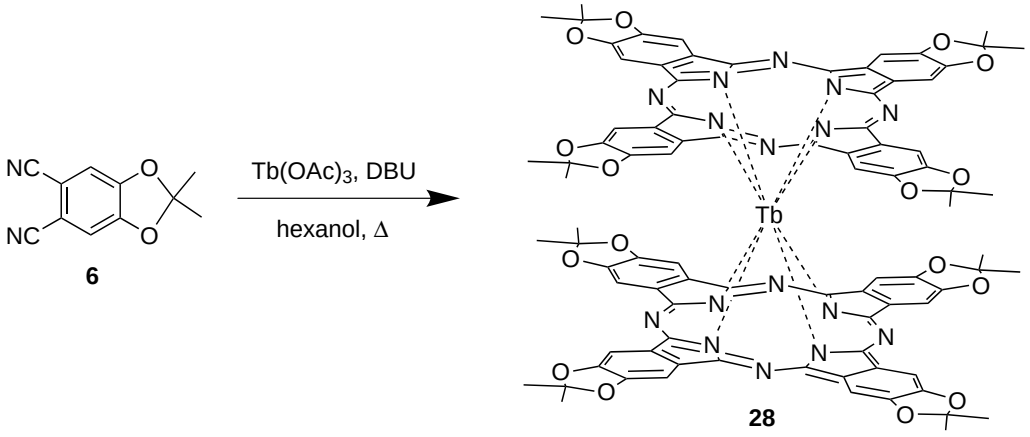

In a flame dried Schlenk under argon was introduced 4,5-isopropylidenedioxy phthalonitrile **6** (0.5 mmol, 100 mg, 1.0 eq.), and the Schlenk was degassed and purged with argon 3 times. Dry hexanol (1,5ml) was added with a syringe. DBU (0.25 mmol, 38 mg, 0.5 eq.) was added, and after stirring for 5 min under argon, $Tb(OAc)_3.[H_2O]_6$ (0.08 mmol, 35mg, 0.16 eq.) was added at once. The mixture was then warmed up in a sand bath to reflux at 160ºC for 16h. The course of the reaction was monitored by UV-Vis. After this time, the mixture was cooled to room temperature and acetonitrile was added to precipitate the complex. The dark green precipitate was filtered and dried in air. It was then purified by column chromatography of silica gel and by repeated size exclusion chromatography (on Biobeads SX1) using in both cases toluene as an eluent. The title compound was obtained (21 mg, 19%) as a dark green powder.

M.W.: 1760.5 g.mol^{-1}. **m.p.:** > 300 ºC.**MS m/z:** 1759 (M^+). **FT-IR:** 2985 (w), 2921 (w), 2852 (w), 2782 (w), 1732 (w), 1599 (w), 1456 (s), 1387 (s), 1315 (m), 1270 (s), 1206 (s), 1125 (m), 1068 (s), 1010 (m), 976 (s), 860 (s), 837 (s), 752 (m), 723 (m), 680 (w) cm^{-1}. **UV-Vis** (log(ε)): 292 (4.90), 336 (4.90), 371 (5.03), 483 (4.52), 581 (4.17), 605 (4.40), 667 (5.13) nm.

4,5-Bis(dodecylthio)phthalonitrile (10) [6]

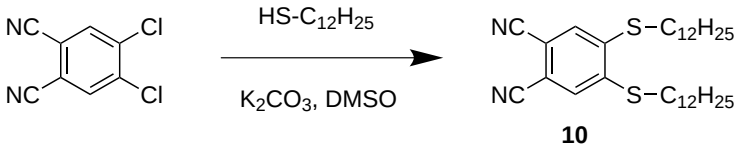

10

Potassium carbonate (500 mg, 3.62 mmol, 8.7 eq.) was suspended in DMSO and the mixture was sonicated for 5 minutes. Dodecan-1-thiol (202 mg, 1 mmol, 2.4 eq.) and 4,5-dichlorophthalonitrile (82 mg, 0.42 mmol, 1 eq.) were added and the mixture was stirred at room temperature for 12 hours. Water was added to precipitate the reaction products which were filtered out and dried. The obtained solids were washed with pentane to remove the excess of thiol, affording 4,5-bis(dodecylthio)phthalonitrile **10** as a white crystalline solid (143 mg, 65%).

M.W.: 528.9 g.mol^{-1}. **m.p.:** 66 ºC. **FT-IR:** 3075 (w), 2918 (s), 2850 (s), 2231 (m), 1685 (w), 1563 (s), 1456 (s), 1431 (m), 1378 (w), 1349 (m), 1269 (w), 1225 (m), 1114 (s), 953 (w), 933 (m), 898 (m), 869 (m), 780 (w), 762 (w), 763 (m), 721 (s), 691 (m) cm^{-1}. **^{1}H NMR** (250 MHz, $CDCl_3$) δ 7.41 (s, 2 H, Ar-**H**), 3.01 (t, *J* = 7.3 Hz, 4 H, -S-**CH_2**-), 1.86 – 1.60 (m, 4 H, -S-CH_2-**CH_2**-), 1.27 (s, 36 H, -S-CH_2-CH_2-(**CH_2**)$_9$-), 0.88 (t, *J* = 6.6 Hz, 6 H, -**CH_3**). **^{13}C NMR** (63 MHz, $CDCl_3$) δ 144.63, 128.53, 116.03, 111.44, 33.12, 32.28, 29.98, 29.91, 29.79, 29.70, 29.45, 29.26, 28.44, 23.05, 14.48 ppm.

Octachlorophthalocyanine (11)

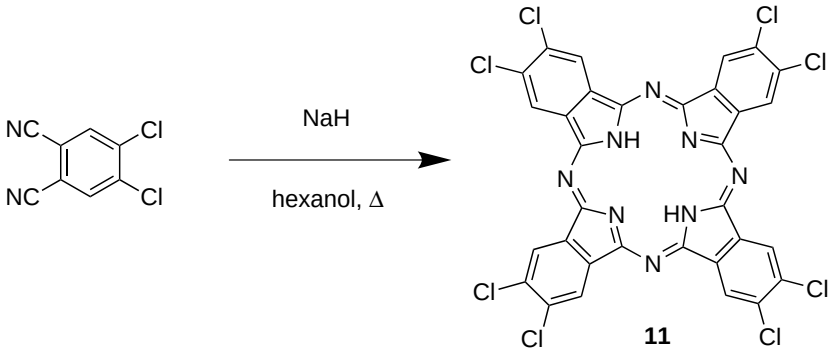

11

4,5-Dichlorophthalonitrile (200 mg, 1.0 mmol, 1 eq.) was dissolved in n-hexanol (3 mL). Sodium hydride 60% in oil (90 mg, 2.2 mmol, 2.2 eq.) was added and the mixture

[6] A. G. Gurek, T. Basova, D. Luneau, C. Lebrun, E. Koltsov, A. K. Hassan and V. Ahsen, *Inorg. Chem.* **2006**, *45*, 1667-1676.

was warmed to 100ºC for 12h. After that time the reaction was cooled down, acetonitrile (20 mL) was added and the mixture was filtrated. The obtained dark green solids (53 mg) were practically insoluble in all common solvents. It was identified as containing a mixture of hexa (**11**-6 Cl), hepta (**11**-7 Cl) and octachlorophthalocyanine (**11**-8 Cl) by LDI-TOF mass spectrometry.

M.W.: 11-6 Cl 721.2 g.mol^{-1}. **MS m/z:** 775.3 ([NaM^{+}]).

M.W.: 11-7 Cl 755.6 g.mol^{-1}. **MS m/z:** 749.1 ([NaLiM^{-}]), 768.6 ([Na$_2$M^{-}]).

M.W.: 11-8 Cl 790.1 g.mol^{-1}. **MS m/z:** 789.6 (M^{-}), 812.1 ([NaM^{-}])

Dihexyl-4,5-dichlorophthalate (12) [8]

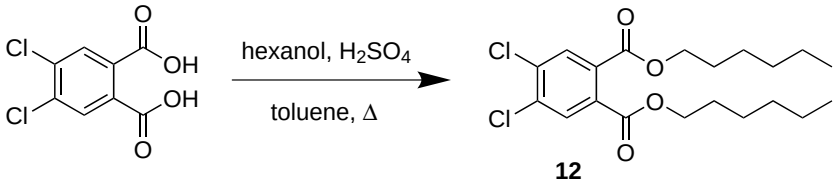

12

In a round bottom flask under nitrogen were introduced 4,5-dichlorophthalic acid (20 mmol, 4.7 g, 1.0 eq.), and n-hexanol (90 mmol, 9.2 g, 4.5 eq.) in toluene (30 mL). Concentrated sulfuric acid (1 mL) was added, and the flask equipped with a Dean-Stark apparatus was heated at reflux temperature for 15 h. The resulting mixture was cooled to room temperature, washed with water (50 mL) and 10% aqueous $NaHCO_3$ (50mL), dried over $MgSO_4$ and evaporated in vacuum. The residues were purified by column chromatography of silica gel using hexane/DCM 1:1 as an eluent, affording 3.7 g (46%) of a colorless oil characterized as **12**.

M.W.: 403.3 g.mol^{-1}. **^{1}H NMR** 360 MHz, ($CDCl_3$): δ 7.79 (Ar-*H*, s, 2 H), 4.29 (-O-C*H*$_2$-, t, J=6.6 Hz, 4 H), 1.72 (-O-CH$_2$-C*H*$_2$, m, 4 H), 1.20-1.45 (-O-CH$_2$-CH$_2$-(C*H*$_2$)$_3$-CH$_3$, m, 12 H), 0.90 (-CH$_2$-CH$_3$, t, J=6.7 Hz, 6 H) ppm.

[8] B. Tylleman, R. Gomez-Aspe, G. Gbabode, Y. H. Geerts and S. Sergeyev, *Tetrahedron* **2008**, *64*, 4155-4161.

Di-tert-butyl-4,5-dichlorophthalate (13)

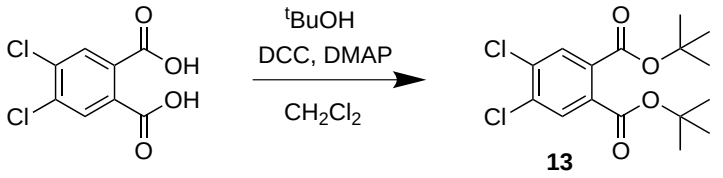

13

In a round bottom flask under nitrogen were dissolved 4,5-dichlorophthalic acid (10 mmol, 2.35 g, 1.0 eq.), DMAP (1.47 mmol, 0.18 g, 0.15 eq.) and 2-methylpropan-2-ol (40 mmol, 3.0 g, 4.0 eq.) in DCM (10 mL). The flask was cooled to 0 ºC and DCC (22 mmol, 4.5 g, 2.2 eq.) was added, and the resulting mixture was stirred at 0 ºC for 15 min and then at room temperature for 12h. The precipitated urea was then filtered off and washed thoroughly with DCM. The combined organic phases were evaporated on a rotary evaporator and the obtained solids were purified by silica gel column chromatography using DCM as an eluent, affording di-tert-butyl-4,5-dichlorophthalate **13** as a white solid (2.40 g, 69%).

M.W.: 347.2 g.mol-1. **FT-IR:** 3105 (w), 2978 (m), 2952 (m), 1722 (s), 1587 (w), 1556 (w), 1471 (m), 1458 (m), 1383 (m), 1367 (m), 1358 (m), 1301 (s), 1281 (s), 1258 (s), 1246 (s), 1159 (s), 1123 (s), 1086 (s), 1037 (m), 937 (w), 896 (w), 883 (w), 844 (s), 802 (w), 790 (w), 775 (w), 751 (w), 733 (w) cm^{-1}. **^{1}H NMR** 250 MHz, ($CDCl_3$): δ 7.69 (Ar-H, s, 2 H), 1.57 (-O-C(CH_3)$_3$, s, 18 H) ppm. **^{13}C NMR** 63 MHz, ($CDCl_3$): δ 164.8, 134.9, 133.4, 130.8, 83.0, 28.1 ppm.

N-pentadecyl-4,5-dichlorophthalimide (14)

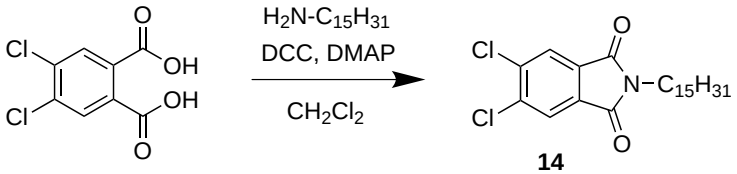

14

In a round bottom flask under nitrogen were dissolved 4,5-dichlorophthalic acid (10 mmol, 2.35 g, 1.0 eq.), Pentadecylamine (16 mmol, 3.6 g, 1.6 eq.) and DMAP (1.47 mmol, 0.18 g, 0.15 eq.) in DCM (10 mL). The flask was cooled to 0 ºC and DCC (22 mmol, 4.5 g, 2.2 eq.) was added, and the resulting mixture was stirred at 0 ºC for 15 min and then at room temperature for 12h. The precipitated urea was then filtered off and

washed thoroughly with DCM. The combined organic phases were evaporated on a rotary evaporator and the obtained solids were purified by silica gel column chromatography using DCM as an eluent, affording N-pentadecyl-4,5-dichlorophthalimide **14** as a white solid (2.5 g, 59%).

M.W.: 426.4 g.mol^{-1}. **MS m/z:** 425.3 (M^-). **m.p.:** 80 ºC. **FT-IR:** 3100 (w), 2947 (m), 2918 (s), 2850 (s), 1775 (m), 1758 (w), 1688 (s), 1614 (w), 1603 (w), 1470 (m), 1434 (m), 1384 (s), 1350 (s), 1343 (m), 1331 (m), 1310 (m), 1269 (w), 1225 (w), 1191 (m), 1159 (w), 1140 (m), 1103 (m), 1080 (w), 1061 (w), 1041 (m), 1009 (m), 979 (w), 851 (w), 933 (w), 906 (m), 892 (w), 853 (m), 790 (w), 759 (w), 743 (s), 736 (s), 707 (s) cm^{-1}. **^{1}H NMR** (360 MHz, $CDCl_3$): δ 7.91 (Ar-*H*, s, 2 H), 3.66 (-N-C*H*$_2$-, t, J=7.3 Hz, 2 H), 1.59 (-N-CH$_2$-C*H*$_2$-,m, 2 H), 1.24 (-N-CH$_2$-CH$_2$-(C*H*$_2$)$_{12}$-CH$_3$, m, 24 H), 0.87 (-CH$_2$-C*H*$_3$, t, J=7.0 Hz, 3 H) ppm. **^{13}C NMR** (63 MHz, $CDCl_3$): δ 166.4, 138.7, 131.3, 125.3, 38.5, 31.9, 29.7, 29.6, 29.5, 29.4, 29.3, 29.1, 28.4, 26.8, 22.7, 14.1 ppm.

***(S)*-N-1-phenylethyl-4,5-dichlorophthalimide (15)**

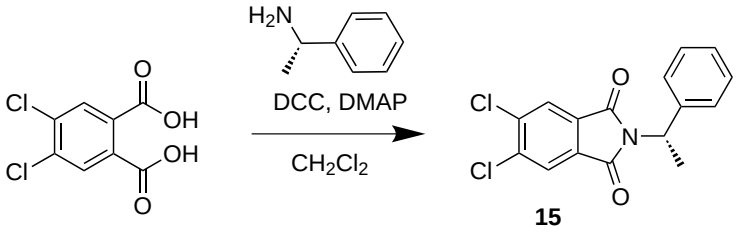

15

In a round bottom flask under nitrogen were dissolved 4,5-dichlorophthalic acid (10 mmol, 2.35 g, 1.0 eq.), DMAP (1.47 mmol, 0.18 g, 0.15 eq.) and *(S)*-1-Phenylethylamine (11 mmol, 1.3 g, 1.1 eq.) in DCM (10 mL). The flask was cooled to 0 ºC and DCC (30 mmol, 6.2 g, 3.0 eq.) was added, and the resulting mixture was stirred at 0 ºC for 15 min and then at room temperature for 12h. The precipitated urea was then filtered off and washed thoroughly with DCM. The combined organic phases were evaporated on a rotary evaporator and the obtained solids were purified by silica gel column chromatography using DCM as an eluent, affording *(S)*-N-1-phenylethyl-4,5-dichlorophthalimide **15** as a white solid (2.2 g, 69%).

M.W.: 390.2 g.mol^{-1}. **m.p.:** 120 ºC.**FT-IR:** 3465 (w), 6094 (w), 3069 (w), 3022 (w), 2985 (w), 2945 (w), 2119 (w), 1771 (m), 1718 (s), 1705 (s), 1614 (m), 1586 (m), 1493 (m), 1456 (m), 1387 (s), 1379 (s), 1354 (s), 1347 (s), 1287 (m), 1214 (m), 1191 (m),

1154 (s), 1138 (m), 1103 (m), 1093 (m), 1050 (m), 1029 (m), 996 (w), 977 (w), 948 (w), 903 (m), 896 (m), 792 (m), 771 (m), 760 (s), 750 (s), 699 (s) cm^{-1}. **^{1}H NMR** (400 MHz, $CDCl_3$): δ 7.87 (Cl-Ar-*H*, s, 2 H), 7.45-7.55 (-N-CH(CH_3)-Ar-*H*, m, 2 H), 7.25-7.35 (-N-CH(CH_3)-Ar-*H*, m, 3 H), 5.54 (-N-C*H*(CH_3)-, q, J=7.3Hz, 1 H), 1.91 (-N-CH(C*H*$_3$)-, d, J=7.3Hz, 3H) ppm. **^{13}C NMR** (63 MHz, $CDCl_3$): δ 166.3, 139.9, 139.0, 131.2, 128.7, 128.0, 127.5, 125.4, 50.3, 17.5 ppm. **[α]** $^{25}_{546}$ = 3.75 $deg.cm^2.g^{-1}$.

Dihexyl-4,5-dicyanophthalate (16) [8]

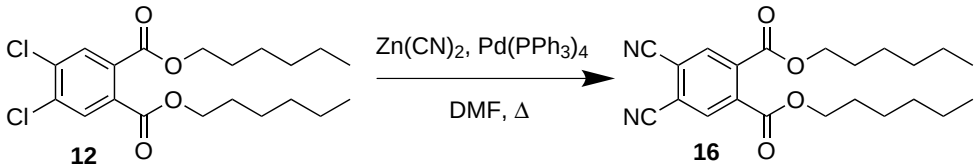

In a round-bottomed flask under argon were introduced dihexyl-4,5-dichlorophthalate **12** (2.5 mmol, 1.0 g, 1.0 eq.), $Pd(PPh_3)_4$ (0.50 mmol, 0.57 g, 0.20 eq.) and zinc(II) cyanide (3.0 mmol, 0.35 g, 1.2 eq.). DMF (5 mL) was added and the mixture was gently stirred at 120 ºC over 2 h. after this time, concentrated ammonia was added (30 mL), and the solid residues were filtered, dried and directly purified by column chromatography of silica gel using toluene as an eluent affording 0.82 g (86%) of a white crystalline solid characterized as **16**.

M.W.: 384.5 $g.mol^{-1}$. **FT-IR:** 3118 (w), 3053 (w), 2954 (m), 2929 (m), 2860 (m), 2238 (w), 1716 (s), 1557 (w), 1496 (w), 1467 (m), 1388 (m), 1376 (m), 1302 (s), 1269 (s), 1215 (s), 1139 (s), 1078 (w), 1045 (w), 0003 (w), 935 (m), 906 (m), 842 (w), 819 (w), 794 (m), 770 (m), 728 (m), 666 (w) cm^{-1}. **^{1}H NMR** 360 MHz, ($CDCl_3$): δ 8.12 (Ar-*H*, s, 2 H), 4.35 (-O-C*H*$_2$-, t, J=6.6 Hz, 4 H), 1.74 (-O-CH_2-C*H*$_2$, m, 4 H), 1.20-1.45 (-O-CH_2-CH_2-(C*H*$_2$)$_3$-CH_3, m, 12 H), 0.90 (-CH_2-CH_3, t, J=6.7 Hz, 6 H) ppm. **^{13}C NMR** (63 MHz, $CDCl_3$) δ 164.51, 136.87, 134.19, 118.42, 114.40, 67.67, 31.72, 28.69, 25.86, 22.86, 14.33.

Di-tert-butyl-4,5-dicyanophthalate (17)

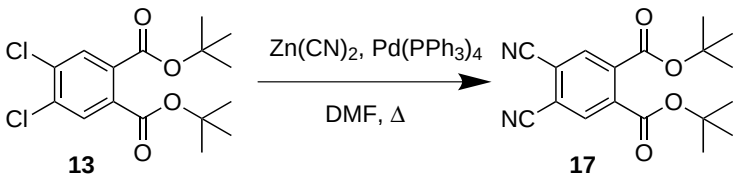

In a round-bottomed flask under argon were introduced di-tert-butyl-4,5-dichlorophthalate **13** (2.9 mmol, 1.0 g, 1.0 eq.), $Pd(PPh_3)_4$ (0.58 mmol, 0.67 g, 0.20 eq.) and zinc(II) cyanide (3.5 mmol, 0.41 g, 1.2 eq.). DMF (5.8 mL) was added and the mixture was gently stirred at 120 ºC over 2 h. after this time, concentrated ammonia was added (30 mL), and the solid residues were filtered, dried and directly purified by column chromatography of silica gel using toluene as an eluent affording 0.91 g (32%) of a white crystalline solid characterized as **17**.

M.W.: 328.4 $g.mol^{-1}$. **m.p.:** 64 ºC. **FT-IR:** 2982 (w), 2935 (w), 2235 (w), 1719 (s), 1605 (w), 1554 (w), 1475 (w), 1461 (w), 1391 (m), 1368 (s), 1310 (s), 1295 (m), 1277 (m), 1260 (m), 1219 (m), 1163 (s), 1131 (s), 1037 (w), 1006 (w), 926 (m), 911 (w), 868 (w), 844 (s), 816 (m), 799 (w), 778 (w), 760 (w), 739 (w), 666 (w) cm^{-1}. **^{1}H NMR** 250 MHz, ($CDCl_3$): δ 8.03 (Ar-*H*, s, 2 H), 1.60 (-O-C(CH_3)$_3$, s, 18 H) ppm. **^{13}C NMR** 63 MHz, ($CDCl_3$): δ 163.3, 138.0, 133.9, 117.5, 114.4, 84.8, 28.1 ppm.

N-pentadecyl-4,5-dicyanophthalimide (18)

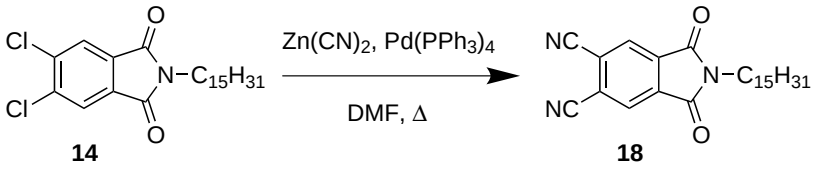

In a round-bottomed flask under argon were introduced N-pentadecyl-4,5-dichlorophthalimide **14** (2.3 mmol, 1.0 g, 1.0 eq.), $Pd(PPh_3)_4$ (0.47 mmol, 0.54 g, 0.20 eq.) and zinc(II) cyanide (2.8 mmol, 0.33 g, 1.2 eq.). DMF (4.7 mL) was added and the mixture was gently stirred at 120 ºC over 2 h. After this time, concentrated ammonia was added (30 mL), and the solid residues were filtered, dried and directly purified by column chromatography of silica gel using toluene as an eluent affording 0.51 g (54%) of a white crystalline solid characterized as **18**.

M.W.: 407.6 g.mol^{-1}. **m/z:** 407.4 (M^-). **m.p.:** 88 ºC. **FT-IR:** 3111 (w), 3050 (w), 2962 (w), 2918 (s), 2850 (s), 2240 (w), 1868 (w), 1781 (m), 1717 (s), 1705 (s), 1623 (w), 1470 (m), 1440 (w), 1416 (w), 1397 (s), 1370 (m), 1358 (m), 1331 (m), 1283 (w), 1271 (w), 1250 (w), 1227 (w), 1205 (w), 1186 (w), 1166 (w), 1151 (w), 1088 (s), 1027 (w), 1003 (w), 970 (w), 961 (w), 939 (m), 888 (w), 849 (w), 814 (w), 788 (m), 768 (w), 745 (s), 719 (s) cm^{-1}. **^{1}H NMR** (360 MHz, $CDCl_3$): δ 8.25 (Ar-*H*, s, 2 H), 3.74 (-N-C*H*$_2$-, t, J=7.2 Hz, 2 H), 1.69 (-N-CH$_2$-C*H*$_2$-, m, 2H), 1.25 (-N-CH$_2$-CH$_2$-(C*H*$_2$)$_{12}$-CH$_3$, m, 24H), 0.88 (-CH$_2$-CH$_3$, t, J=6.9Hz, 3H) ppm. **^{13}C NMR** (63 MHz, $CDCl_3$): δ 164.8, 135.5, 127.9, 121.3, 114.2, 39.1, 31.9, 29.7, 29.6, 29.5, 29.4, 29.3, 29.0, 28.3, 26.8, 22.7, 14.1 ppm.

***(S)*-N-1-Phenylethyl-4,5-dicyanophthalimide (19)**

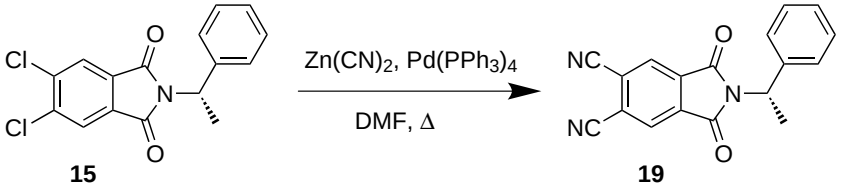

15 **19**

In a round-bottomed flask under argon were introduced *(S)*-N-1-phenylethyl-4,5-dichlorophthalimide **15** (3.1 mmol, 1.0 g, 1.0 eq.), $Pd(PPh_3)_4$ (0.62 mmol, 0.72 g, 0.20 eq.) and zinc (II) cyanide (3.7 mmol, 0.44 g, 1.2 eq.). DMF (6.2 mL) was added and the mixture was gently stirred at 120 ºC over 2 h. after this time, concentrated ammonia was added (30 mL), and the solid residues were filtered, dried and directly purified by column chromatography of silica gel using toluene as an eluent affording 0.68 g (72%) of a white crystalline solid characterized as **19**.

M.W.: 301.3 g.mol^{-1}. **m.p.:** 163 ºC. **FT-IR:** 3121 (w), 3062 (w), 2922 (w), 2243 (w), 1779 (m), 1713 (s), 1494 (w), 1457 (w), 1416 (w), 1389 (m), 1362 (s), 1318 (s), 1239 (w), 1214 (w), 1161 (m), 1113 (w), 1096 (m), 1072 (m), 1023 (w), 1003 (w), 993 (w), 920 (m), 904 (s), 849 (w), 805 (m), 771 (m), 741 (s), 723 (m), 701 (s) cm^{-1}. **^{1}H NMR** (250 MHz, $CDCl_3$): δ 8.21 (CN-Ar-**H**, s, 2 H), 7.4-7.55 (-N-CH(CH$_3$)-Ar-**H**, m, 2 H), 7.27-7.40 (-N-CH(CH$_3$)-Ar-**H**, m, 3 H), 5.58 (-N-C*H*(CH$_3$)-, q, J=7.2 Hz, 1 H), 1.94 (-N-CH(C*H*$_3$)-, d, J=7.2 Hz, 3 H) ppm. **^{13}C NMR** (63 MHz, $CDCl_3$): δ 164.6, 139.0, 135.3, 128.9, 128.5, 128.0, 127.6, 121.2, 114.2, 51.2, 17.4 ppm. $[\alpha]_{546}^{25}$ = -0.26 deg.cm^2.g^{-1}.

Octakishexyl phthalocyanine-2,3,9,10,16,17,23,24-octacarboxylate (23)

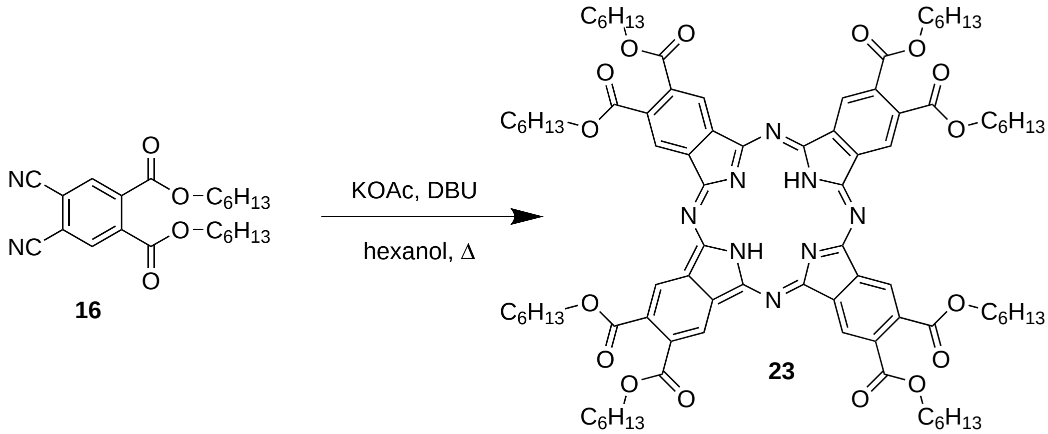

In a dry Schlenk tube under argon were introduced dihexyl-4,5-dicyanophthalate **16** (0.20 mmol, 80 mg, 4.0 eq.), KOAc (0.20 mmol, 20 mg, 4.0 eq.) and DBU (0.20 mmol, 30 mg, 4.0 eq.). n-Hexanol (0.5 mL) was added and the mixture was heated at 150ºC over 12 h, the hexanol was removed by liquid-liquid extraction of hexane and acetonitrile, and the hexane phase containing the free base phthalocyanine was evaporated, and the product was purified by repeated size exclusion column chromatography on BioBeads SX-1 medium using toluene as an eluent to afford 27 mg (34%) of a dark green waxy material characterized as **23**.

M.W.: 1539.9 g.mol^{-1}. **MS m/z:** 1538.4 (M^+), 1539.4 (M^-). **FT-IR:** 3442 (w), 3286 (w), 2953 (m), 2927 (m), 2855 (m), 1723 (s), 1626 (w), 1584 (w), 1506 (w), 1467 (m), 1381 (w), 1334 (m), 1317 (m), 1272 (s), 1241 (s), 1225 (w), (s), 1174 (m), 1134 (w), 1116 (m), 1082 (s), 1009 (m), 936 (m), 918 (w), 898 (m), 835 (w), 791 (w), 762 (s), 743 (s), 694 (w), 668 (m) cm^{-1}. **^{1}H NMR** (360 MHz, $CDCl_3$): δ 9.59 (s, 8 H, Ar-**H**), 4.66 (t, *J* = 7.1 Hz, 16 H, -COO-**CH_2**-), 2.04 (m, 16 H, -COO-CH_2-**CH_2-**), 1.77-1.35 (m, 48 H, -COO- CH_2- CH_2**-(CH_2)$_3$-**), 1.00 (t, *J* = 6.9 Hz, 24 H, -**CH_3**) ppm. **^{13}C NMR** (91 MHz, $CDCl_3$) δ 167.53, 134.54, 124.34, 66.70, 31.66, 28.78, 25.82, 22.70, 14.13 ppm. **Elemental Analysis (%):** Calculated C, 68.64; H, 7.46; N, 7.28. Found C, 68.50; H, 7.33; N, 7.32.

N,N,N,N-Tetrapentadecyl-29H,31H-2,3,9,10,16,17,23,24-phthalocyanine-tetradicarboximide (24)

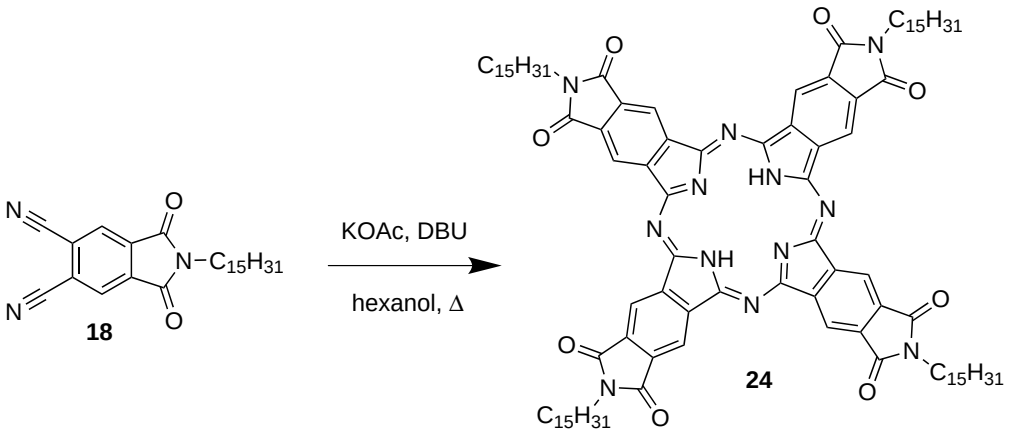

In a dry schlenck under argon were introduced N-pentadecyl-4,5-dicyanophthalimide **18** (0.24 mmol, 100 mg, 4.0 eq.), KOAc (0.24 mmol, 24 mg, 4.0 eq.) and DBU (0.24 mmol, 37 mg, 4.0 eq.). n-hexanol (1.5 mL) was added and the mixture was heated at 150ºC over 12 h. After this time, glacial acetic acid was added (5 mL) and the precipitated dark solids were dissolved in toluene and purified by repeated size exclusion chromatography on BioBeads SX-1 medium using toluene as an eluent, affording 37 mg (37 %) of a dark green solid characterized as **24**.

M.W.: 1632.2 g.mol^{-1}. **MS m/z:** 1631.8 (M^-), 1632.3 (M^+). **FT-IR:** 3289 (m), 2920 (s), 2851 (s), 1765 (s), 1708 (s), 1579 (s), 1466 (m), 1435 (m), 1390 (s), 1363 (s), 1208 (m), 1161 (w), 1113 (m), 1065 (w), 912 (w), 816 (w), 732 (s) cm^{-1}. **UV-Vis** (log(ε)): 715(4.56), 676 (4.58), 657(4.36), 644(4.37), 616(4.26), 360(4.48) nm.

Bis(N,N,N,N-tetrapentadecyl-29H,31H-2,3,9,10,16,17,23,24-phthalocyaninato-tetradicarboximide)terbium(III) (29)

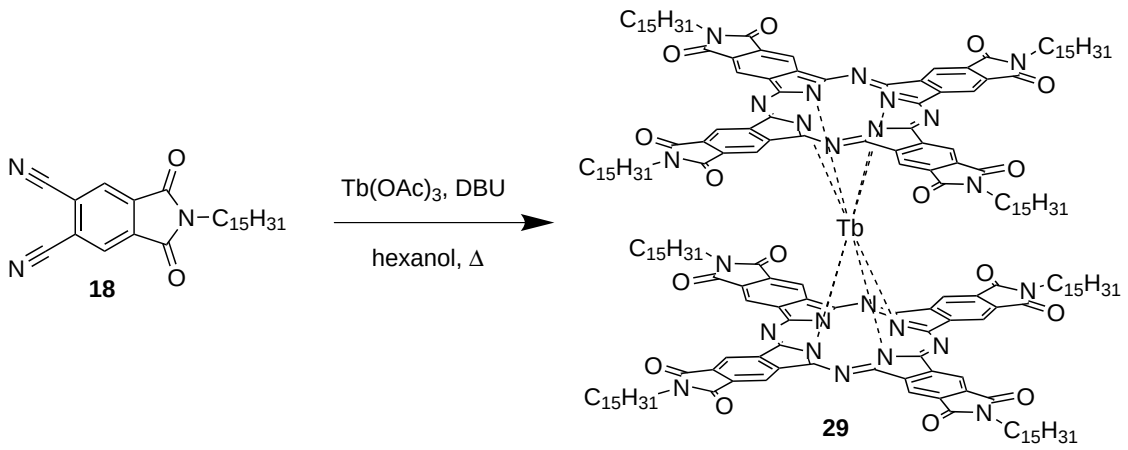

In a flame dried Schlenk tube under argon was introduced N-pentadecyl-4,5-dicyanophthalimide **18** (0.17 mmol, 70 mg, 1.0 eq.). The Schlenk was degassed and was purged with argon 3 times. Dry hexanol (0.5 ml) was added with a syringe. DBU (0.086 mmol, 13 mg, 0.5 eq.) was added, and after stirring for 5 min under argon, $Tb(OAc)_3.[H_2O]_6$ (0.027 mmol, 12.2 mg, 0.16 eq.) was added at once. The mixture was then warmed up in a sand bath to reflux at 160 ºC for 14 h. The course of the reaction was monitored by UV-Vis absorption spectroscopy. After that time, the mixture was dried in vacuum to remove the hexanol. The obtained waxy solid was purified by column chromatography of silica gel using chloroform / AcOH - 99/1 as an eluent. Two thin bands were eluted containing the metal free phthalocyanine and an unidentified impurity, respectively. The deep dark blue band remaining at the top of the column was then eluted using THF as an eluent and was characterized as the anionic for of complex **29**. The obtained fraction was then purified by repeated size exclusion chromatographies on BioBeads-SX1 medium, using toluene as an eluent, affording the title compound (27 mg, 37%) as a waxy green-blue material.

M.W.: 3419.3 $g.mol^{-1}$. **MS m/z:** 3419.7 (M^+). **FT-IR:** 2921 (s), 2851 (s), 1767 (s), 1705 (s), 1465 (m), 1436 (m), 1404 (m), 1386 (m), 1358 (s), 1215 (m), 115 (s), 1066 (s), 911 (m), 813 (w), 786 (w), 735 (s), 660 (m) cm^{-1}. **UV-Vis** (log(ε)): 917(3.52), 681(5.18), 614(4.40), 467(4.32), 359(4.81), 338(4.76) nm.

Bibliography

[1] H. E. Gottlieb, V. Kotlyar, A. Nudelman, *J. Org. Chem.* **1997**, *62*, 7512-7515.
[2] S. A. Macgregor, E. McInnes, R. J. Sorbie, L. J. Yellowlees, in *Molecular Electrochemistry of Inorganic, Bioinorganic and Organometallic Compounds* (Eds.: A. J. L. Pombeiro, J. A. McCleverty), Kluwer Academic Publishers, **1993**, pp. 503-518.
[3] M. Kohn, *J. Am. Chem. Soc.* **1951**, *73*, 480.
[4] K. Binnemans, J. Sleven, S. De Feyter, F. C. De Schryver, B. Donnio, D. Guillon, *Chem. Mater.* **2003**, *15*, 3930-3938.
[5] E. Gomar-Nadal, C. Rovira, D. B. Amabilino, *Tetrahedron* **2006**, *62*, 3370-3379.
[6] A. G. Gurek, T. Basova, D. Luneau, C. Lebrun, E. Koltsov, A. K. Hassan, V. Ahsen, *Inorg. Chem.* **2006**, *45*, 1667-1676.
[7] R. P. Linstead, M. Whalley, *J. Chem. Soc.* **1952**, 4839-4846.
[8] B. Tylleman, R. Gomez-Aspe, G. Gbabode, Y. H. Geerts, S. Sergeyev, *Tetrahedron* **2008**, *64*, 4155-4161.

CHAPTER 8

CONCLUSIONS

In the present work, the synthesis and the magnetic properties of new double-decker terbium phthalocyanine complexes were studied with several compounds in a variety of oxidation states, morphologies, and reduced dimensionalities, leading to the following main conclusions:

- Neutral lanthanide double-decker phthalocyanine complexes deposited on highly oriented pyrolitic graphite maintain their slow magnetic relaxation rates. The complexes in a submonolayer structure were indeed shown to behave essentially like the bulk material by performing XMCD measurements at the terbium $M_{4,5}$ edge. They displayed magnetization hysteresis at a temperature of 7 K and presented an XAS absorption spectrum identical to the bulk complex, which demonstrated how the $4f^8$ system is unscathed.

- The anionic double-decker phthalocyanine complexes on the other hand are strongly affected by the vicinity of the graphite surface when deposited as a submonolayer. They provided an XAS spectrum quasi-identical to that of the neutral complex, and also displayed a magnetization hysteresis at 7 K, indicating that the anion is oxidized under these conditions and is therefore not as robust as the neutral system.

- MCD measurements on dilute frozen solutions of a double-decker phthalocyanine complex proved the actual single-molecule behavior of a collection of isolated complexes in a diamagnetic solvent glass. The non-aggregated state of the molecules was demonstrated. The SMM behavior was shown to exist for neutral, anionic and cationic complexes. Contrary to what was expect, based on ac magnetic susceptibility measurements, the best redox state in terms of magnetic bistability is the neutral complex, which shows a higher coercive field and larger remnant magnetization than the

other two redox states. The MCD detected magnetization hysteresis of the complex at low temperature in a dilute solvent glass was shown to be quite different from that of the bulk complex, possibly due to the removal of dipolar magnetic interactions.

- The magnetic properties of a liquid-crystalline double-decker phthalocyanine terbium complex was probed in a variety of bulk frozen – quenched – states, demonstrating the existence of two magnetically non-equivalent species with different relaxation rates in the solid state. The ratio between the two species can be reversibly tuned by adjusting the cooling rates from the isotropic liquid state. The existence of these slow and fast relaxing species was assigned to molecular distortions of the superparamagnetic complexes.

All in all, it was shown that the single-molecule magnetic behavior of a series of terbium double-decker phthalocyanine complex is qualitatively affected by the redox state of the molecule and the superstructure in which it is incorporated, with changes in blocking temperature and shape of the magnetization hysteresis. Nevertheless, the SMM behavior was also shown to be quite robust since neither the chemical substitution of the phthalocyanines, the hybridization with a graphite surface, the oxidation or reduction of the system, or the morphology of the solid state remove this property of the system.

APPENDIX I

MAGNETIC CIRCULAR DICHROISM

Magnetic circular dichroism (MCD) is a spectroscopic method that consists in recording the difference of absorption of a sample with left and right circularly polarized light (lcp and rcp, respectively) in the presence of a magnetic field. Contrary to natural circular dichroism (CD), MCD spectroscopy does not rely on the natural optical activity of the studied compounds and may be used to characterize almost all kinds of aromatic molecules.

The MCD signal arises from the same electronic transitions as those observed in UV-Vis absorption spectroscopy but the selection rules are different, and hence so are the intensities of the MCD band with respect to the UV-Vis ones. The information obtained from MCD spectra is complementary to that of UV-Vis spectra in the fact that it provides information on the ground and excited state degeneracies, and complements therefore the UV-Vis spectroscopy to solve the electronic structure of the studied molecules.

Since the MCD intensity follows a Beer-Lambert law and additionally is proportional to the magnetic field B, the magnitude ΔA is a signed quantity given by the following eqution:

$$\Delta A = A_{-} - A_{+} = \Delta\varepsilon_M clB$$

where A_{-} is the lcp absorption, A_{+} is the rcp absorption, ε_M is the molar apsorption coefficient of the sample, c is the concentration of the sample and l is the pathlength of the cell used to perform the experiment. The detailed expression of ΔA provides the following expression:

$$\Delta A/E = (\Delta\varepsilon cl)/E = \gamma\mu_B B\left[-A_1\frac{\partial f(E)}{\partial E} + \left(B_0 + \frac{C_0}{kT}\right)f(E)\right]$$

where f(E) is the lineshape function that depends on the enrgy E associated to the incident wavelength. The latter equation defines thus the three spectral features

composing any MCD spectrum: the derivative-shaped Faraday A term and the two absorption-shaped terms, called Faraday B and C terms.

A Faraday A term of positive sign appears as a positive lobe at an energy higher than the crossing point, while one of negative sign appears as a positive lobe at an energy lower than the crossing point. This term is a result of an orbitally degenerate excited state and a non-degenerate ground state, and are predicted only in molecules possessing at least a three-fold axis of symmetry.

Due to the Zeeman splitting of the orbitally degenerate excited state and the MCD selection rules, the lcp absorption and the rcp absorptions are shifted in opposite directions, giving rise to the characteristic derivative lineshape of the Faraday A term, centered on the energy of the non polarized absorption (see Figure I-1).

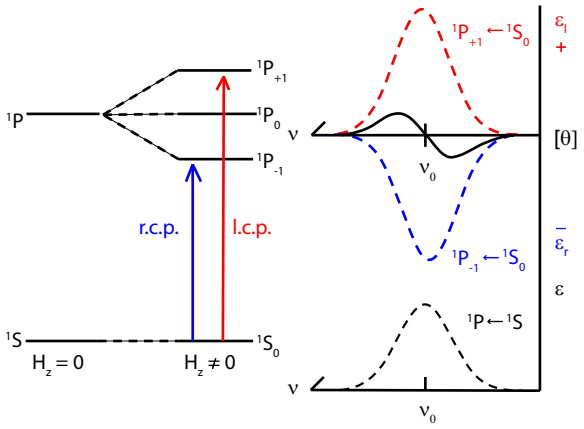

Figure I-1. Faraday A term originated from an orbitally degenerate excited state and a non-degenerate ground state. Polarized absorptions (above, dotted lines), are responsible for the MCD lineshape (above, full line) while an unpolarized absorption (below) is responsible for the absorption band.

The Faraday B terms are Gaussian-shaped absorption bands of either positive or negative sign and are observed when an transition towards an excited state is mixed with nearby transitions by the effect of a magnetic field.

When two B terms of wavelength ν_0 and ν_1 are interacting, they give spectral envelopes of opposite sign (see Figure I-2). When the energy splitting between the two interacting terms (i.e. $\Delta\nu = \nu_0 - \nu_1$) is small, the observed MCD curve looks like a derivative-shape Faraday A term and they are therefore called pseudo A term.

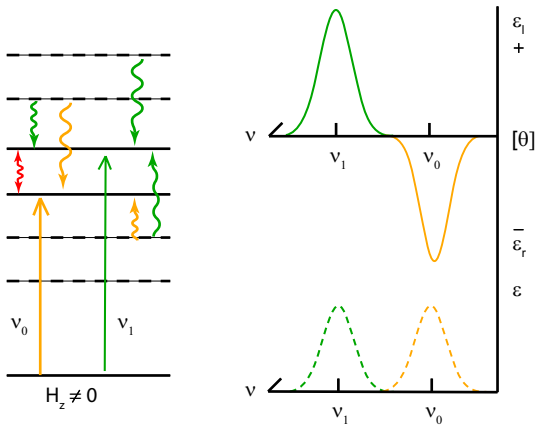

Figure I-2. Interacting transitions responsible for two Faraday B terms (left) and their appearance as a pseudo A term (right)

The difference between an A term and the pseudo A term is that in an A term the crossing point is observed at the absorption peak wavelength ν_0 (see Figure I-1) whereas in a pseudo A term the positive and negative lobes are centered on the absorption peaks at ν_0 and ν_1 and the crossing point is observed in between these two wavelengths.

Finally, the Faraday C terms appear as a Gaussian-shaped band of either positive or negative sign, similar in shape to a non interacting B term. These terms arise from an orbitally degenerate ground-state and a non-degenerate excited state (see Figure I-3), and the intensity is inversely proportional to the temperature, as a result of the change in the Boltzmann distribution over the magnetic field splitted orbital component of the degenerate ground-state.

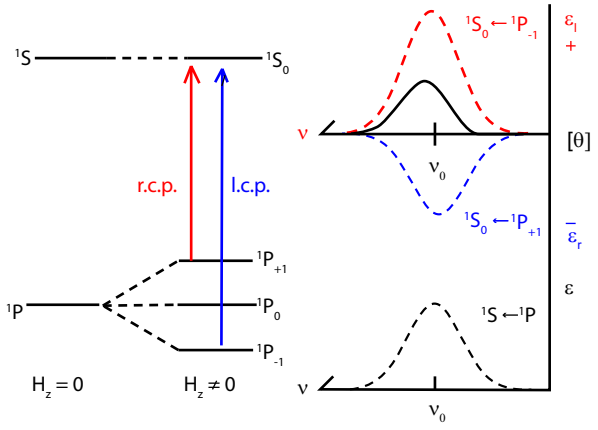

Figure I-3. Faraday C terms originate from an orbitally degenerate ground-state. Polarized absorptions (above, dotted lines), resulting MCD lineshape (above, full line) and unpolarized absorption (below) for a Faraday C term.

The distinctive characteristics of a Faraday C term are that it is observed as a Gaussian-shaped band close (but rigorously not at the same wavelength) to the corresponding absorption band and presents an intensity that is inversely proportional to temperature. It is important to stress that for diamagnetic atoms or molecules, the ground-state is by definition non-degenerate and there is therefore no occurrence of C terms.

The analysis of MCD spectra and the assignment of the observed bands to A, B and C terms correlated with UV-Vis absorptions allows to assign the observed transitions to a certain electronic transition and they permit to gain knowledge on the degenerate ground-state and excited states which finally allows determination of the electronic structure of the studied compounds.

This technique has been especially used in the study of porphyrins and phthalocyanines which are strongly absorbing and highly symmetric aromatic molecules and therefore provide high quality MCD spectra with large intensities.[1]

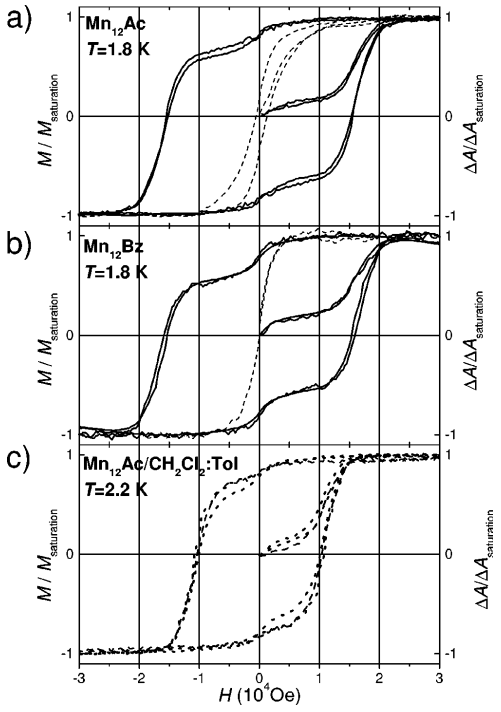

Figure I-4. Field dependence of SQUID magnetization and MCD at 21200 cm^{-1} (black curves) for $Mn_{12}Ac$ (a) and $Mn_{12}Bz$ (b).[3] In (a) and (b), the black solid curves indicate the magnitude of the MCD in 1:1 CH_2Cl_2:toluene glasses, while the dashed lines correspond to the relevant SMM in a 1:2 CH_3CN:DMF glass. For (c), the dotted curve indicates the magnetization of $Mn_{12}Ac/CH_2Cl_2$:toluene, while the black curves represent MCD measurements at 21200 cm^{-1} (dotted line) and 19 700 cm^{-1} (dashed line).

[1] N. Kobayashi and K. Nakai, *Chem. Commun.* **2007**, 4077-4092.

The MCD intensity being directly proportional to the magnetization of individual molecules,[2-4] it is possible to record MCD detected magnetization hysteresis (see Figure I-4). Magnetic circular dichroism spectroscopy is therefore also a powerful tool to study the magnetization of collections of isolated single-molecule magnets in a solvent glass.

[2] E. J. L. McInnes, E. Pidcock, V. S. Oganesyan, M. R. Cheesman, A. K. Powell and A. J. Thomson, *J. Am. Chem. Soc.* **2002**, *124*, 9219-9228.

[3] N. Domingo, B. E. Williamson, J. Gomez-Segura, P. Gerbier, D. Ruiz-Molina, D. B. Amabilino, J. Veciana and J. Tejada, *Phys. Rev. B* **2004**, *69*, 052405.

[4] P. Gerbier, N. Domingo, J. Gomez-Segura, D. Ruiz-Molina, D. B. Amabilino, J. Tejada, B. E. Williamson and J. Veciana, *J. Mater. Chem.* **2004**, *14*, 2455-2460.

APPENDIX II

X-RAY MAGNETIC CIRCULAR DICHROISM

II-1 Definition and conventions

X-ray magnetic circular dichroism (XMCD) spectroscopy is a core-level spectroscopy that consists in recording the difference in X-ray absorption spectra of a magnetized sample towards circularly polarized x-rays.[1] Using the sign conventions of Baudelet et al.,[2] the incident light direction is taken along the +**z** axis, and the magnetic field B is applied along the –**z** direction to align the magnetization of the probed material.

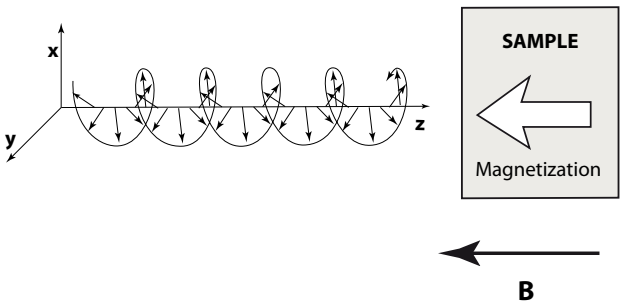

Figure II-1. Schematics of the sign convention used in XMCD

In these conditions, the positive (resp. negative) helicity corresponds to the right (resp. left) circularly polarized X-rays. The XMCD signal $\Delta\mu$ is given by the difference in X-ray absorption spectra of positive μ_+ and negative μ_- helicities as a function of the applied magnetic field **B**:

$$\Delta\mu = \mu_+(\mathbf{B}) - \mu_-(\mathbf{B}) = \mu_R(\mathbf{B}) - \mu_L(\mathbf{B})$$

II-2 Principles and nomenclature

XMCD is based on X-ray absorption spectroscopy (XAS) with a source of polarized X-rays and in the presence of a magnetic field. The nomenclature that applies to XMCD

[1] T. Funk, A. Deb, S. J. George, H. Wang and S. P. Cramer, *Coord. Chem. Rev.* **2005**, *249*, 3-30.
[2] F. Baudelet, C. Giorgetti, S. Pizzini, C. Brouder, E. Dartyge, A. Fontaine, J. P. Kappler and G. Krill, *J. Electron Spectrosc. Relat. Phenom.* **1993**, *62*, 153-156.

for the probed transitions is therefore the same as that used for XAS, which is the Barkla notation.[3] Upon X-ray absorption, a core hole is created with the excitation of a core electron to the valence states.

The transitions are named depending on the core-hole that is created. They are labeled with their main quantum number n, their angular quantum number l, and the total angular momentum $l + s$ or $l - s$ (Table II-1). The shells with same n are given the same letter, and they are indexed and sorted first by principal quantum number, then by angular quantum number and finally in increasing order of total angular momentum. The K shell is only constituted by the 1s orbitals and does not need indexing. The L shell comprises the 2s and 2p orbitals.

Table II-1. Nomenclature for core-level spectra.

	Core-holes								
Orbital	1s	2s	$2p_{1/2}$	$2p_{3/2}$	3s	$3p_{1/2}$	$3p_{3/2}$	$3d_{3/2}$	$3d_{5/2}$
Label	K	L_1	L_2	L_3	M_1	M_2	M_3	M_4	M_5

When exciting an electron from the 2p orbitals, the core-hole created has a spin of 1/2 or -1/2, therefore the 2p orbitals having $l = 1$, the total angular momentum is either $1 - 1/2 = 1/2$ or $1 + 1/2 = 3/2$. The 2p core-holes are named $2p_{1/2}$ and $2p_{3/2}$ and they are labeled as L_2 and L_3, respectively, since L_1 is attributed to the 2s core-hole. If talking about the 2p orbitals in their globality, one usually refers to the $L_{2,3}$ edge. The same rules apply to the labeling of the M shell core-holes and the list of orbitals and edge labels are given in Table II-1.

II-3 Chemical specificity

XMCD, like all core-level spectroscopies, is element specific. Indeed, the spectroscopic transitions of every element is associated with a specific range in energy of the incident X-rays. This feature allows one not only to determine the chemical nature of the materials under study but to perform element specific studies of the magnetization.

[3] C. G. Barkla, *Philosophical Magazine Series 6* **1911**, *22*, 396-412.

For instance, in a mixed material containing different magnetic metals, it is possible to record element specific magnetization curves, or to determine the magnetic coupling between the different metals by comparison of the sign of the XMCD spectra of the different elements. A good example is the study of $Fe_3Gd_3O_{12}$ by Rudolf et *al.*,[4] who employed XMCD to determine which element was dominating the magnetic behavior of the material as a function of temperature (see Figure II-2). At 300 K, the strong negative XMCD signal of the Fe-L_2 edge demonstrates that the iron dominates the magnetic behavior of the system, and the small positive XMCD signal of the Gd M_4 edge indicates that it is antiferromagnetically coupled to the Fe.

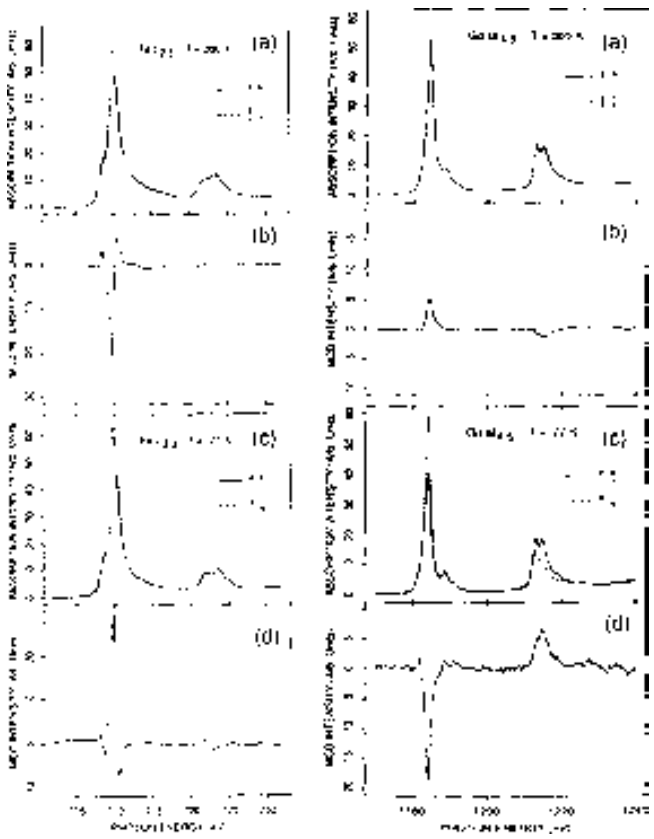

Figure II-2. The Fe L-edge (left) and Gd M-edge (right) XMCD spectra of $Fe_3Gd_3O_{12}$ at different temperatures.

On the contrary, at lower temperature (77 K), it is the Gd-M_4 edge that presents a strong negative XMCD signal, indicating the predominance of Gd at this temperature, while the Fe-L_2 presents a strong positive XMCD signal, which again demonstrates the antiferromagnetic coupling between Fe and Gd ions.

[4] P. Rudolf, F. Sette, L. H. Tjeng, G. Meigs and C. T. Chen, *J. Magn. Magn. Mater.* **1992**, *109*, 109-112.

II-4 Detection methods

The measurement of XMCD spectra requires a source of polarized X-rays and they are usually performed in synchrotron radiation facilities.

XMCD is essentially the measurement of relative absorption coefficients. All the methods classically used for XAS can be used. The three most used methods are transmission, fluorescence and electron yield (see Figure II-3).

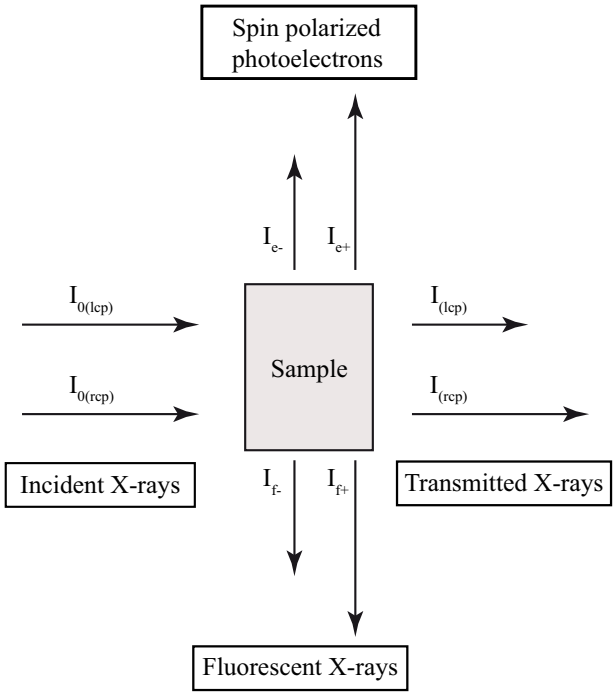

Figure II-3. Schematic of a XMCD experiment. I_0 is the incident beam intensity, I is the transmitted intensity while I_f and I_e are the intensities of the emitted fluorescence and photoelectrons, respectively.

In transmission mode, the signal is obtained by direct comparison of the incident intensity, I_0, and the transmitted intensity, I. This method works beautifully for thin metal foils but it is difficult to prepare high quality defect free thin samples with coordination complexes. For this reason the practical use of the transmission mode is quite limited in the study of inorganic complexes.

In the so-called electron yield mode, the photoelectrons emitted by the sample are measured either by directly detecting the emitted electrons or indirectly by monitoring the compensating flow of electrons from the ground to the sample. It is important to stress that electron emission is limited to the first 25-50 Å of the surface of the sample only and are therefore a sensitive probe of surface effects.

Finally, it is possible to measure the fluorescent X-rays emitted by the sample upon irradiation. The fluorescence detected excitation spectrum is not necessarily the same as the absorption spectrum. Nevertheless, in practical applications this method usually provides accurate values of Sz and Lz, and the influence on magnetization curves is fairly limited since these require only relative values.

II-5 Sum rules

One of the specificities of XMCD spectroscopy is that it allows one to determine the projections of the spin and angular momentum of the studied samples. This can be done by sum rules, that is, by simply integrating the obtained spectra.

For transition metal $L_{2,3}$-edges for instance, the sum rules for a powder sample are given by:

$$\langle L_z \rangle = \frac{2(A+B)}{3C} n_h \; and \; \langle S_z \rangle = \frac{A-2B}{2C} n_h$$

Where A is the integrated area under the XMCD L_3 feature, B is the integrated area under the L_2-edge feature and C is the integrated area under the XAS absorption curves (see Figure II-4).

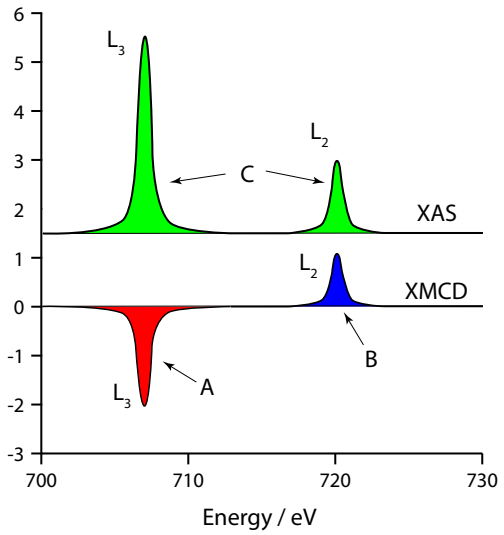

Figure II-4. Illustration of the A,B and C integrals used for the calculation of L_z and S_z by sum rules on the $L_{2,3}$ edges of transition metals.

The analytical expression of the sum rules given above is limited to the $L_{2,3}$ edge of transition metals, but if one derives the proper sum rules, the applicability of the method

is general, and XMCD is therefore a powerful tool to determine the spin and angular contributions to the magnetic moment.

II-6 Conclusions

XMCD is a highly sensitive element specific high energy probe of the magnetization of a material. Depending on the material under study it can be used to derive the spin and orbital contributions to the total magnetic moment, to measure element specific magnetization curves, to determine the magnetic coupling between the different magnetic centers of the compounds. Its high sensitivity has also been shown lately to make it a powerful tool for the study of the magnetization of submonolayer samples of inorganic superparamagnets on a surface.[5, 6]

[5] M. Mannini, P. Sainctavit, R. Sessoli, C. Cartier dit Moulin, F. Pineider, M. A. Arrio, A. Cornia and D. Gatteschi, *Chem. Eur. J.* **2008**, *14*, 7530-7535.

[6] M. Mannini, F. Pineider, P. Sainctavit, C. Danieli, E. Otero, C. Sciancalepore, A. M. Talarico, M.-A. Arrio, A. Cornia, D. Gatteschi and R. Sessoli, *Nat. Mater.* **2009**, *8*, 194-197.

APPENDIX III

ARTICLES

J|A|C|S COMMUNICATIONS

Published on Web 01/25/2010

Probing the Magnetic Properties of Three Interconvertible Redox States of a Single-Molecule Magnet with Magnetic Circular Dichroism Spectroscopy

Mathieu Gonidec,[†,§] E. Stephen Davies,[‡] Jonathan McMaster,*[,‡] David B. Amabilino,*[,†] and Jaume Veciana*[,†,§]

Institut de Ciència de Materials de Barcelona (CSIC) and Networking Research Center on Bioengineering, Biomaterials and Nanomedicine (CIBER-BBN), Campus Universitari de Bellaterra, E-08193 Bellaterra, Barcelona, Spain, and School of Chemistry, University of Nottingham, University Park, Nottingham NG7 2RD, U.K.

Received November 11, 2009; E-mail: vecianaj@icmab.es; amabilino@icmab.es; j.mcmaster@nottingham.ac.uk

Single-molecule magnets (SMMs), which are capable of exhibiting magnetic bistability[1] and present unique quantum properties,[2,3] have a range of potential applications in nanoscience including information storage[4] and molecular spintronics.[5] The anionic double-decker phthalocyanine complexes of Tb, Dy, and Ho behave as single-molecule magnets.[6,7] While efforts have been made to study the magnetic behavior of their one- and two-electron oxidized forms,[8,9] no magnetic hysteresis data have been reported. Herein, we present the spectroelectrochemical characterization of the anionic, neutral, and cationic equivalents of a terbium double-decker complex (**1**, Figure 1) and report a study of the corresponding hysteresis of magnetization using magnetic circular dichroism (MCD) spectroscopy in frozen dilute solutions at low temperature (1.5 K). Our results show that low temperature MCD spectroscopy is a viable and powerful technique to study the magnetization properties of this interesting family of compounds.

MCD spectroscopy has been shown to be a powerful tool for the optical detection of the magnetic behavior of Mn_{12} cluster SMMs.[10−13] An advantage that MCD spectroscopy offers, when compared to standard magnetometric measurements, is high sensitivity; this allows measurements of the magnetization of a collection of isolated molecules in dilute frozen solutions with diamagnetic solvents, thus minimizing the effect of intermolecular magnetic interactions and facilitating measurements at the single-molecule level.

We synthesized the neutral complex **1** following a previously reported procedure.[14] The redox properties of **1** were determined by cyclic voltammetry (Figure S1), and the oxidation and reduction processes at $E_{1/2} = 0.45$ and 0.09 V vs SCE, respectively, were studied further by UV/vis spectroelectrochemistry at 273 K. The spectroscopic changes in the absorption spectra associated with the one-electron electrochemical interconversions of $[Pc_2Tb]^{+/0/-}$ are shown in Figure S2. These demonstrate that $[Pc_2Tb]^{+/0/-}$ species may be electrogenerated reversibly and are stable on the time scale of the experiment. The UV/vis spectra of $[Pc_2Tb]^{+/0/-}$ (Figure 1) show the characteristic absorption bands of double-decker phthalocyanine complexes, including Soret bands at 387, 371, and 358 nm and Q bands at 705, 663, 624 nm, respectively.[15] In the case of $[Pc_2Tb]^{+/0}$, the characteristic π-radical band is observed at 495 and 475 nm, respectively.[15]

The samples for MCD spectroscopy, as solutions in CH_2Cl_2 with 0.8 M $[NBu_4][BF_4]$, were frozen in liquid nitrogen, which afforded glasses of suitable quality for optical measurements. In situ absorption spectra support the absence of aggregation of $[Pc_2Tb]^{+/0/-}$ under the conditions used (Figure S3−S5), an important feature of these experiments in which we probe the magnetic properties of a collection of molecules for which intermolecular magnetic interactions are minimized.

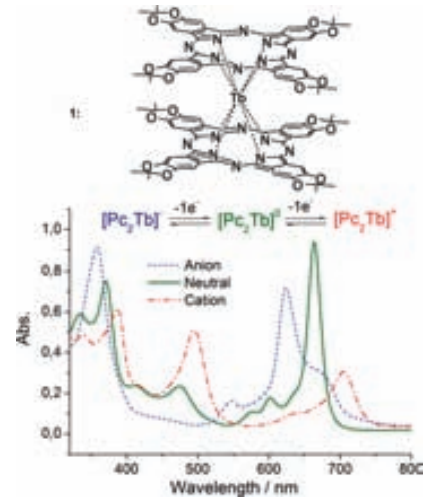

Figure 1. UV/vis absorption spectrum of solution of $[Pc_2Tb]^0$, in CH_2Cl_2 with 0.4 M $[NBu_4][BF_4]$, and of solutions of $[Pc_2Tb]^{+/-}$ generated electrochemically from $[Pc_2Tb]^0$. All spectra recorded at 273 K.

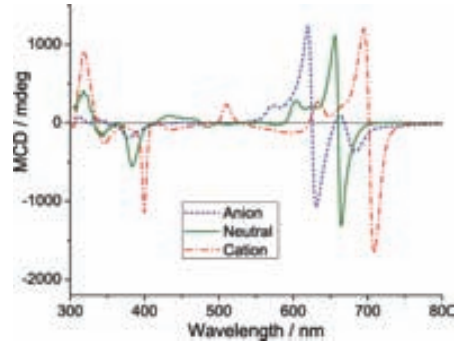

Figure 2. MCD spectra of solutions of $[Pc_2Tb]^{+/0/-}$ at 1.5 K and 7 T in CH_2Cl_2 with 0.8 M $[NBu_4][BF_4]$.

The rich MCD spectra of solutions of $[Pc_2Tb]^{+/0/-}$ (Figure 2) contain prominent temperature and field dependent pseudo-A terms at 701, 660, and 624 nm, respectively, that correspond to the intense Q-band features in the UV/vis absorption spectra (Figure 1). In addition, the fingerprint π-radical band of $[Pc_2Tb]^0$ and $[Pc_2Tb]^+$ show temperature-dependent MCD bands of opposite sign at 484 and 510 nm, respectively.

[†] Institut de Ciència de Materials de Barcelona (CSIC).
[§] CIBER-BBN.
[‡] University of Nottingham.

10.1021/ja9095895

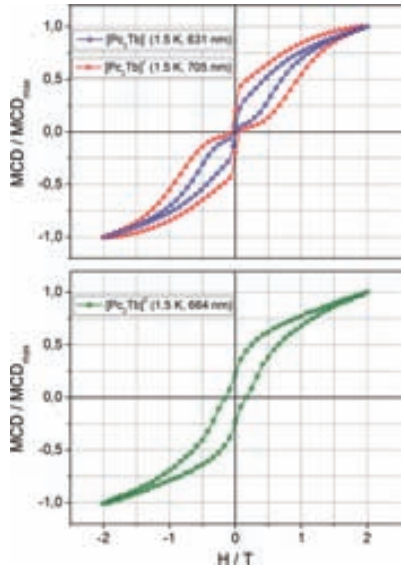

Figure 3. Hysteresis curves of the normalized MCD intensity vs B recorded at 1.5 K and a sweep rate of 1 T·min^{-1} for the Q-band of $[Pc_2Tb]^{+/-}$ (top) and $[Pc_2Tb]^0$ (bottom). The symbols represent 1 of every 5 data points.

The MCD intensity was monitored at 705, 664, and 631 nm for $[Pc_2Tb]^{+/0/-}$, respectively, over a $B = \pm 2$ T field range at a sweep rate of 1 T·min^{-1} and plotted as magnetization hysteresis curves (Figure 3). The field dependent MCD intensity of solutions of $[Pc_2Tb]^{+/-}$ recorded at 705 and 631 nm, respectively, (Figure 3, top) both present butterfly shaped hysteresis curves that are almost saturated at $B = \pm 2$ T, with an abrupt drop at $B < 0.09$ T. These data are similar to the hysteresis curves obtained by magnetometry on dilute solid solutions of $[NBu_4][Pc_2Tb]$ in the isostructural diamagnetic $[NBu_4][Pc_2Y]$ host,[16] suggesting that MCD of frozen solutions of $[Pc_2Tb]^{+/0/-}$ is a viable probe of the magnetic properties of isolated $[Pc_2Tb]^{+/0/-}$ complexes. The principal differences between the responses for $[Pc_2Tb]^+$ and $[Pc_2Tb]^-$ include a larger coercive field (0.071 T compared to 0.023 T) and a stronger remnant signal (0.198 as compared to 0.065 of the saturated signal intensity) for $[Pc_2Tb]^+$.

The sharp drop in magnetization at $B < 0.09$ T for the dilute solid solution of $[Pc_2Tb]^-$ arises from eight $|Jz> ||Iz>$ states which are brought to resonance by the Zeeman splitting.[17] This resonance only occurs at low field because of the small energy differences between these states. The very similar behaviors observed in the MCD of frozen solutions of $[Pc_2Tb]^{+/-}$, especially the coincidence of the change in magnetization around $B = \pm 0.09$ T, suggest that the source of their magnetic behavior is closely related. The difference in the width of their hysteresis curves above approximately 0.2 T suggests that the $|Jz>$ multiplet splitting is larger for $[Pc_2Tb]^+$ than for $[Pc_2Tb]^-$. This is consistent with the temperature dependence of the maximum in the imaginary component of the ac-susceptibility measurements previously reported for these oxidation states.[9] The field dependent MCD of $[Pc_2Tb]^0$ recorded as a frozen solution at 664 nm exhibits different hysteresis behavior as compared to those recorded for $[Pc_2Tb]^{+/-}$. Notably, the hysteresis is maintained over the whole range of magnetic field, between ± 1.5 T, and does not narrow around $B = 0$ T. Consequently, the coercive field is larger for $[Pc_2Tb]^0$ (0.16 T) than for $[Pc_2Tb]^{+/-}$ in these frozen solutions. The derivatives of the hysteresis cycles of $[Pc_2Tb]^{+/0/-}$ show features at *ca.* $\pm 0.4-0.5$ T that may arise from quantum tunneling effects (Figures S6−S8), although the sharp decrease in the gradient at 0 T strongly indicates that in all three systems there is relatively little tunneling at zero field. The relatively smooth profile of the hysteresis of $[Pc_2Tb]^0$ suggests that tunneling is not dominant in this complex when compared to $[Pc_2Tb]^{+/-}$.

To conclude, the optical MCD technique used here for the characterization of bis(phthalocyaninato)lanthanide-based SMMs does not rely on the preparation of solid solutions and on the identification of suitable isostructural diamagnetic hosts to minimize intermolecular magnetic interactions. Furthermore, the MCD method can be used to probe the magnetic properties of a range of different redox states of the same complex under essentially the same frozen solution conditions. While data from magnetic susceptibility studies suggest that the cationic form, $[Pc_2Tb]^+$, is more attractive for SMM applications,[8,9] we show that, under the conditions of our experiment, the neutral complex, $[Pc_2Tb]^0$, has a greater coercive field than the oxidized or reduced states.

Acknowledgment. This work was supported by the Marie Curie EST FuMaSSEC, EU NoE MAGMANet (515767-2), EMOCIONA (CTQ2006-06333/BQU) projects and by CIBER de Bioingeniería, Biomateriales y Nanomedicina (CIBER-BBN, promoted by ISCIII), Spain.

Supporting Information Available: Cyclic voltammetry, spectroelectrochemistry, *in situ* absorption data of the frozen samples, derivatives of the hysteresis cycles. This material is available free of charge via the Internet at http://pubs.acs.org.

References

(1) Gatteschi, D.; Sessoli, R.; Villain, J. *Molecular Nanomagnets*; Oxford University Press: Oxford, 2006.
(2) Gatteschi, D.; Sessoli, R. *Angew. Chem., Int. Ed.* **2003**, *42*, 268–297.
(3) Wernsdorfer, W.; Sessoli, R. *Science* **1999**, *284*, 133–135.
(4) Cavallini, M.; Gomez-Segura, J.; Ruiz-Molina, D.; Massi, M.; Albonetti, C.; Rovira, C.; Veciana, J.; Biscarini, F. *Angew. Chem., Int. Ed.* **2005**, *44*, 888–892.
(5) Rocha, A. R.; Garcia-Suarez, V. M.; Bailey, S. W.; Lambert, C. J.; Ferrer, J.; Sanvito, S. *Nat. Mater.* **2005**, *4*, 335–339.
(6) Ishikawa, N.; Sugita, M.; Ishikawa, T.; Koshihara, S.-y.; Kaizu, Y. *J. Am. Chem. Soc.* **2003**, *125*, 8694–8695.
(7) Ishikawa, N.; Sugita, M.; Wernsdorfer, W. *J. Am. Chem. Soc.* **2005**, *127*, 3650–3651.
(8) Ishikawa, N.; Sugita, M.; Tanaka, N.; Ishikawa, T.; Koshihara, S.-Y.; Kaizu, Y. *Inorg. Chem.* **2004**, *43*, 5498–5500.
(9) Takamatsu, S.; Ishikawa, T.; Koshihara, S.-Y.; Ishikawa, N. *Inorg. Chem.* **2007**, *46*, 7250–7252.
(10) McInnes, E. J. L.; Pidcock, E.; Oganesyan, V. S.; Cheesman, M. R.; Powell, A. K.; Thomson, A. J. *J. Am. Chem. Soc.* **2002**, *124*, 9219–9228.
(11) Domingo, N.; Williamson, B. E.; Gomez-Segura, J.; Gerbier, P.; Ruiz-Molina, D.; Amabilino, D. B.; Veciana, J.; Tejada, J. *Phys. Rev. B* **2004**, *69*, 052405.
(12) Gerbier, P.; Domingo, N.; Gomez-Segura, J.; Ruiz-Molina, D.; Amabilino, D. B.; Tejada, J.; Williamson, B. E.; Veciana, J. *J. Mater. Chem.* **2004**, *14*, 2455–2460.
(13) Cheesman, M. R.; Oganesyan, V. S.; Sessoli, R.; Gatteschi, D.; Thomson, A. J. *Chem. Commun.* **1997**, 1677–1678.
(14) Ivanov, A. V.; Svinareva, P. A.; Zhukov, I. V.; Tomilova, L. G.; Zefirov, N. S. *Russ. Chem. Bull. Int. Ed.* **2006**, *55*, 281–286.
(15) Ishikawa, N. *J. Porphyrins Phthalocyanines* **2001**, *5*, 87–101.
(16) Ishikawa, N.; Sugita, M.; Wernsdorfer, W. *Angew. Chem., Int. Ed.* **2005**, *44*, 2931–2935.
(17) Ishikawa, N.; Sugita, M.; Ishikawa, T.; Koshihara, S.-Y.; Kaizu, Y. *J. Phys. Chem. B* **2004**, *108*, 11265–11271.

JA9095895

Probing the magnetic properties of three interconvertible redox states of a single-molecule magnet with MCD

Mathieu Gonidec,[†] E. Stephen Davies,[‡] Jonathan McMaster,*[,‡]

David B. Amabilino,*[,†] Jaume Veciana*[,†]

Institut de Ciència de Materials de Barcelona (CSIC)-Networking Research Center on Bioengineer in, Biomaterials and Nanomedicine (CIBER-BBN), Campus Universitari de Bellaterra, E-08193 Bellaterra, Barcelona, Spain, and School of Chemistry, University of Nottingham, University Park, Nottingham, NG7 2RD, U.K.

[†] Institut de Ciència de Materials de Barcelona - CSIC.

[‡] University of Nottingham.

1. Cyclic voltammetry of $[Pc_2Tb]^0$

Dichloromethane (Fisher) was freshly distilled under an atmosphere of dinitrogen from calcium hydride then passed through a short column of alumina immediately prior to use.

Cyclic voltammetric studies were carried out using an Autolab PGSTAT20 potentiostat. Standard cyclic voltammetry was carried out under an atmosphere of argon using a three-electrode arrangement in a single compartment cell. A glassy carbon working electrode, a Pt wire secondary electrode and a saturated calomel reference electrode, chemically isolated from the test solution *via* a bridge tube containing electrolyte solution and fitted with a porous vycor frit, were used in the cell. Compensation for internal resistance was not applied. Potentials are quoted *versus* SCE. Decamethylferrocene (Fc*) was used as the internal reference ($E_{1/2}$ Fc^{*+}/Fc^* = -0.01 V vs. SCE). The difference between $E_{1/2}$ Fc^+/Fc and $E_{1/2}$ Fc^{*+}/Fc^* recorded as an independent experiment under identical conditions was 0.52 V.

Figure S1: Cyclic voltammetry of a 4.5×10^{-4} M solution of $[Pc_2Tb]^0$ in CH_2Cl_2 with 0.4 M $[NBu_4][BF_4]$ recorded at 0.1 $V.s^{-1}$

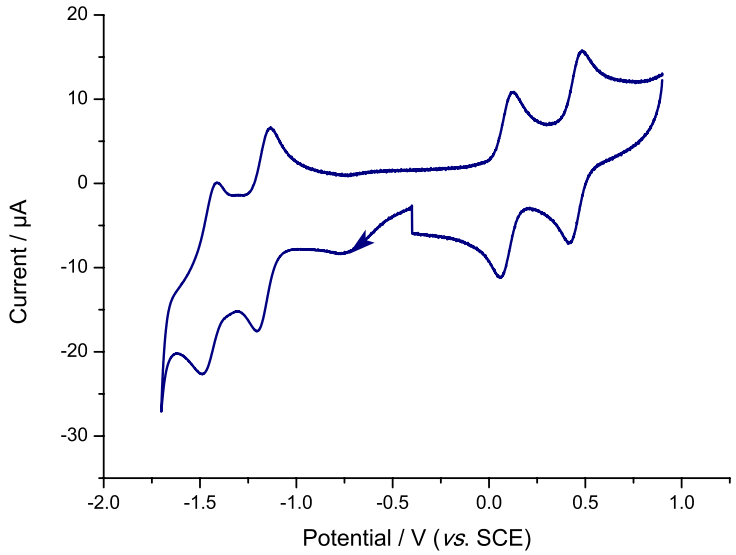

Cyclic voltammetric studies for $[Pc_2Tb]^0$ show one oxidation, at $E_{1/2}$ 0.45 V vs. SCE, and three reduction processes at $E_{1/2}$ 0.09 , -1.16 and -1.45 V *vs.* SCE, respectively. The redox processes centered at $E_{1/2}$ 0.45, 0.09 and -1.16 were all determined to be chemically reversible by UV/Vis spectroelectrochemistry at 273 K.

2. UV/Vis spectroelectrochemical studies

The UV/vis spectroelectrochemical experiments were carried out with an optically transparent electrochemical (OTE) cell (modified quartz cuvette, optical pathlength: 0.5 mm).[1] A three-electrode configuration, consisting a Pt/Rh gauze working electrode, a Pt wire secondary electrode (in a fritted PTFE sleeve) and a saturated calomel electrode, chemically isolated from the test solution *via* bridge tube containing electrolyte solution and terminated in a porous frit, was used in the cell. The potential at the working electrode was controlled by a Sycopel Scientific Ltd. DD10M potentiostat. The UV/vis spectra were recorded on a Perkin Elmer Lambda 16 spectrophotometer.

[1] S. A. Macgregor, E. McInnes, R. J. Sorbie and L. J. Yellowlees, *Molecular Electrochemistry of Inorganic, Bioinorganic and Organometallic Compounds*, A. J. L. Pombeiro and J. A. McCleverty (eds.), Kluwer Academic Publishers, 1993, 503.

Figure S3: Electrochemical conversion of a 1.48×10^{-4} M solution of $[Pc_2Tb]^0$ to $[Pc_2Tb]^-$ applying a potential of -0.15 V *vs.* SCE (top) and of $[Pc_2Tb]^0$ to $[Pc_2Tb]^+$ applying a potential of 0.59 V *vs.* SCE (bottom) in CH_2Cl_2 with 0.4 M $[NBu_4][BF_4]$

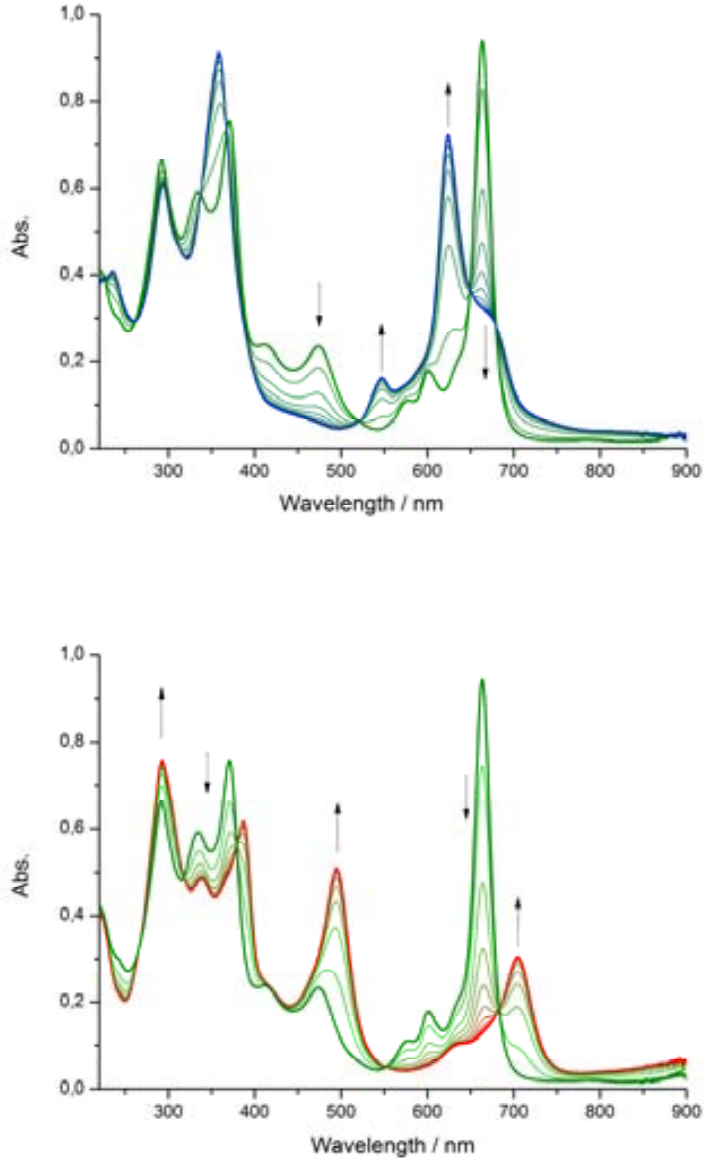

3. Magnetic circular dichroism and in situ UV/Vis absorption spectra

Solutions of $[Pc_2Tb]^{+/0/-}$ for the MCD spectroscopic measurements were prepared in CH_2Cl_2 containing 0.8 M of NBu_4BF_4. The anionic state was prepared by bulk electrolysis of a 1.11×10^{-4} M solution of $[Pc_2Tb]^{\mathbf{0}}$ and the solution of $[Pc_2Tb]^{+}$ was generated by the chemical oxidation of a solution of $[Pc_2Tb]^{\mathbf{0}}$ with a *ca.* 3×10^{-3} M solution of bromine in 0.8 M NBu_4BF_4 in CH_2Cl_2. The samples solutions were loaded into cells of *ca.* 2 mm path-length constructed from quartz discs separated by a Teflon spacer and frozen in liquid nitrogen. In situ UV/Vis absorption data were recorded simultaneously with the MCD data.

Figure S4: Comparison of a room temperature UV/Vis spectrum of $[Pc_2Tb]^{-}$ and the spectrum of the frozen solution of $[Pc_2Tb]^{-}$ recorded in situ at 1.5 K.

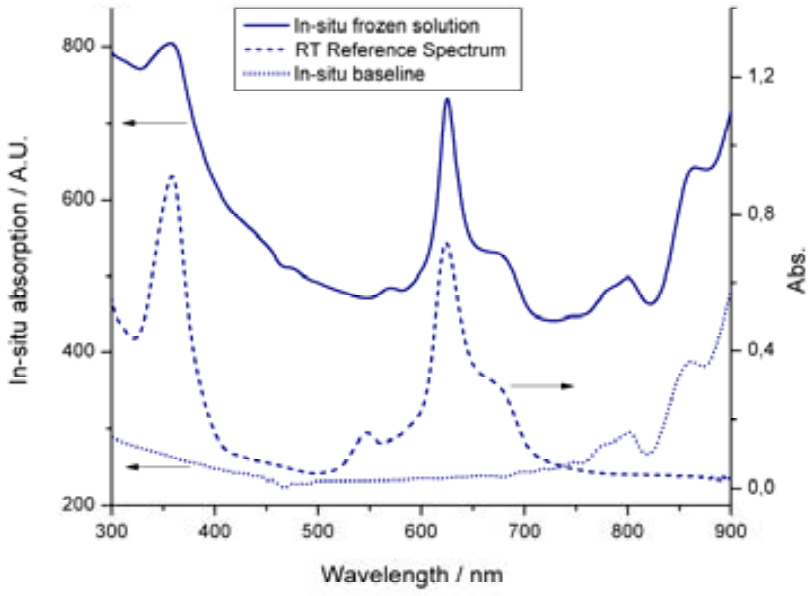

Figure S5: Comparison of a room temperature UV/Vis spectrum of $[Pc_2Tb]^0$ and the spectrum of the frozen solution of $[Pc_2Tb]^0$ recorded in situ at 1.5 K.

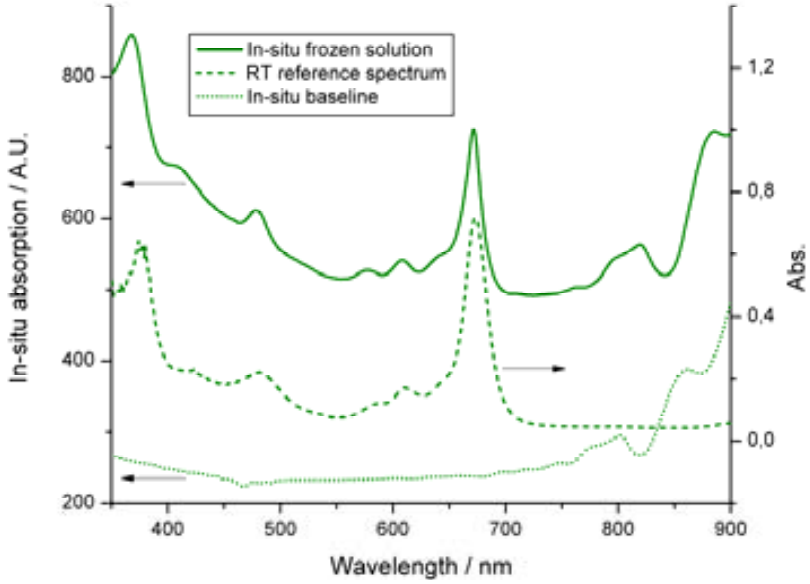

Figure S6: Comparison of a room temperature UV/Vis spectrum of $[Pc_2Tb]^+$ and the spectrum of the frozen solution of $[Pc_2Tb]^+$ recorded in situ at 1.5 K.

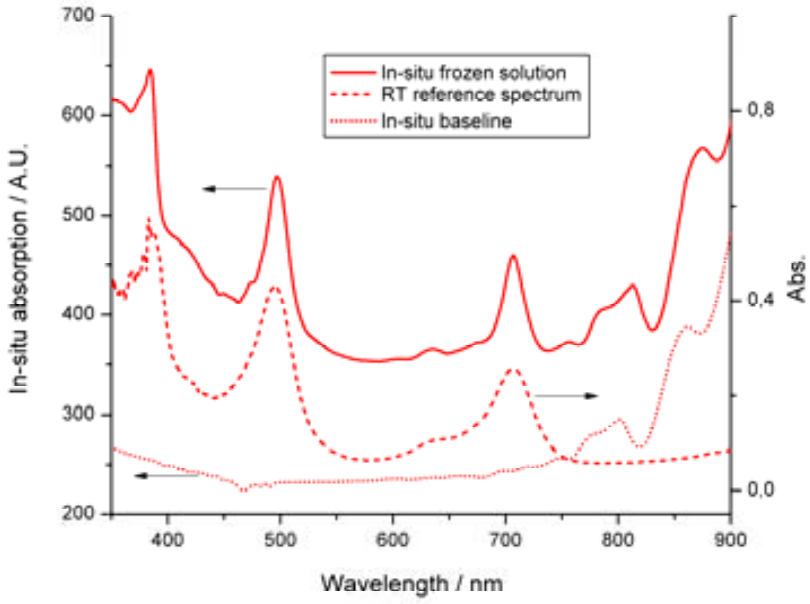

4. Derivative of the hysteresis cycles

Figure S7: Derivative of the hysteresis curve of the normalized MCD intensity *vs*. H recorded at 1.5 K and a sweep rate of 1 T.min^{-1} at 630 nm for $[Pc_2Tb]^-$ and enlargement of the same. The data are shown for 2.5 H±2 T cycles.

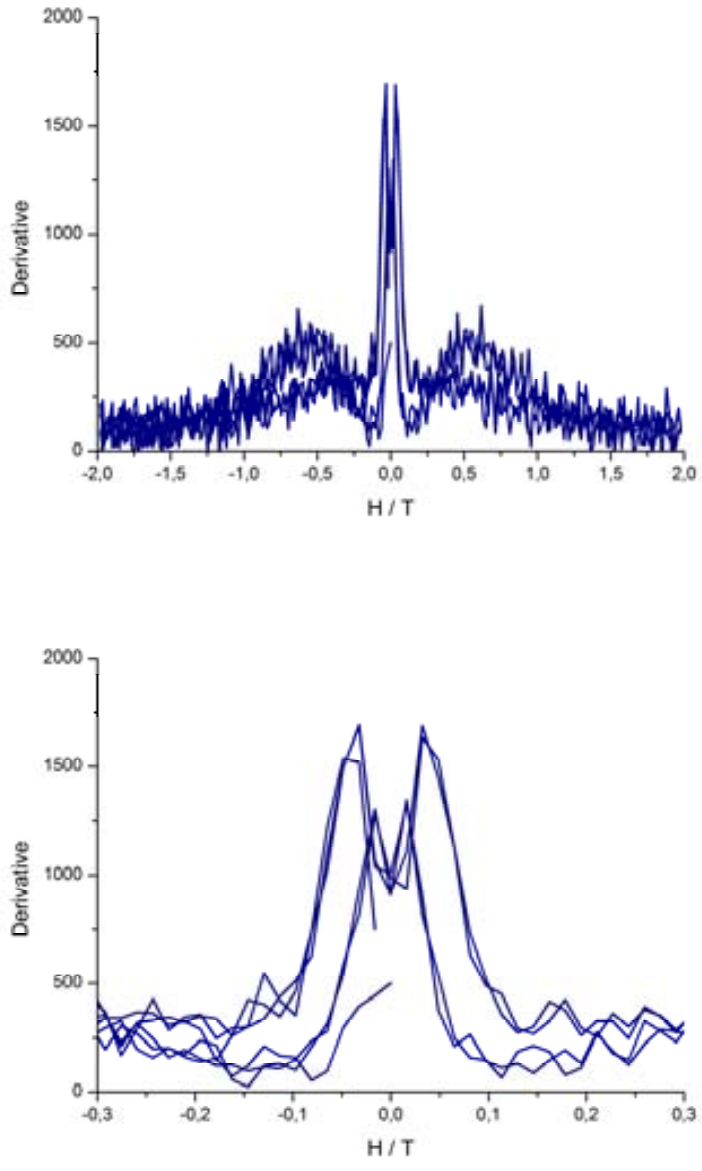

Figure S8: Derivative of the hysteresis curve of the normalized MCD intensity *vs*. H recorded at 1.5 K and a sweep rate of 1 T.min^{-1} at 675 nm for $[Pc_2Tb]^0$ and enlargement of the same. The data are shown for 4 H±2 T cycles.

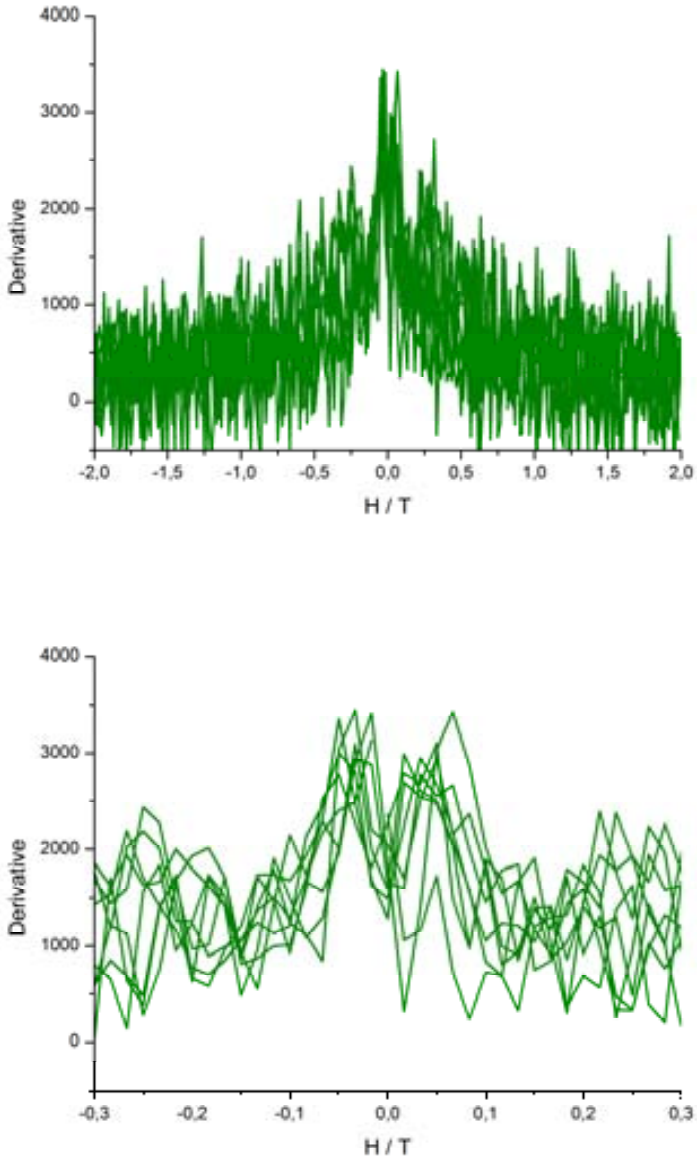

Figure S9: Derivative of the hysteresis curve of the normalized MCD intensity *vs*. H recorded at 1.5 K and a sweep rate of 1 T.min^{-1} at 714 nm for $[Pc_2Tb]^+$ and enlargement of the same. The data are shown for 2.5 H±2 T cycles.

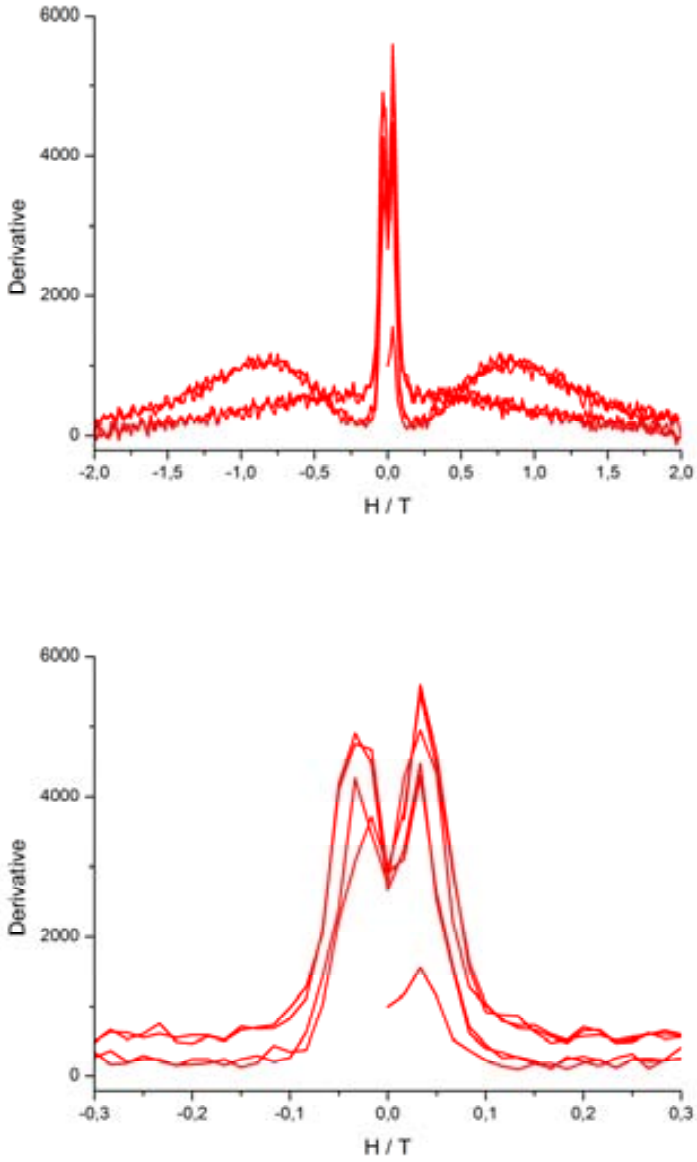

DOI: 10.1002/anie.200905007

Single-Molecule Magnets

A Liquid-Crystalline Single-Molecule Magnet with Variable Magnetic Properties**

Mathieu Gonidec, Fernando Luis, Àlex Vílchez, Jordi Esquena, David B. Amabilino, and Jaume Veciana**

Dedicated to Jean-Pierre Sauvage on the occasion of his 65th birthday

Single-molecule magnets (SMMs) are attractive because they present magnetic bistability of each isolated molecule,[1] thus enabling the discovery of a wide variety of intriguing phenomena and the possibility of preparing multifunctional molecular nanosystems.[2] The so-called double-decker lanthanide complexes of phthalocyanines, in which a lanthanide ion with a large total angular momentum is coordinated between two parallel phthalocyanine derivatives, are particularly attractive because of their relatively high blocking temperatures.[3–5]

Our interest in these systems arose from the possibility of using organic synthesis to functionalize the SMM core. In particular, we have been engaged in a program aimed at preparing chiral SMMs which might show interesting chiroptical phenomena,[6,7] such as magnetochiral dichroism (MChD), which could be useful for data storage and processing.[8] To facilitate processing of SMMs and related materials, the incorporation of long alkyl chains is advantageous, and we were particularly attracted by liquid-crystalline phases, as previously carried out with a Mn_{12} SMM[9] and spin-crossover iron(II) compounds.[10]

For this reason, we prepared compound **1**, a chiral derivative of the double-decker terbium complex. It behaves both as a liquid crystal at room temperature and as a single-molecule magnet at low temperatures. Importantly, when the material is cooled at different rates, the magnetic properties vary because of different degrees of supramolecular order. Herein we describe the preparation and characterization of this liquid-crystalline terbium double-decker phthalocyanine complex and how its mesomorphic properties can be used as a tool to adjust its magnetic properties reversibly at will. The terbium ion is used as a direct and very sensitive probe of the structural changes occurring at low temperatures, at which magnetic relaxation is dominated by direct tunneling transitions.

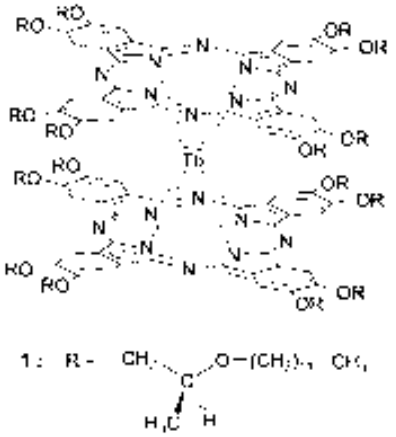

The chiral metal-free (free-base) phthalocyanine **5**, bearing eight identical stereocenters, was prepared in three steps from 4,5-dibromocatechol (Scheme 1) and the chiral bromoalkyl compound **2** derived from methyl lactate by a known procedure.[11]

Compound **3** was converted into the bis(cyano) derivative **4** using zinc(II) cyanide,[12] and the purified compound was cyclized in *n*-hexanol using lithium metal to give **5**. The corresponding terbium double-decker complex **1** was prepared by reacting **5** with anhydrous terbium chloride and lithium bis(trimethylsilyl)amide with minor changes from a published method.[13] The new compound was thoroughly purified by column chromatography, and was characterized by MALDI-TOF mass spectrometry, IR, UV/Vis absorption spectroscopy, circular dichroism spectroscopy, and elemental

[*] M. Gonidec, Prof. D. B. Amabilino, Prof. J. Veciana
Departament de Nanociència Molecular i Materials Orgànics, Institut de Ciència de Materials de Barcelona, Consejo Superior de Investigaciones Científicas (CSIC), Networking Research Center on Bioengineering, Biomaterials and Nanomedicine (CIBER-BBN)
Campus de la U.A.B., 08193 Bellaterra (Spain)
Fax: (+34) 93-580-5729
E-mail: amabilino@icmab.es
vecianaj@icmab.es
Homepage: http://www.icmab.es/nmmo/
Dr. F. Luis
Instituto de Ciencia de Materiales de Aragón, CSIC-Universidad de Zaragoza and Departamento de Física de la Materia Condensada, Universidad de Zaragoza
C/Pedro Cerbuna 12, 50009 Zaragoza (Spain)
À. Vílchez, Dr. J. Esquena
Institut de Química Avançada de Catalunya, CSIC, Barcelona (Spain)

[**] We warmly thank Amable Bernabé for recording the LDI-TOF MS and IR spectra. This work was supported by the Marie Curie EST FuMaSSEC, EU NoE MAGMANet (515767-2), EMOCIONA (CTQ2006-06333/BQU), Grup de Recerca de Catalunya (2009 SGR-516) and Molecular Nanoscience (CSD2007-00010) and Molchip (MAT2009-13977-C03) projects

Supporting information for this article is available on the WWW under http://dx.doi.org/10.1002/anie.200905007.

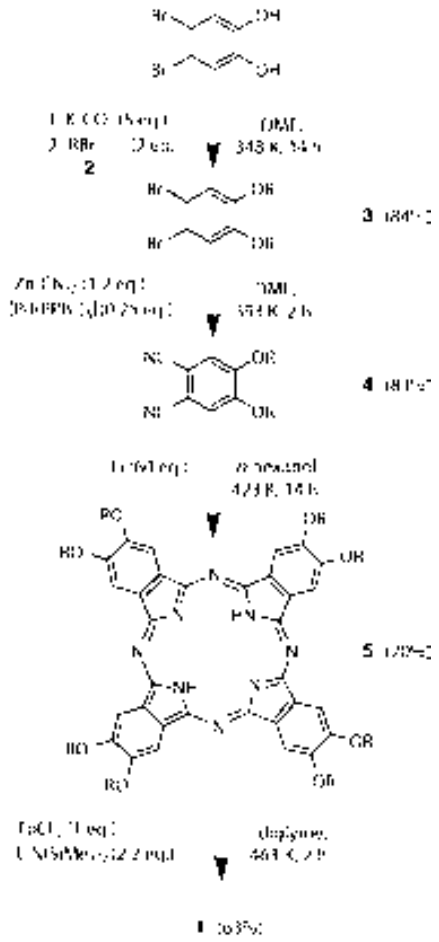

Scheme 1. Synthesis of **1** from 4,5-dibromocatechol and (*S*)-1-bromo-2-dodecyloxypropane (RBr; **2**).

analysis. The absorption spectrum of **1** shows the characteristic bands of neutral double-decker complexes,[14] and the optical activity of the compound was shown by circular dichroism spectroscopy, with Cotton effects at 668, 610, 455, and 368 nm (see the Supporting Information).

Polarized optical microscopy (POM) shows that compound **1** is mesomorphic at room temperature, with a clearing point at 304 K and an optical texture that suggests a columnar (Col) mesophase (see the Supporting Information). Upon cooling from the isotropic (I) liquid, some hexagonal dendritic growth could be observed in the optical texture of **1** under uncrossed polarizing filters at 298 K. The observation of this fan-like texture suggests a homeotropic alignment on glass of a columnar hexagonal (Col_h) mesophase.[15–18]

Differential scanning calorimetry (DSC) shows only one endothermic peak (see the Supporting Information) at 261 K corresponding to the $Cr \rightarrow Col_h$ transition with $\Delta H = 86.1\ kJ\,mol^{-1}$ and $\Delta S = 340.7\ J\,K^{-1}\,mol^{-1}$, but does not show any peak near 304 K corresponding to the clearing point observed by POM, presumably because of the small enthalpy difference between the two phases.

Small-angle X-ray scattering (SAXS) was used to confirm the nature of the observed mesophase. Only three reflections (see the Supporting Information) could be observed in the small angle region (0–8°) at 298 K, with d spacing ratios of $1:\sqrt{3}:2$, thus allowing unambiguous identification of a hexagonal lattice. The observed reflections, obeying $(h^2+hk+k^2)^{1/2} = d/d_{hkl}$, were labeled (100), (110), and (200). This observation confirms the hexagonal columnar mesophase, which is qualitatively consistent with previously reported mesomorphic double-decker compounds of cerium[15–17] and various lanthanides.[18,19]

The phase behavior of the free-base phthalocyanine **5** is found to be qualitatively similar to the behavior of **1**. It also presents a hexagonal columnar mesophase, as evidenced by POM and SAXS (see the Supporting Information). Nevertheless, the clearing point is much lower in complex **1** than in **5** (304 K compared with 415 K), as occurs in analogous systems.[18–20]

The properties of single-molecule magnets can be very sensitive to the structural changes in the solid state. Differences of magnetic behavior have been seen in dodecamanganese complexes and attributed to Jahn–Teller isomerism in the coordination sphere of the manganese ion.[21] It has also been shown that the degree of dipolar interactions and also changes in the matrix arrangements around the molecular core of double-decker lanthanide complexes can influence the magnetic behavior of these compounds.[22,23] For this reason, the mesomorphism of **1** can be seen as a tool to tune the superstructure and probe the robustness of its magnetic properties in a variety of discrete structural situations. As the SMM behavior and magnetic ordering occur at low temperatures, the sample can be kinetically trapped in a given structural state, and its magnetic properties measured at low temperature. Using suitable rates of cooling, a structurally disordered sample $\mathbf{1}_{dis}$, an intermediate partially ordered sample $\mathbf{1}_{po}$, or an ordered crystalline state $\mathbf{1}_{cr}$ can be prepared from the same specimen.

Alternating current magnetic susceptibility measurements of $\mathbf{1}_{dis}$ and $\mathbf{1}_{cr}$ as a function of temperature and frequency of the oscillating magnetic field were carried out with a SQUID magnetometer. The disordered sample $\mathbf{1}_{dis}$ was prepared by warming up the material to the isotropic phase ex-situ at 333 K for 2 minutes and quenching at 150 K inside the susceptometer. The ordered sample $\mathbf{1}_{cr}$ was prepared entirely in situ by warming up the same sample again and cooling it down slowly at a controlled rate. By doing so, any change in composition is ruled out, and the only difference from one sample to the other being the structure that is reached in the frozen state.

The temperature dependence of the in-phase (χ_M') and out-of-phase (χ_M'') susceptibilities measured at several frequencies of the two samples (see Supplementary Information) proved to be very similar to previously reported neutral double-decker complexes of terbium.[24] The $\chi_M' T$ product of the ordered and disordered samples converge above 54 K and for all the studied frequencies (0.5–1488 Hz) to approximately the same value (9.2–9.6 $emu\,mol^{-1}$). Similarly, the $\chi_M''(T)$ curves of $\mathbf{1}_{dis}$ and $\mathbf{1}_{cr}$ show qualitatively the same behavior under the above-mentioned conditions. Having a closer look at the data however, the appearance of a second drop can be observed in the $\chi_M'(T)$ curves corresponding to the disordered sample, which becomes more evident below 15 Hz. The peak

in $\chi_M''(T)$ also appears to be shifted up by about 2–3 K and the divergence at low temperature is notably higher for the disordered sample $\mathbf{1}_{dis}$ with respect to the ordered one $\mathbf{1}_{cr}$ (see the Supporting Information).

The difference between the magnetization dynamics of $\mathbf{1}_{cr}$ and $\mathbf{1}_{dis}$ samples shows up more clearly in the frequency-dependent plots of the magnetic susceptibility (Figure 1).

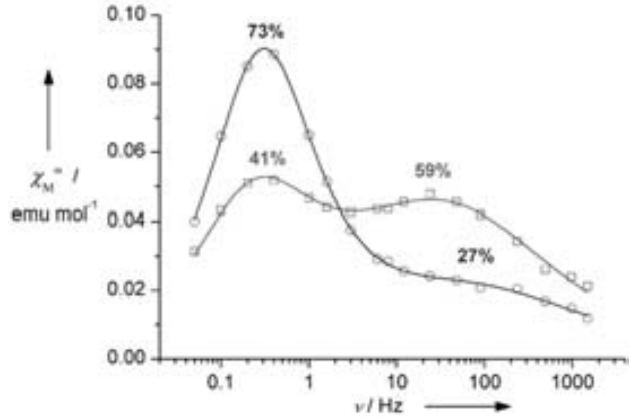

Figure 1. $\chi_M''(\upsilon)$ for the sample $\mathbf{1}_{dis}$ (□) and $\mathbf{1}_{cr}$ (○) at 25 °C. The solid lines are best fits to a Cole–Cole model.

Although, the former sample shows mainly one peak centered at 0.3 Hz in the χ_M'' versus υ plot at 25 K, the disordered sample clearly shows two peaks, which are centered at 0.3 and 40 Hz. This result is evidence of the coexistence of two different magnetic relaxation processes, meaning that the sample behaves magnetically as a mixture of two different entities. As changes in the chemical composition can be ruled out, the nature of these slow and fast relaxing species must be associated with different molecular conformations or supramolecular arrangements. These structural changes can modify the anisotropy parameters and the intermolecular dipolar interactions, both of which may play a role in determining the magnetic relaxation rates. Deciding which of these two effects dominates requires a more detailed and quantitative analysis, which we describe in what follows.

The $\chi_M''(\upsilon)$ curves were fitted as the weighted sum of two Cole–Cole functions [Eq. (1)][25]

$$\chi''(\omega) = \sum_{i=1,2} (\chi_{\tau_i} - \chi_{S_i}) x_i \frac{(\omega\tau_i)^{1-\alpha_i}\cos(\pi\alpha_i/2)}{1 + 2(\omega\tau_i)^{1-\alpha_i}\sin(\pi\alpha_i/2) + (\omega\tau_i)^{2-2\alpha_i}} \qquad (1)$$

where τ_1 and τ_2 are the relaxation times of the fast and slow magnetic species, respectively, and $x_1 = 1 - x_2$ is the fraction of the former. The results show that the percentage of slowly relaxing species was almost doubled, changing from 41 % to 73 % upon switching from $\mathbf{1}_{dis}$ to $\mathbf{1}_{cr}$, which indicates that the more slowly relaxing fraction is characteristic of the ordered or crystalline state. After letting the sample equilibrate at room temperature (i.e., in the mesophase) for several weeks, it was quenched again to 150 K using the same procedure as that used for $\mathbf{1}_{dis}$. The magnetic characterization reveals that the ratio of slowly relaxing species in this partially ordered sample $\mathbf{1}_{po}$ dropped even lower than in the disordered sample $\mathbf{1}_{dis}$ to a value of only 32 %. The reversibility of the process was checked by submitting the sample to the same thermal treatments after several months. The new data proved to be identical to the first set (see the Supporting Information).

A deeper insight into the nature of the two species, and thus also on the influence of the thermal history, is provided by the relaxation times τ_1 and τ_2, which are plotted in Figure 2 as a function of the reciprocal temperature.

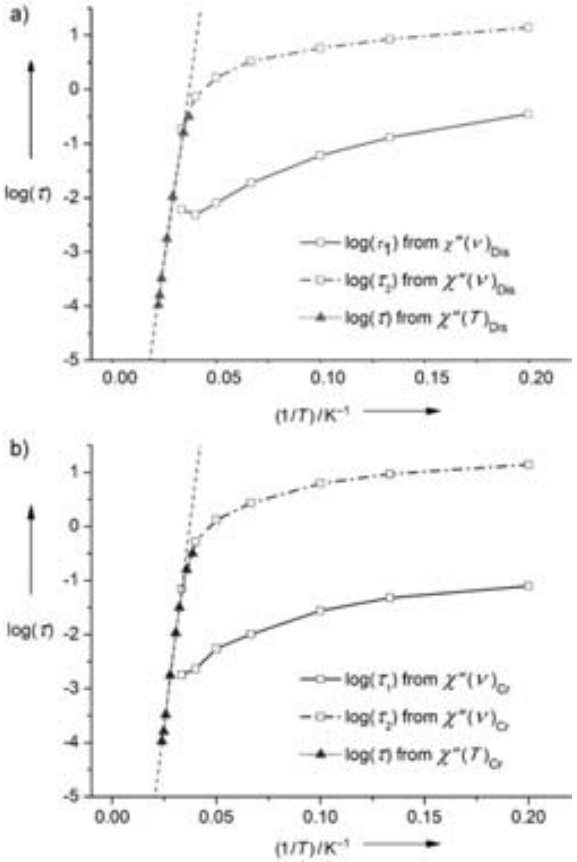

Figure 2. Log(τ) versus $1/T$ plots for a) $\mathbf{1}_{dis}$ and b) $\mathbf{1}_{cr}$. Key: —— □ log(τ_1), –•–• □ log(τ_2) obtained from $\chi_M''(\upsilon)$. ▲ log(τ) obtained from $\chi''(T)$. τ_1 and τ_2 are the relaxation times of the fast and slow species, respectively.

We find that for the two samples, log(τ_2) is proportional to $1/T$ for $T > 30$ K, and becomes weakly dependent on T (more specifically $\tau_2 \propto T^{-1}$; see the Supporting Information) at lower temperatures. This behavior shows a crossover from a thermally activated Orbach mechanism that is predominant at high temperature to a direct or phonon-induced tunneling process taking over at $T < 30$ K. The Arrhenius analysis gives $\Delta_{obs} = 4.80 \times 10^2$ cm^{-1} for sample $\mathbf{1}_{cr}$ and $\Delta_{obs} = 4.22 \times 10^2$ cm^{-1} for sample $\mathbf{1}_{dis}$, which is in agreement with previously reported barrier height in neutral terbium double-deckers.[3] A crucial observation is that the relaxation times of the two species diverge dramatically in the low-temperature or tunneling regime, where τ_1 becomes two orders of magnitude shorter than τ_2. The same applies under magnetic fields (see the

Supporting Information), which should tend to suppress the influence of dipolar interactions. The strong difference between τ_1 and τ_2 must then be associated with changes in the molecular conformation. Tunneling rates are determined by the intensity and symmetry of the off-diagonal anisotropy terms present in the spin Hamiltonian which, in its turn, reflect the local molecular symmetry and are, for this reason, extremely sensitive to even very weak distortions in the plane perpendicular to the easy magnetic axis.[26,27] Based on these observations, we assign the origin of the fast relaxing species, characteristic of the disordered $\mathbf{1}_{dis}$ sample, to intramolecular distortions.

Although the coexistence of two different relaxation processes is a common feature in some SMMs,[9,21] it is the first time that it is observed in lanthanide double-decker complexes, and it is the only system in which the ratio between these responses has been shown to be reversibly modified by simple thermal treatments.

In conclusion, we have shown the important influence that the structural environment of a single-molecule magnet has on its magnetic behavior, taking advantage of the phase behavior of the complex. A reversible change of the magnetic properties was achieved by simple heating and cooling cycles. The absence of compositional change was demonstrated by the reversibility of the process, thus providing evidence for the structural origin of the modification of the magnetic behavior, because of variations in the arrangement of the molecules. This discovery was made possible by the synthesis of a room-temperature liquid-crystalline molecular material whose phase behavior depends critically on the chiral substituents.

Received: September 7, 2009
Revised: December 3, 2009
Published online: January 27, 2010

Keywords: lanthanides · liquid crystals · magnetic properties · metallomesogens · single-molecule studies

[1] D. Gatteschi, R. Sessoli, J. Villain, *Molecular Nanomagnets*, Oxford University Press, Oxford, **2006**.
[2] See, for example: a) D. Gatteschi, L. Bogani, A. Cornia, M. Mannini, L. Sorace, R. Sessoli, *Solid State Sci.* **2008**, *10*, 1701 – 1709; b) M. Cavallini, C. Albonetti, F. Biscarini, *Adv. Mater.* **2009**, *21*, 1043 – 1053; c) E. Vucic, H. M. H. F. Sanders, F. Arena, E. Terreno, S. Aime, K. Nicolay, E. Leupold, M. Dathe, N. A. J. M. Sommerdijk, Z. A. Fayad, W. J. M. Mulder, *J. Am. Chem. Soc.* **2009**, *131*, 406 – 407; d) I. P. Suzdalev, *Russ. Chem. Rev.* **2009**, *78*, 249 – 282.
[3] N. Ishikawa, M. Sugita, T. Ishikawa, S.-y. Koshihara, Y. Kaizu, *J. Phys. Chem. B* **2004**, *108*, 11265 – 11271.
[4] N. Ishikawa, M. Sugita, T. Ishikawa, S.-y. Koshihara, Y. Kaizu, *J. Am. Chem. Soc.* **2003**, *125*, 8694 – 8695.
[5] N. Ishikawa, *Polyhedron* **2007**, *26*, 2147 – 2153.
[6] P. Gerbier, N. Domingo, J. Gomez-Segura, D. Ruiz-Molina, D. B. Amabilino, J. Tejada, B. E. Williamson, J. Veciana, *J. Mater. Chem.* **2004**, *14*, 2455 – 2460.
[7] N. Domingo, P. Gerbier, J. Gomez, D. Ruiz-Molina, D. B. Amabilino, J. Tejada, J. Veciana, *Polyhedron* **2003**, *22*, 2355 – 2358.
[8] C. Train, R. Gheorghe, V. Krstic, L.-M. Chamoreau, N. S. Ovanesyan, G. L. J. A. Rikken, M. Gruselle, M. Verdaguer, *Nat. Mater.* **2008**, *7*, 729 – 734.
[9] a) E. Terazzi, C. Bourgogne, R. Welter, J.-L. Gallani, D. Guillon, G. Rogez, B. Donnio, *Angew. Chem.* **2008**, *120*, 500 – 505; *Angew. Chem. Int. Ed.* **2008**, *47*, 490 – 495.
[10] a) M. Seredyuk, A. B. Gaspar, V. Ksenofontov, Y. Galyametdinov, M. Verdaguer, F. Villain, P. Gütlich, *Inorg. Chem.* **2008**, *47*, 10232 – 10245; b) A. B. Gaspar, M. Seredyuk, P. Gütlich, *Coord. Chem. Rev.* **2009**, *253*, 2399 – 2413; c) A. B. Gaspar, M. Seredyuk, P. Gütlich, *J. Mol. Struct.* **2009**, *924–926*, 9 – 19.
[11] E. Gomar-Nadal, C. Rovira, D. B. Amabilino, *Tetrahedron* **2006**, *62*, 3370 – 3379.
[12] A. G. M. Barrett, G. R. Hanson, A. J. P. White, D. J. Williams, A. S. Micallef, *Tetrahedron* **2007**, *63*, 5244 – 5250.
[13] T. Gross, F. Chevalier, J. S. Lindsey, *Inorg. Chem.* **2001**, *40*, 4762 – 4774.
[14] A. De Cian, M. Moussavi, J. Fischer, R. Weiss, *Inorg. Chem.* **1985**, *24*, 3162 – 3167.
[15] F. Nekelson, H. Monobe, Y. Shimizu, *Chem. Commun.* **2006**, 3874 – 3876.
[16] F. Nekelson, H. Monobe, M. Shiro, Y. Shimizu, *J. Mater. Chem.* **2007**, *17*, 2607 – 2615.
[17] F. Nekelson, H. Monobe, Y. Shimizu, *Mol. Cryst. Liq. Cryst.* **2007**, *479*, 205 – 211.
[18] K. Ban, K. Nishizawa, K. Ohta, A. M. Van de Craats, J. M. Warman, I. Yamamoto, H. Shirai, *J. Mater. Chem.* **2001**, *11*, 321 – 331.
[19] a) K. Binnemans, J. Sleven, S. De Feyter, F. C. De Schryver, B. Donnio, D. Guillon, *Chem. Mater.* **2003**, *15*, 3930 – 3938; b) K. Binnemans, C. Gorller-Walrand, *Chem. Rev.* **2002**, *102*, 2303 – 2346.
[20] Z. Belarbi, C. Sirlin, J. Simon, J. J. Andre, *J. Phys. Chem.* **1989**, *93*, 8105 – 8110.
[21] S. M. J. Aubin, Z. Sun, H. J. Eppley, E. M. Rumberger, I. A. Guzei, K. Folting, P. K. Gantzel, A. L. Rheingold, G. Christou, D. N. Hendrickson, *Inorg. Chem.* **2001**, *40*, 2127 – 2146.
[22] a) N. Ishikawa, M. Sugita, W. Wernsdorfer, *Angew. Chem.* **2005**, *117*, 2991 – 2995; *Angew. Chem. Int. Ed.* **2005**, *44*, 2931 – 2935.
[23] F. Branzoli, P. Carretta, M. Filibian, G. Zoppellaro, M. J. Graf, J. R. Galán-Mascarós, O. Fuhr, S. Brink, M. Ruben, *J. Am. Chem. Soc.* **2009**, *131*, 4387 – 4396.
[24] N. Ishikawa, M. Sugita, N. Tanaka, T. Ishikawa, S.-y. Koshihara, Y. Kaizu, *Inorg. Chem.* **2004**, *43*, 5498 – 5500.
[25] K. S. Cole, R. H. Cole, *J. Chem. Phys.* **1941**, *9*, 341 – 351.
[26] A. Cornia, R. Sessoli, L. Sorace, D. Gatteschi, A. L. Barra, C. Daiguebonne, *Phys. Rev. Lett.* **2002**, *89*, 257201.
[27] M. Evangelisti, F. Luis, F. L. Mettes, N. Aliaga, G. Aromí, J. J. Alonso, G. Christou, L. J. de Jongh, *Phys. Rev. Lett.* **2004**, *93*, 117202.

Angewandte Chemie
Eine Zeitschrift der Gesellschaft Deutscher Chemiker

Supporting Information

69451 Weinheim, Germany

A Liquid-Crystalline Single-Molecule Magnet with Variable Magnetic Properties**

Mathieu Gonidec, Fernando Luis, Àlex Vílchez, Jordi Esquena, David B. Amabilino, and Jaume Veciana**

anie_200905007_sm_miscellaneous_information.pdf

1. Experimental techniques

^{1}H NMR spectra were recorded on a Bruker Avance DPX-360 spectrometer. The non deuterated solvent peak was used as an internal reference to calibrate the spectra ($CDCl_3$, 7.26 ppm).

Mass spectra were recorded on a Bruker Ultraflex LDI-TOF spectrometer.

UV-Vis absorption spectra were collected on a Varian Cary 5000 spectrometer and Circular Dichroism data were recorded on a Jasco J275 spectropolarimeter.

The phase transition temperatures enthalpies and entropies were measured by Differential Scanning Calorimetry on a Mettler-Toledo DSC-822e/400 calorimeter.

Small Angle X-ray Scattering data were recorded using a S3 MICRO instrument (Hecus X-ray Systems, Graz, Austria) with point beam focalization.

Polarized Optical Micrographs were recorded with an Olympus DP20 camera on an Olympus BX51 microscope. The temperature was controlled by a Linkam Scientific TMS94 control unit.

Magnetic susceptibility measurements were done on a Quantum Design MPMS-XL-5 magnetometer equipped with a SQUID sensor. The sample consisted of 37 mg of complex **1** introduced in a gelatine capsule. The magnetic signal of this sample holder was measured separately and then subtracted from the experimental data. In any case, it is completely negligible with respect to the sample signal in the experimental conditions (temperature and magnetic field) of our experiments.

2. Synthetic procedures

1,2-dibromo-4,5-bis((S)-2-(dodecyloxy)propoxy)benzene:

To a suspension of K_2CO_3 (22.3 mmol, 3.08 g, 5 eq.) in DMF (44 mL) was added 4,5-dibromocatechol (4.46 mmol, 1.19 g, 1 eq.). The mixture was stirred at 40 ºC for 15 minutes before addition of (S)-1-bromo-2-dodecyloxypropane (8.92 mmol, 2.74 g, 2 eq.). The reaction mixture was then stirred at 75 ºC overnight. Water (100 mL) was added to precipitate the reaction product. After filtration, the solids were dissolved in CH_2Cl_2, dried over $MgSO_4$ and the solvent evaporated. The residue was purified by column chromatography of silicagel using toluene as an eluent. 1,2-dibromo-4,5-bis((S)-2-(dodecyloxy)propoxy)benzene was obtained as a white crystalline solid (2.7 g, 84%). ^{1}H NMR 360 MHz, ($CDCl_3$): δ 7.09 (Ar-*H*, s, 2H), 3.95 (Ar-O-*CH_2*, m, 2H), 3.83 (Ar-O-*CH_2* and *CH*-CH_3, m, 4H), 3.54 (O-*CH_2*-CH_2, t, J=6.7 Hz, 4H), 1.55 (O-CH_2-*CH_2*, m, 4H), 1.39-1.13 (CH-*CH_3* and O-CH_2-CH_2-*$(CH_2)_9$*-CH_3, m, 42H), 0.88 (CH_2-*CH_3*, t, J=6.6 Hz, 6H) ppm.

4,5-bis((S)-2-(dodecyloxy)propoxy)phthalonitrile:

In a dry round-bottom flask under argon were suspended 1,2-dibromo-4,5-bis((S)-2-(dodecyloxy) propoxy)benzene (3.75 mmol, 2.70 g, 1 eq.), tetrakis(triphenylphosphine)palladium(0) (1.04 mmol, 1.20 g, 0.28 eq.) and zinc cyanide (4.50 mmol, 0.528 g, 1.2 eq.) in DMF (7.5 mL). The mixture was then heated at 120 ºC for 2 h after which ammonia (37%, 50 mL) was added, and the resulting precipitate was filtrated, washed with more ammonia (100 mL) and purified by column chromatography of silicagel using toluene as an eluent affording 4,5-bis((S)-2-(dodecyloxy)propoxy)phthalonitrile (1.9 g, 83%) as a white solid. ^{1}H NMR 360 MHz, ($CDCl_3$): δ 7.18 (Ar-*H*, s, 2H), 4.04 (Ar-O-*CH_2*, m, 2H), 3.95 (Ar-O-*CH_2*, m, 2H), 3.95 (*CH*-CH_3, m, 2H), 3.54 (O-*CH_2*-CH_2, m, 4H), 1.55 (O-CH_2-*CH_2*, m, 4H), 1.39-1.14 (CH-*CH_3* and O-CH_2-CH_2-*$(CH_2)_9$*-CH_3, m, 42H), 0.88 (CH_2-*CH_3*, t, J=6.6 Hz, 6H) ppm.

2,3,9,10,16,17,23,24-octakis-((S)-2-(dodecyloxy)propoxy)-phthalocyanine:

In a round bottom flask under nitrogen was added lithium (24.5 mmol, 170 mg, 60 eq.) in n-hexanol (10 mL). The mixture was heated at 100 ºC and stirred until complete disappearance of the lithium. 4,5-bis((S)-2-(dodecyloxy)propoxy)phthalonitrile (1.63 mmol, 1.00 g, 4 eq.) was added and the mixture was stirred at 150 ºC overnight. Methanol was added, and the dark green waxy residue was decanted and washed several times with warm methanol, dissolved in hexane and the insoluble impurities were filtered out. The final residue was purified by repeated size exclusion chromatography (BioBeads SX1) using toluene as an eluent, affording a waxy dark green solid (197 mg, 20%). ^{1}H NMR 360 MHz, ($CDCl_3$): δ 8.08 (N-*H*, s, 1H), 4.67 (N-*H*, s, 1H), 4.08 (Ar-O-*CH_2*, m, 8H), 3.96 (Ar-O-*CH_2*, m, 8H), 3.85 (*CH*-CH_3, m, 8H), 3.57 (O-*CH_2*-CH_2, m, 16H), 1.56 (O-CH_2-*CH_2*, m, 16H), 1.43-1.14 (CH-*CH_3* and O-CH_2-CH_2-*$(CH_2)_9$*-CH_3, m, 168H), 0.87 (CH_2-*CH_3*, m, 24H) ppm. MS *m*/*z*: 2454 (M+), UV-Vis(log(ε)): 700(4.57), 661(4.45), 646(4.05), 636(3.98), 599(3.74), 424(3.86), 354(4.17) nm, Col_h142 I

bis-(2,3,9,10,16,17,23,24-octakis-((S)-2-(dodecyloxy)propoxy)-phthalocyaninato)terbium(III):

In a dry schlenk tube under argon were introduced 2,3,9,10,16,17,23,24-octakis-((S)-2-(dodecyloxy)propoxy)-phthalocyanine (0.031 mmol, 75 mg, 2 eq.) and anhydrous terbium chloride (7.6 µmol, 2.0 mg, 0.5 eq.). The solids were degassed for 10 minutes under vacuum, after which the mixture was cooled to 0 ºC with an ice bath. diglyme (3 mL) and N,N-bis(trimethylsilyl)lithium amide 1 M solution in THF (67 µmol, 67 µL, 4.4 eq.) were added with a syringe. The reaction was then stirred at 0 ºC for 1 h and refluxed for 2 h. After cooling down, methanol was added, and the dark green waxy residue was decanted and washed several times with warm methanol, dissolved in hexane and the insoluble impurities were filtered out. The residue was purified by repeated size exclusion chromatography (BioBeads SX1) using toluene as an eluent, affording a waxy dark green solid (52 mg, 67%). MS *m*/*z*: 5068 (M-), UV-Vis(log(ε)): 668(5.08), 605(4.40), 581(4.18), 483(4.47), 369(4.99), 337(4.90) nm, m.p.: -12 ºC, Col_h 31 I

3. Mass spectroscopy

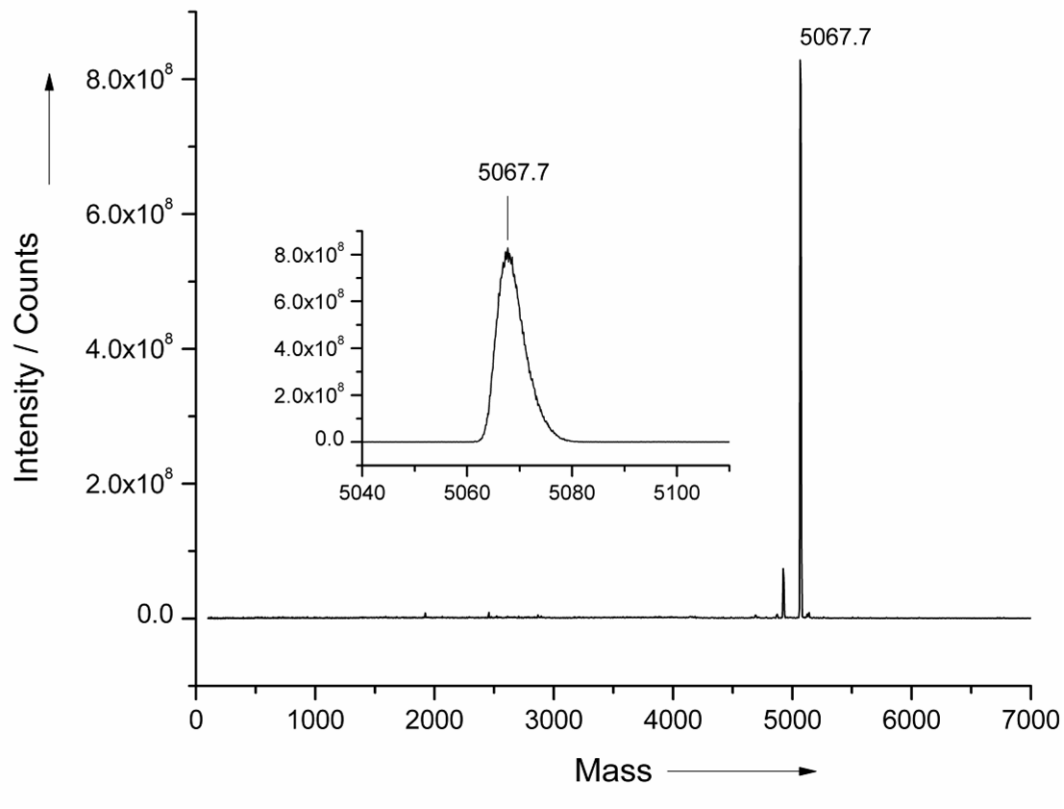

LDI-TOF MS of the terbium double-decker complex **1** with negative polarization , and enlargement of the same (inset)

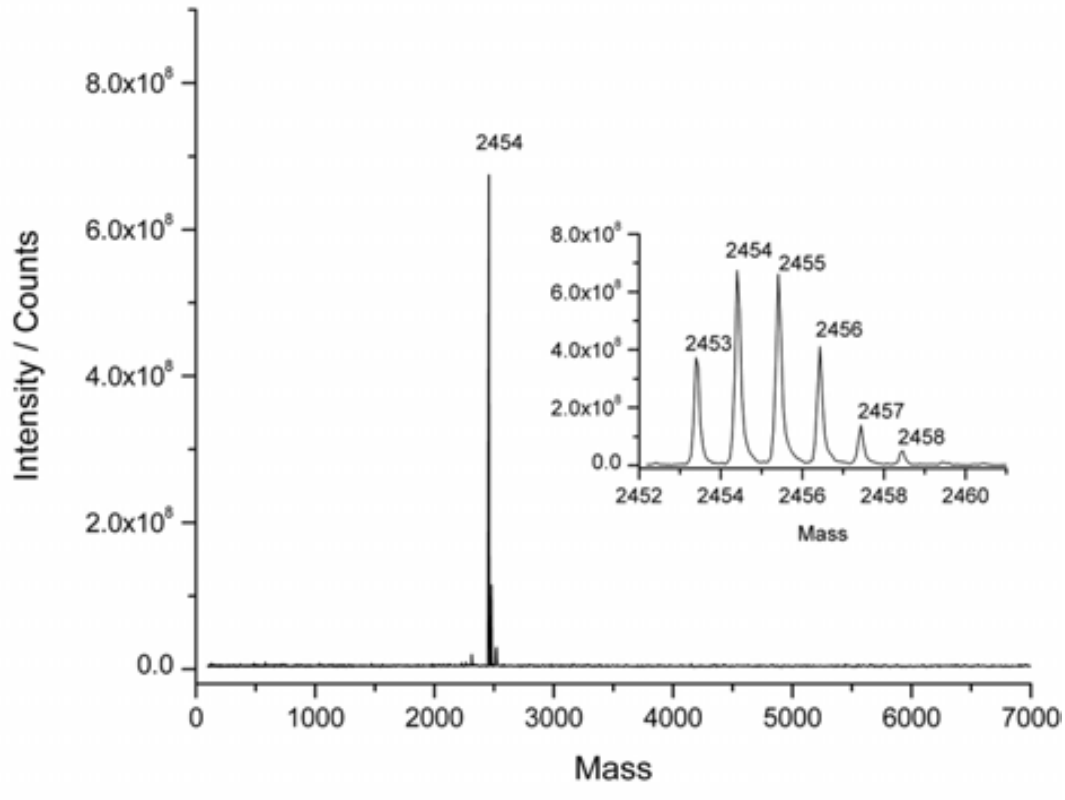

LDI-TOF MS of the free base phthalocyanine **5** with positive polarization, and enlargement of the same (inset)

4. Optical characterizations

4.1 UV-Vis spectra

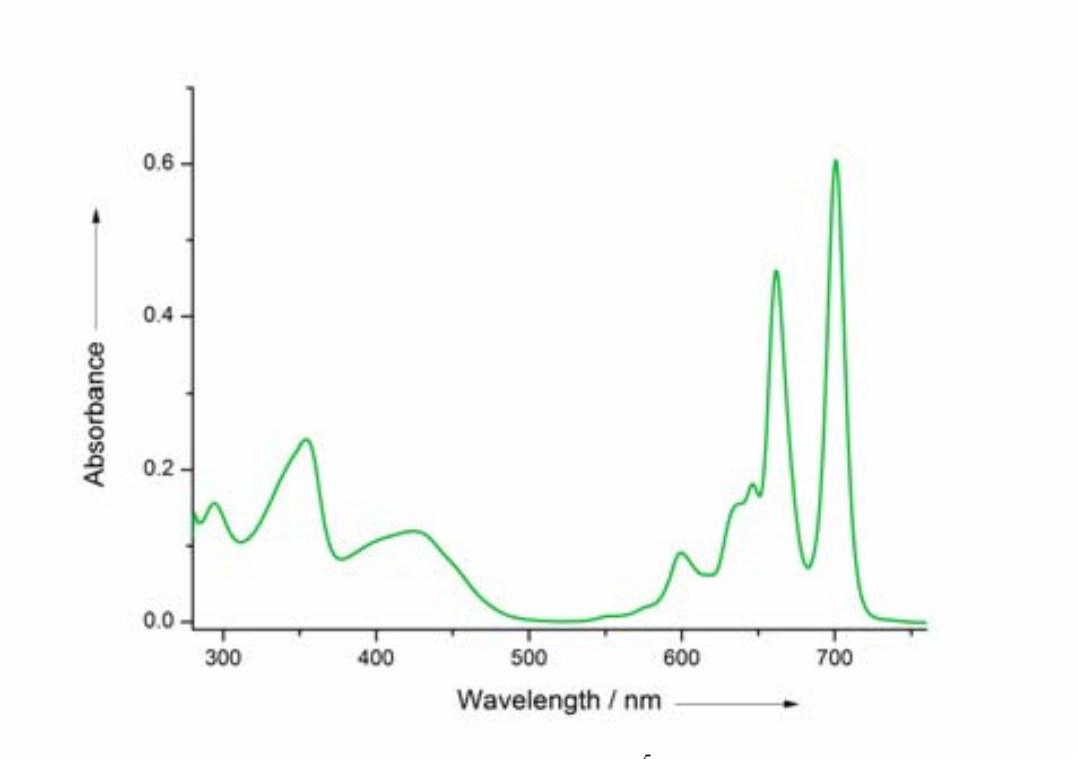

UV-Vis spectrum of a 1.63×10^{-5} M solution
of the metal free phthalocyanine **5** in toluene

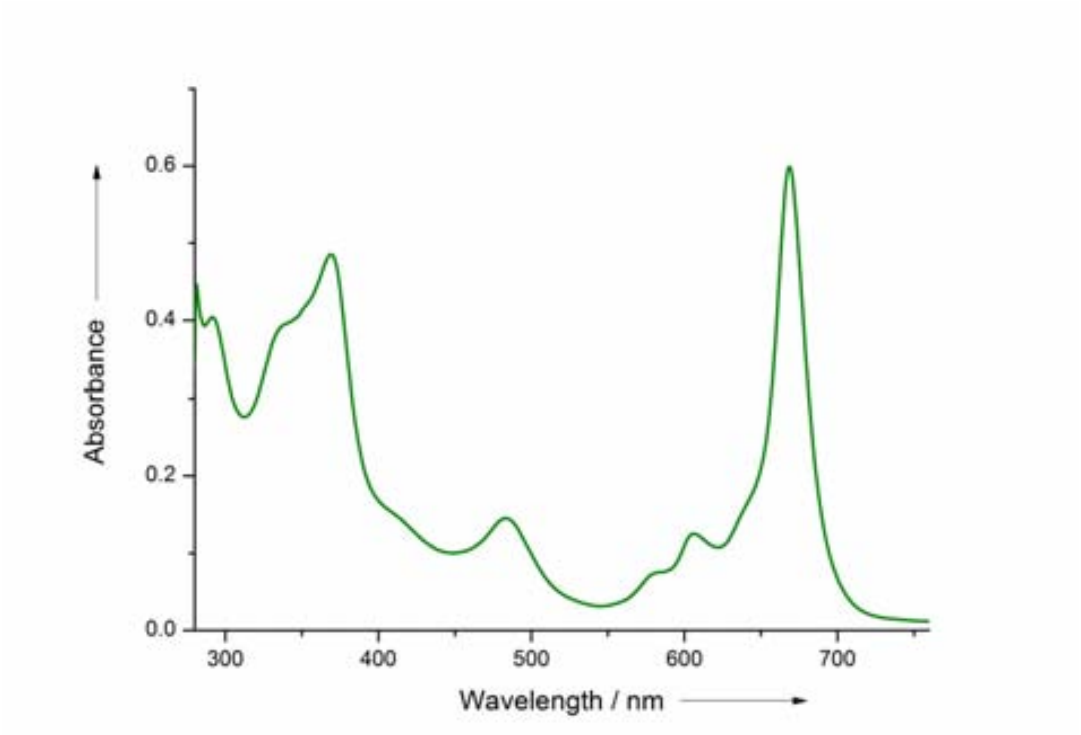

UV-Vis spectrum of a 5.00×10^{-6} M solution
of the terbium double-decker complex **1** in toluene

4.2 Circular dichroism spectra

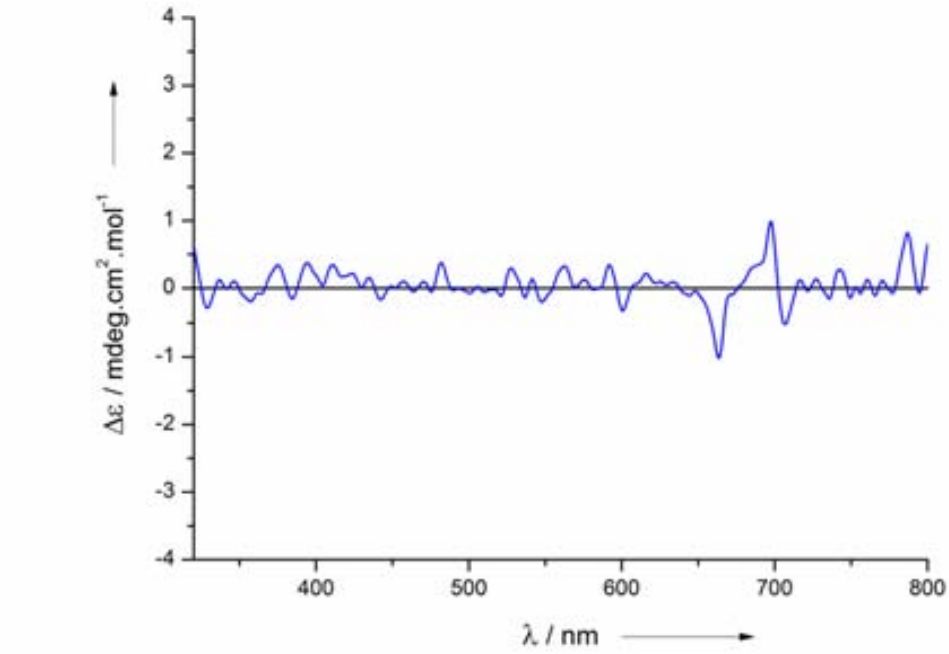

CD spectrum of the free base phthalocyanine **5** in toluene

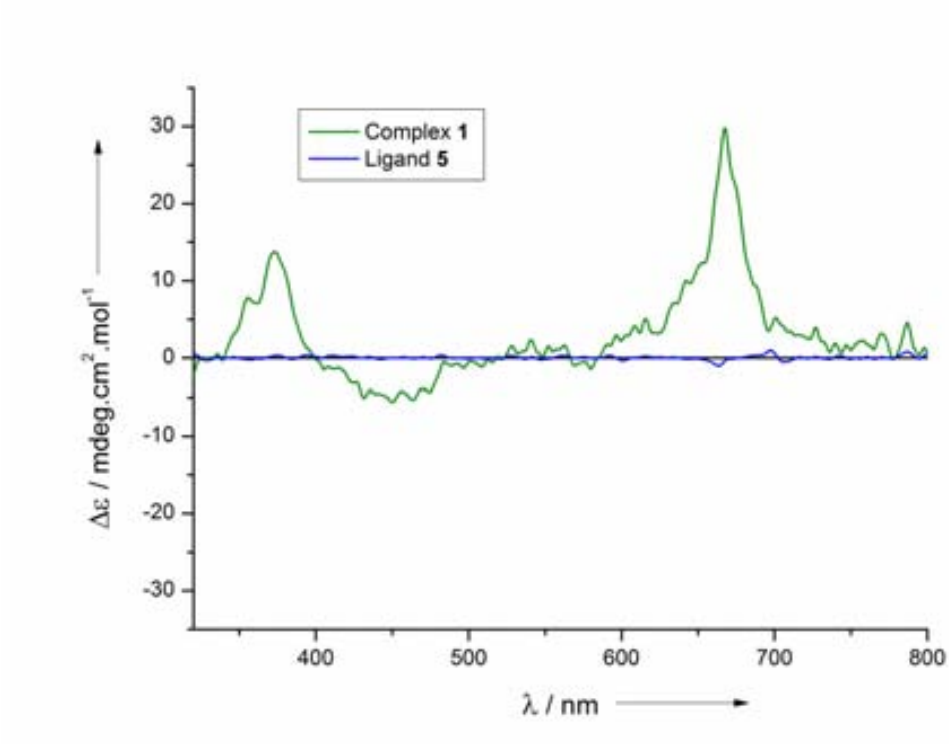

CD spectra of the free base phthalocyanine **5** and the corresponding terbium double-decker complex **1** in toluene

5. Differential scanning calorimetry

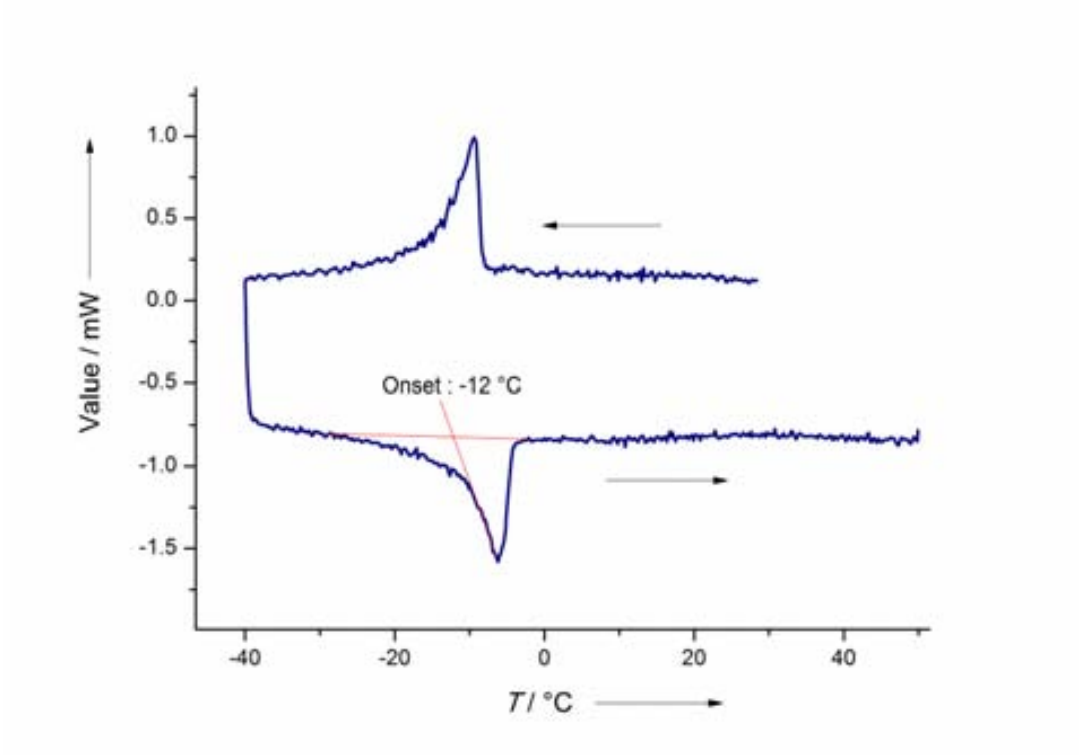

DSC trace of the terbium double-decker complex **1** with cooling and heating rates of 1 ºC.min^{-1}

6. Small angle X-ray scattering

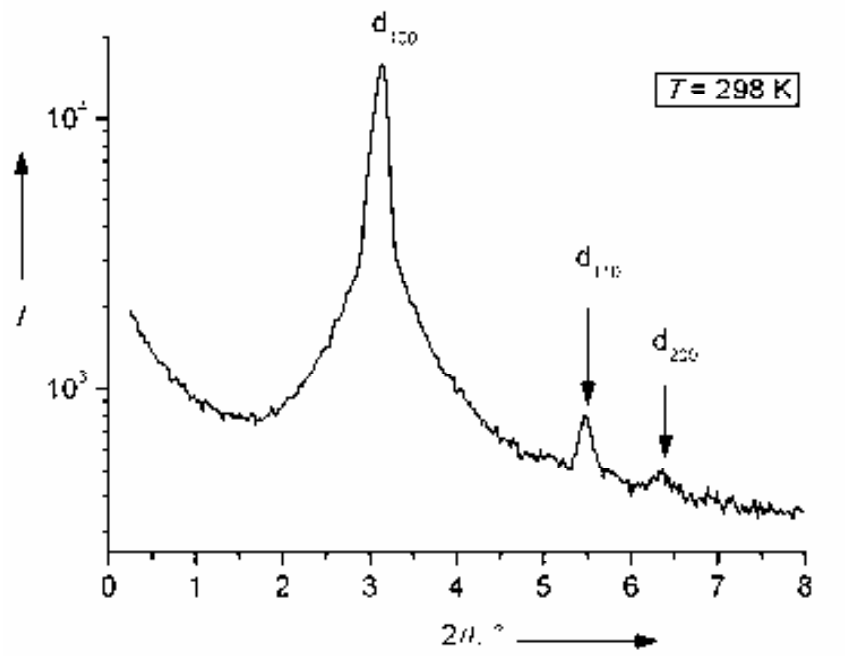

SAXS diffraction pattern of the hexagonal columnar mesophase of **1** at 298 K.

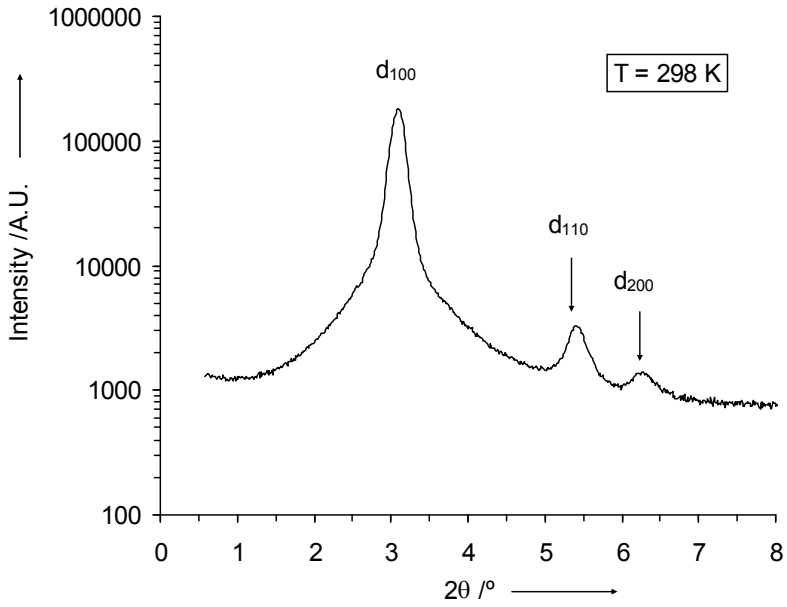

SAXS diffraction pattern of the free base phthalocyanine **5** at 298 K. The repeat distance of the hexagonal columnar mesophase is 3.2 nm, which is the same than for the terbium double-decker complex **1**, within the experimental error.

7. Cooling scheme

The "amorphous" $\mathbf{1}_{Dis}$ sample was quenched very rapidly from the liquid state to 150 K. The temperature of the SQUID's sample chamber was first set to 150 K and the chamber was left open to air, under a strong Helium gas flow that avoids any condensation of air from the atmosphere. Then, the sample was liquefied by warming it up to above 323 K outside the cryostat. Finally, the sample was rapidly introduced inside the chamber. The thermalization to 150 K occurs within timescales shorter than 1-2 minutes. The temperature history recorded in the slow procedure, devised to obtain a crystalline material, is attached below.

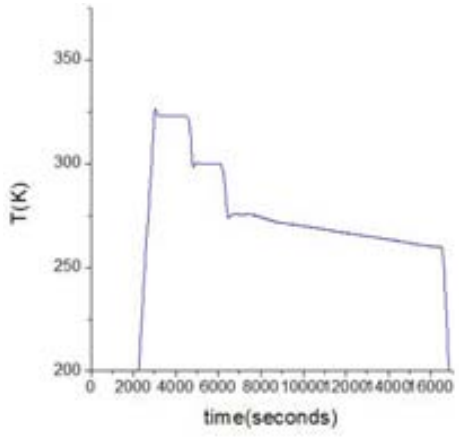

The melting temperature was crossed at a very slow rate (of 0.1 K/minute) and the sample was left to stabilize for half an hour in the liquid phase and the mesophase.

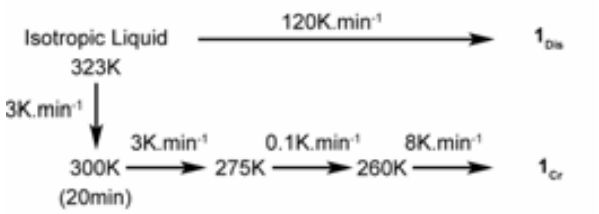

Cooling rates for the preparation of samples $\mathbf{1}_{Dis}$ and $\mathbf{1}_{Cr}$

8. Magnetic properties

8.1 ac magnetic susceptibilities

8.1.1 Sample $\mathbf{1}_{Cr}$

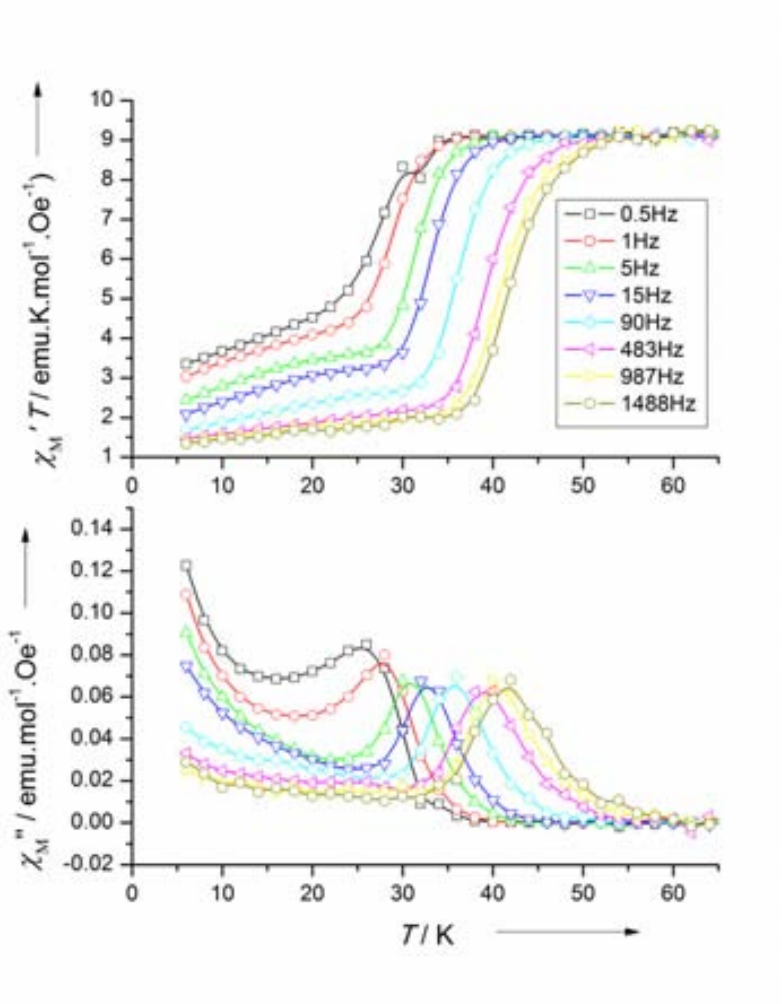

In phase (up) and out of phase (down) ac magnetic susceptibilities of $\mathbf{1}_{Cr}$ versus temperature at 0.5, 1, 5, 15, 90, 483, 987 and 1488 Hz

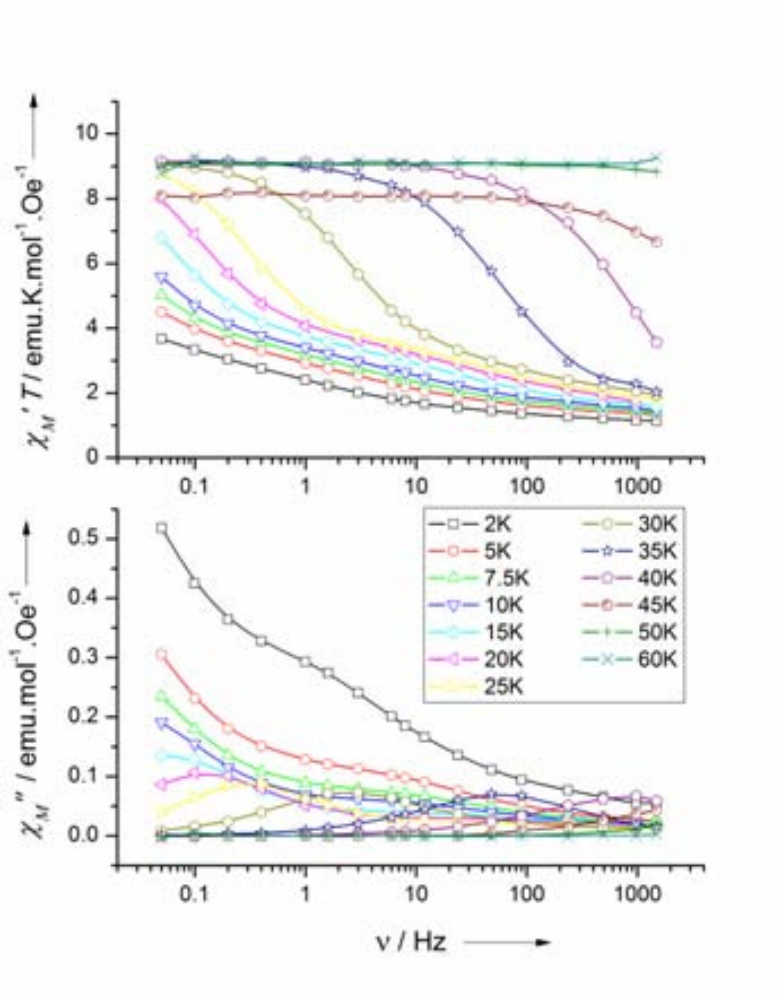

In phase (up) and out of phase (down) ac magnetic susceptibilities of $\mathbf{1_{Cr}}$ versus frequency of the magnetic field at 2, 5, 7.5, 10, 15, 20, 25, 30, 35, 40, 45, 50 and 60 K

8.1.2 Sample $\mathbf{1}_{Dis}$

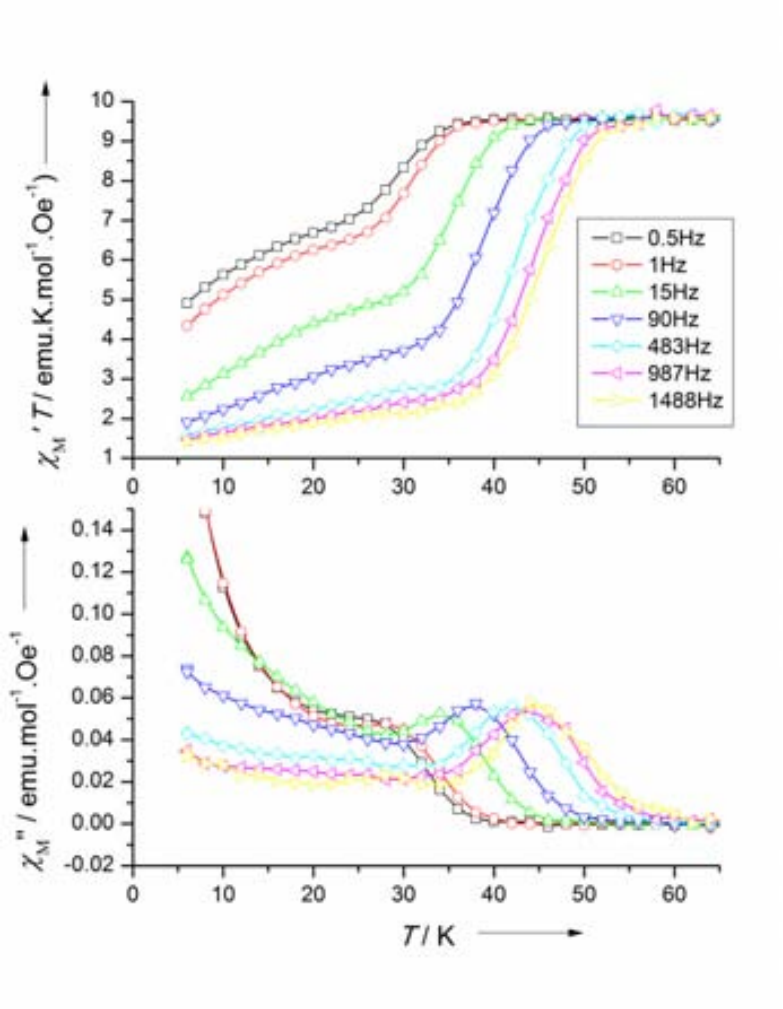

In phase (up) and out of phase (down) ac magnetic susceptibilities of $\mathbf{1}_{Dis}$ versus temperature at 0.5, 1, 15, 90, 483, 987 and 1488 Hz

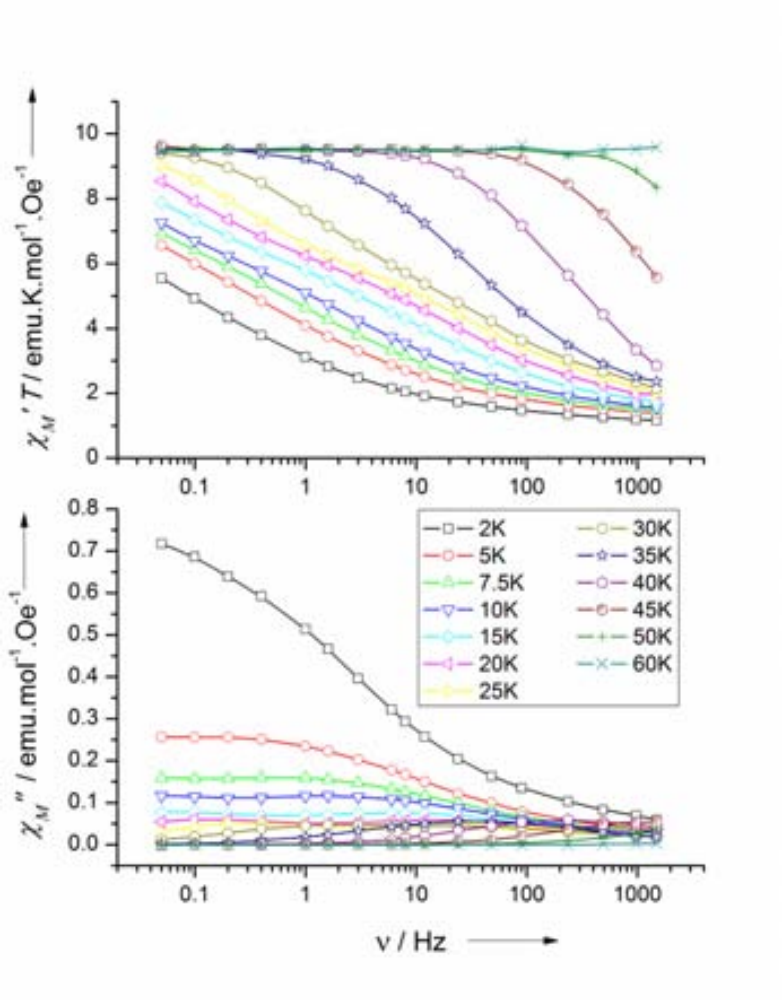

In phase (up) and out of phase (down) ac magnetic susceptibilities of $\mathbf{1}_{\mathbf{Dis}}$ versus frequency of the magnetic field at 2, 5, 7.5, 10, 15, 20, 25, 30, 35, 40, 45, 50 and 60 K

8.2 Fitting of the magnetic susceptibilities

8.2.1 Fitted ac magnetic susceptibilities of 1_{Cr}, 1_{Dis}, $1'_{Cr}$, $1'_{Dis}$ and 1_{PO}

The magnetic susceptibility data were fitted as the sum of two independent Cole-Cole functions using the following equations:

$$\chi''(\omega) = f(\chi_{T1} - \chi_{S1}) \frac{(\omega\tau_1)^{1-\alpha_1} \cos(\pi\alpha_1/2)}{1 + 2(\omega\tau_1)^{1-\alpha_1} \sin(\pi\alpha_1/2) + (\omega\tau_1)^{2-2\alpha_1}} + (1-f)(\chi_{T2} - \chi_{S2}) \frac{(\omega\tau_2)^{1-\alpha_2} \cos(\pi\alpha_2/2)}{1 + 2(\omega\tau_2)^{1-\alpha_2} \sin(\pi\alpha_2/2) + (\omega\tau_2)^{2-2\alpha_2}}$$

$$\chi'(\omega) = f\left(\chi_{S1} + (\chi_{T1} - \chi_{S1}) \frac{1 + (\omega\tau_1)^{1-\alpha_1} \sin(\pi\alpha_1/2)}{1 + 2(\omega\tau_1)^{1-\alpha_1} \sin(\pi\alpha_1/2) + (\omega\tau_1)^{2-2\alpha_1}}\right) + (1-f)\left(\chi_{S2} + (\chi_{T2} - \chi_{S2}) \frac{1 + (\omega\tau_2)^{1-\alpha_2} \sin(\pi\alpha_2/2)}{1 + 2(\omega\tau_2)^{1-\alpha_2} \sin(\pi\alpha_2/2) + (\omega\tau_2)^{2-2\alpha_2}}\right)$$

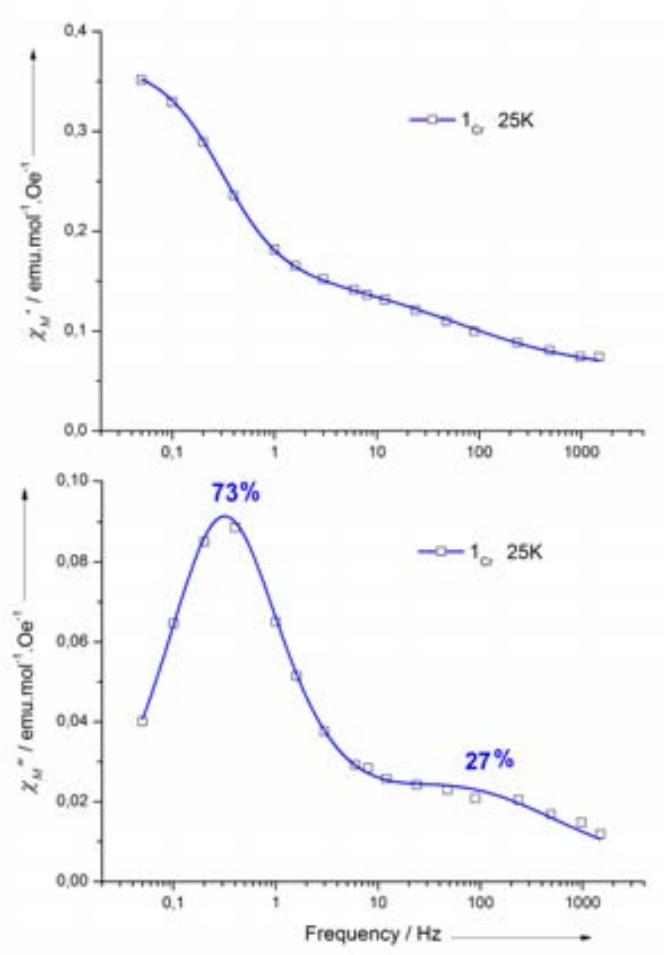

In phase (up) and out of phase (down) ac magnetic susceptibilities of $\mathbf{1_{Cr}}$ versus frequency of the magnetic field at 25K. The solid lines are best fit to a Cole-Cole model.

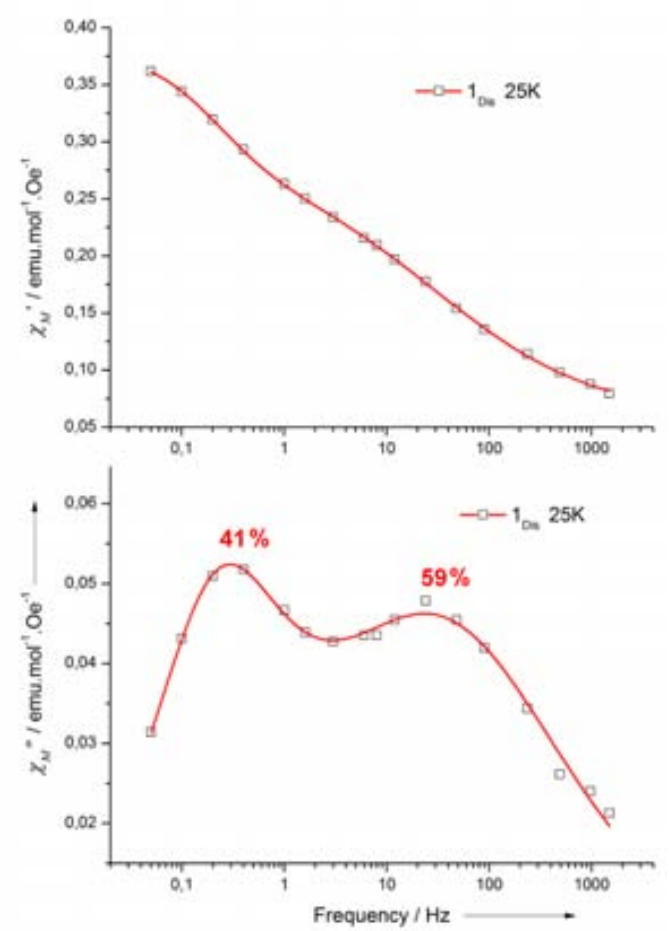

In phase (up) and out of phase (down) ac magnetic susceptibilities of $\mathbf{1_{Dis}}$ versus frequency of the magnetic field at 25K. The solid lines are best fit to a Cole-Cole model.

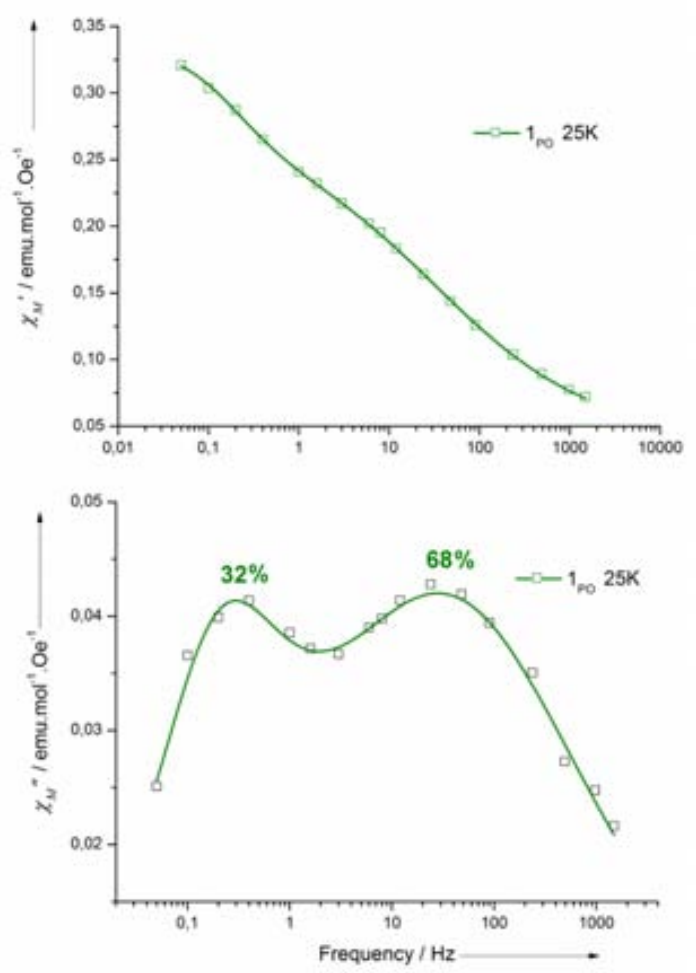

In phase (up) and out of phase (down) ac magnetic susceptibilities of $\mathbf{1_{PO}}$ versus frequency of the magnetic field at 25K. The solid lines are best fit to a Cole-Cole model.

To demonstrate the reversibility of the process, the sample, one year after the first measurements, was subjected to the same heating treatments, affording samples **1'$_{Cr}$** and **1'$_{Dis}$** :

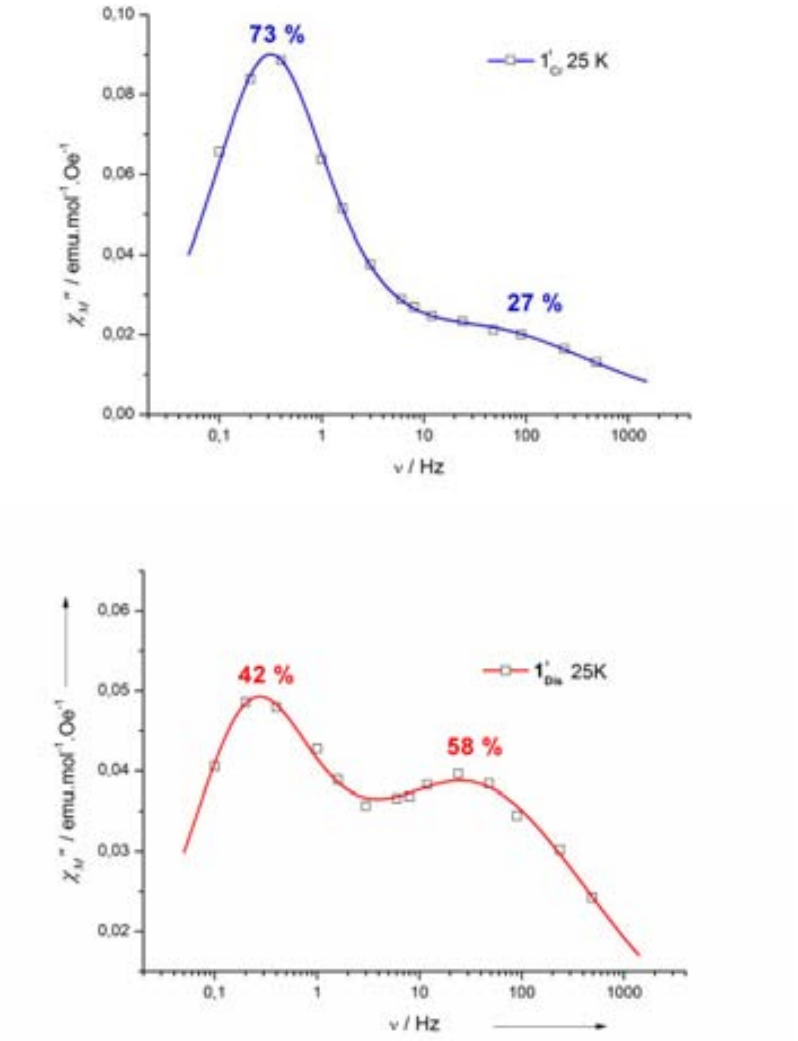

Out of phase ac magnetic susceptibility of **1'$_{Cr}$** (up) and **1'$_{Dis}$** (down) versus frequency of the magnetic field at 25K. The solid lines are best fit to a Cole-Cole model.

8.2.2 Fitting parameters

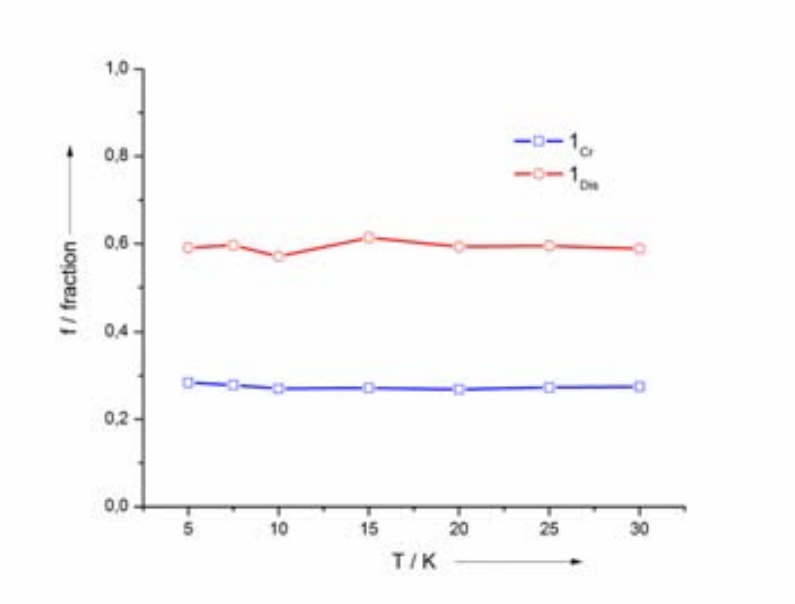

Fitted fraction of the fast process, as a function of temperature for samples **1**$_{Dis}$ (circles) and **1**$_{Cr}$ (squares)

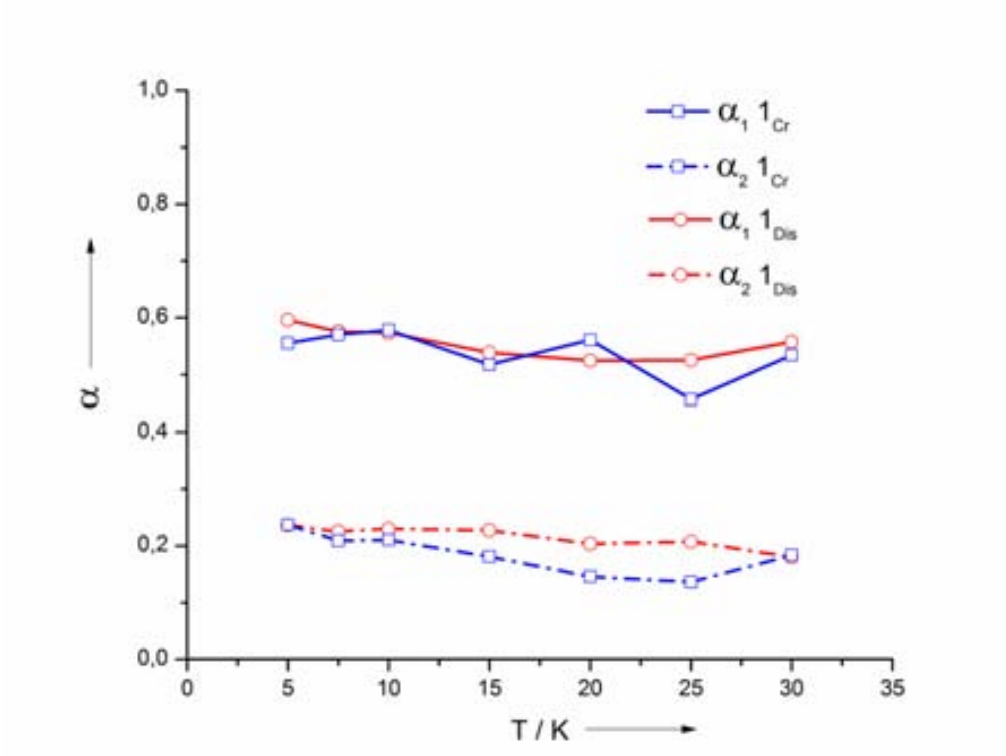

Fitted broadness parameters alpha1 and alpha2 of the fast and slow processes, respectively, as a function of temperature for samples **1**$_{Dis}$ (circles) and **1**$_{Cr}$ (squares)

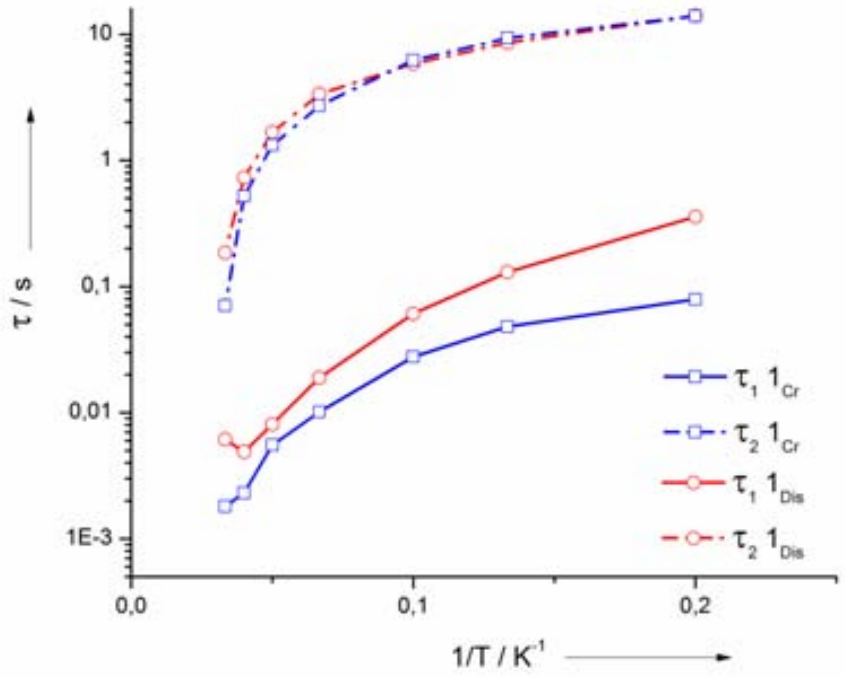

Fitted τ_1 and τ_2 of the fast and slow processes, respectively, as a function of 1/T for samples $\mathbf{1_{Dis}}$ (circles) and $\mathbf{1_{Cr}}$ (squares)

8.3 Plot of τ(T) and Arrhenius analysis

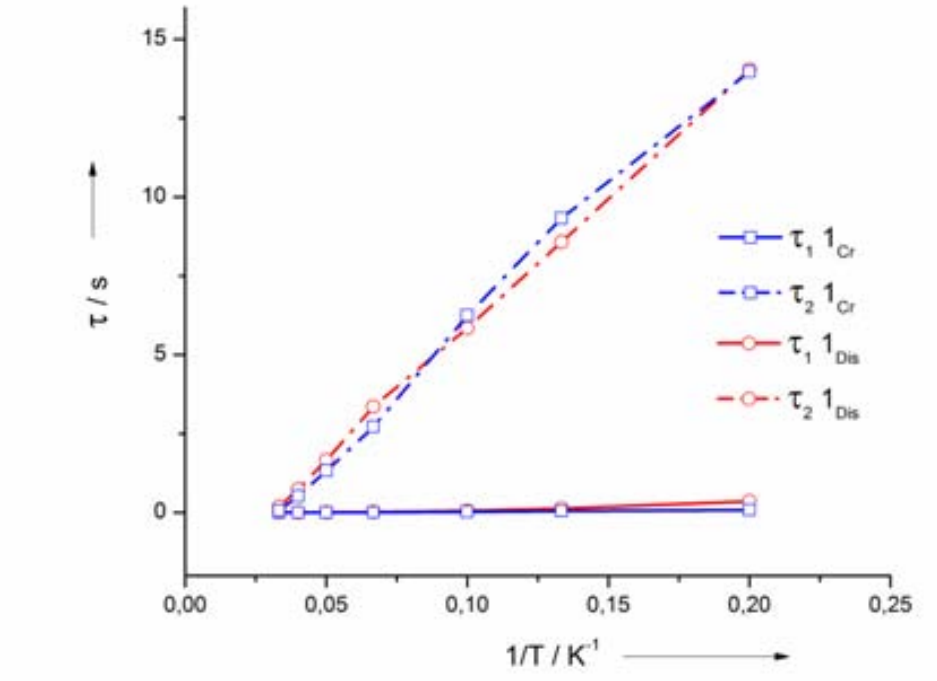

Linear plot of the fitted parameters τ_1 and τ_2 as a function of 1/T for samples 1_{Dis} (circles) and 1_{Cr} (squares) for 5 K < T < 30 K. In this range of temperature, τ_2 (dashed line) is clearly linear in 1/T.

	Δ_{obs} (cm^{-1})	τ_0^{-1} (s^{-1})
1_{Cr}	4.80×10^2	1.44×10^{11}
1_{Dis}	4.22×10^2	5.85×10^9
Ishikawa's $[Pc_2Tb]^0$	4.10×10^2 [a]	6.80×10^8 [a]

Table of the calculated observed barrier Δ_{obs} and pre-exponential factor τ_0^{-1} for the Arrhenius plot of samples 1Cr, 1Dis, and comparison with previously reported values.

[a] N. Ishikawa, M. Sugita, T. Ishikawa, S.-y. Koshihara, Y. Kaizu, *The J. Phys. Chem. B* **2004**, *108*, 11265-11271.

8.4 Equilibrium susceptibilities

The plot below compares the Curie-Weiss fits made for the equilibrium susceptibilities (measured above the blocking temperatures for 90 Hz) of the samples $\mathbf{1}_{\mathbf{Cr}}$ and $\mathbf{1}_{\mathbf{Dis}}$.

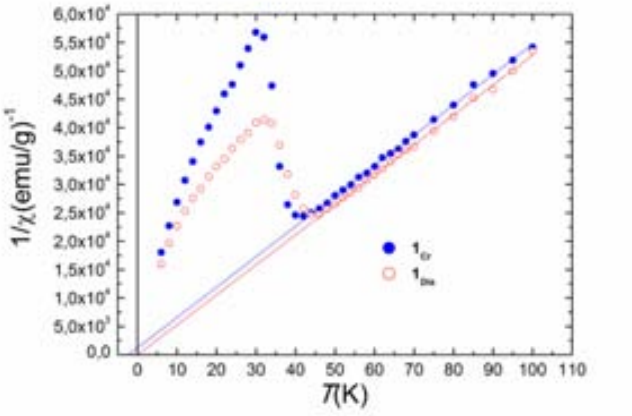

The Curie constants $C(\mathbf{1}_{\mathbf{crys}})$ and $C(\mathbf{1}_{\mathbf{dis}})$ estimated from the fits are virtually the same whereas, by contrast, the Weiss temperature θ, which provides a measure of the strength of intermolecular magnetic interactions, does depend on the thermal treatment. The typical dipolar bias fields, which in a mean field approximation can be taken as proportional to θ, are found to be smaller in the disordered sample $\mathbf{1}_{\mathbf{Dis}}$. This is not surprising, as the molecular packing is expected to be substantially different in the two samples and dipolar interactions, with their long-range character, are sensitive to changes in the intermolecular distances and the crystalline symmetry.

8.5 Field dependence

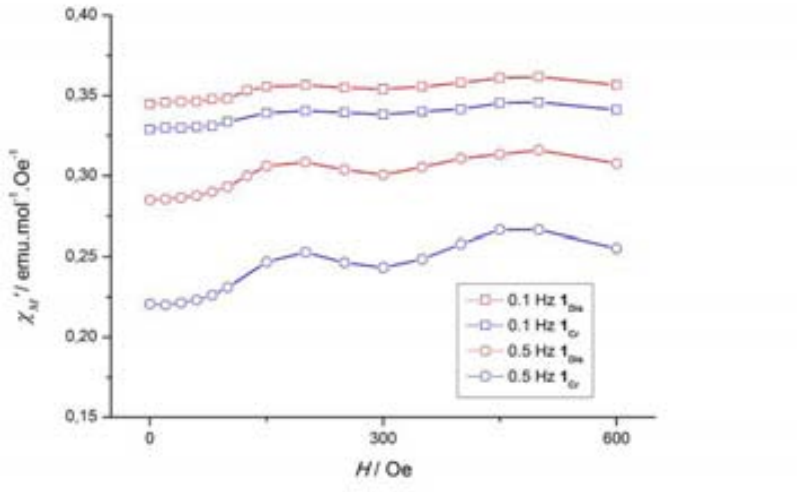

Real component of the ac magnetic susceptibility of sample $\mathbf{1}_{\mathbf{Dis}}$ and $\mathbf{1}_{\mathbf{Cr}}$ measured ar 25 K, at 0.1 and 0.5 Hz as a function of DC magnetic field. The plot shows that, at any frequency and at all fields below 600 Oe, the molecular spins are farther from equilibrium in the $\mathbf{1}_{\mathbf{Cr}}$ sample than they are in the $\mathbf{1}_{\mathbf{Dis}}$ sample.

8.6 3D Graphs of 1_{Cr} and 1_{Dis}

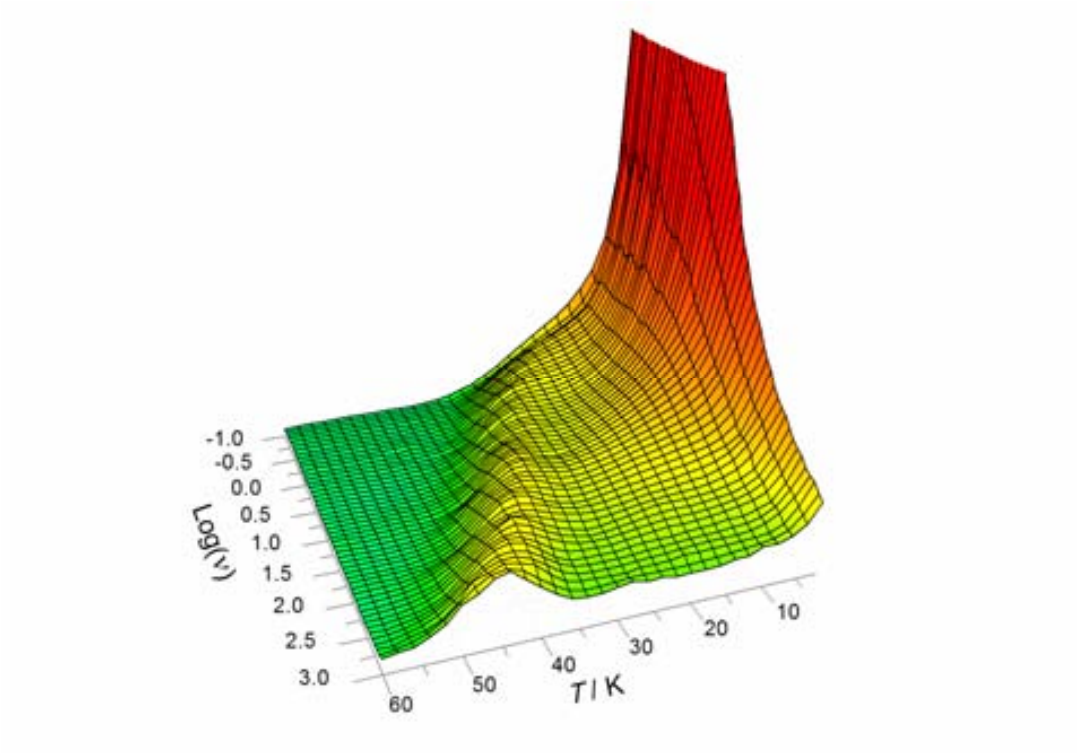

3D graph of $\chi_M''(\log(\nu), T)$ for the structurally disordered sample $\mathbf{1_{Dis}}$

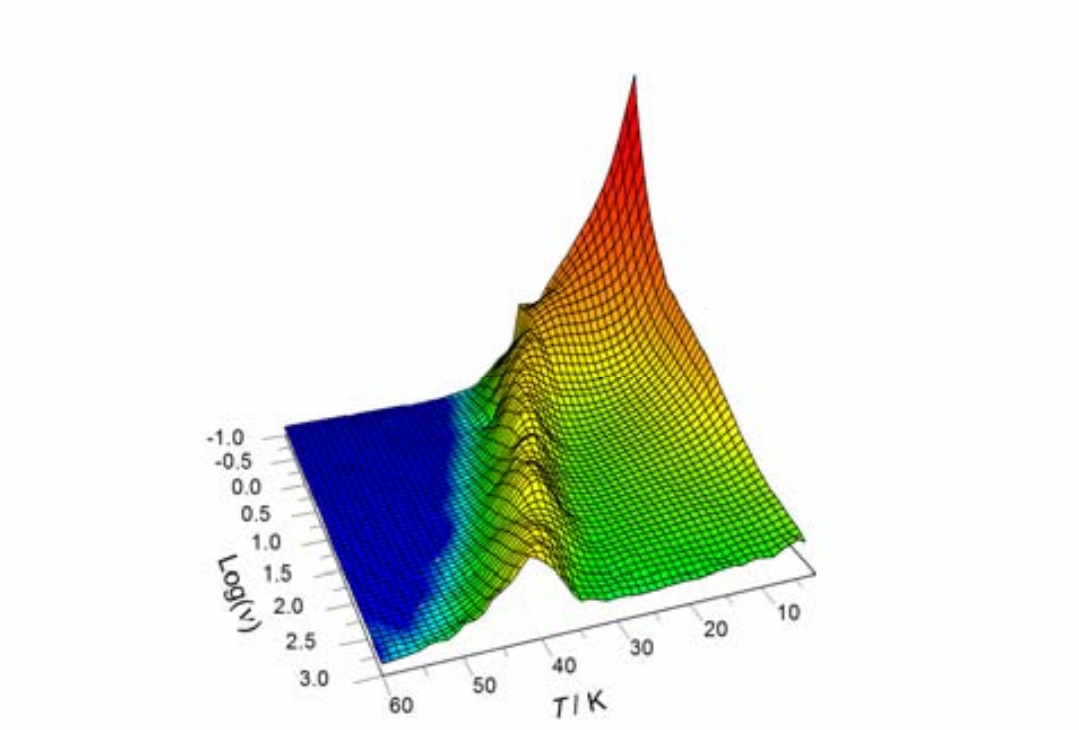

3D graph of $\chi_M''(\log(\nu), T)$ for the sample $\mathbf{1_{Cr}}$

8.7 DC magnetic susceptibility

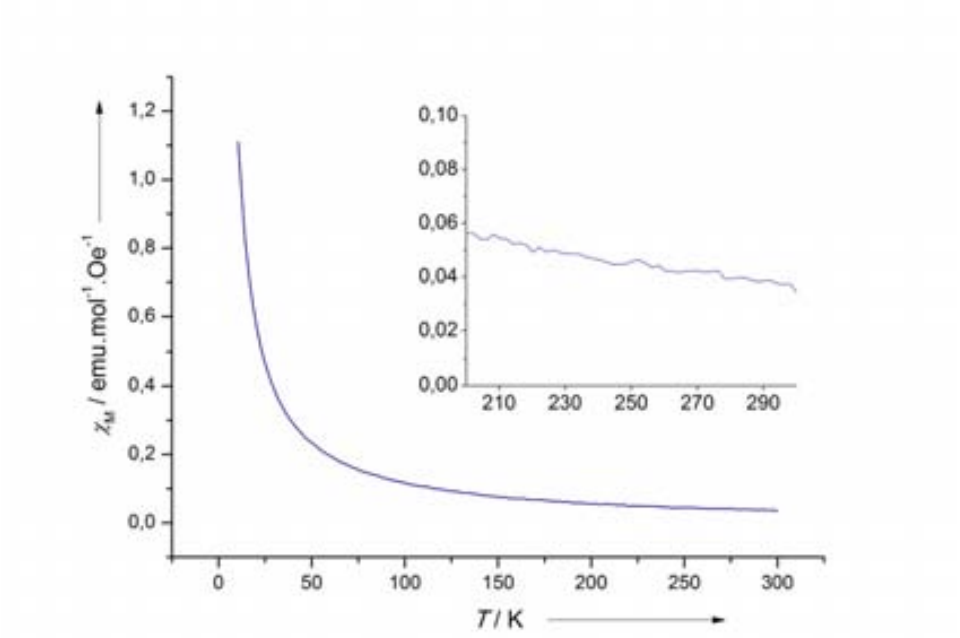

Plot of the dc magnetic susceptibility of compound **1** as a function of temperature. The inset shows the region between 200 and 300 K. As could be expected, no anomaly can be seen at the melting temperature of complex **1** (261 K).

9. Polarized optical microscopy

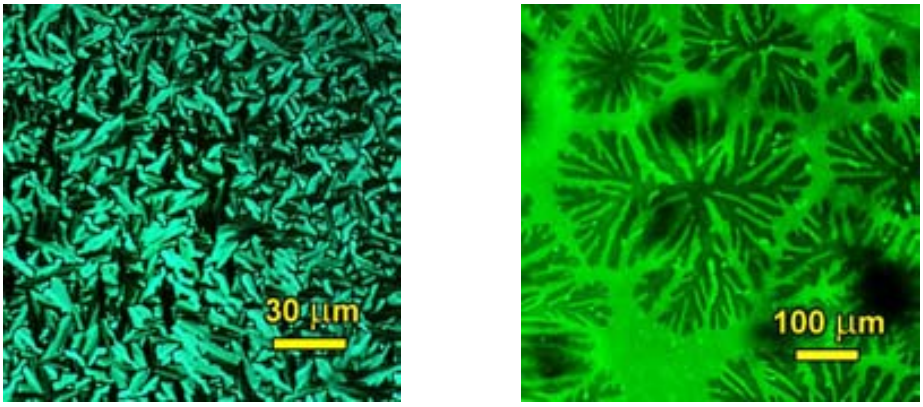

POM images of the mesophase of **1**, showing the optical texture at 298 K with crossed polarizing filters (left) and the fan texture of the homeotropic alignment, as seen with parallel polarizing filters (right).

Polarized optical microscopy was used to characterize the morphology of the different samples. Pictures were taken with crossed polarizing filters and parallel polarizing filters.

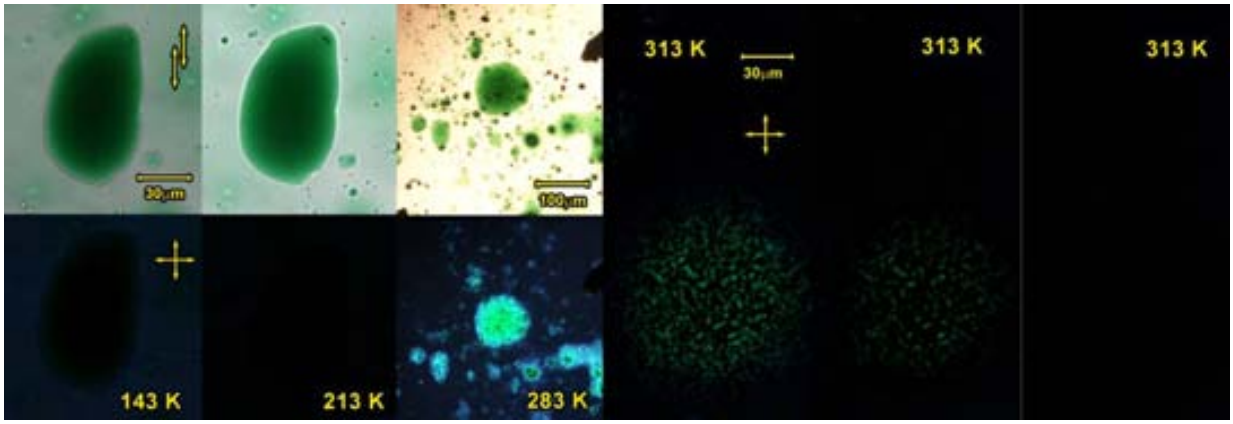

Changes in optical texture while heating a quenched sample of **1** from 143 K to 313 K at 30 K/min. At 143 K the sample looks effectively amorphous, it shows a textured mesophase at 283 K and it melts to an isotropic liquid at 313 K.

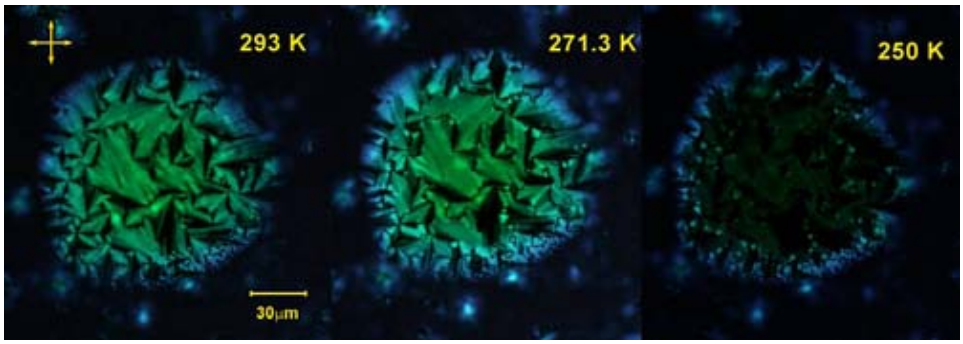

Changes in the optical texture while cooling down from 313 K using the cooling procedure described in section 7.